HIGH PERFORMANCE ES40-DERIVED SILICA MEMBRANES FOR DESALINATION

SHENGNAN WANG

M.Sc.

A thesis submitted for the degree of Doctor of Philosophy at

The University of Queensland in 2016

School of Chemical Engineering

Abstract

Access to potable water has become one of the top 10 global problems facing our contemporary society. Desalination of vast amounts of seawater is a promising measure to ameliorate this stress. Numerous thermal and membrane processes have been employed to desalt seawater, of which reverse osmosis (RO) using polymeric membranes is the most mature technology and has been regarded as the benchmark in current desalination technologies. However, due to the high pressure requirement for RO operation, other membrane processes, such as membrane distillation and pervaporation have been developed as the alternatives to further reduce the energy cost. Furthermore, due to the lack of chemical/thermal stability and high tendency to scaling and fouling of polymeric membranes, novel inorganic membranes, in particular silica derived membranes, are emerging as potential candidates for desalination. The majority of published works on silica membranes utilizes tetraethyl orthosilicate (TEOS) as the silica precursor and interlayers are generally required to reduce the roughness of the porous substrates, followed by 4 to 6 thin-film coatings and calcinations with heating rates of 1–2 $°C$ min^{-1} to form defect free silica membranes, which consume 10–14 days with extra cost. Therefore, the major target of this research is to produce interlayer-free silica membranes fabricated by rapid thermal processing (RTP) for desalination application.

Ethyl silicate 40 (ES40) is used as precursor to prepare silica membranes in this work owing to their superior thermal stability as compared to the TEOS analogous product. Firstly, the sol-gel processing of ES40 was investigated in this thesis. At different temperatures and H_2O/Si ratios, ES40 underwent various degrees of phase separation behaviour and sol-gel reactions. It was found that the hydrolysis and condensation reactions decreased with decreasing reaction temperature. Dense silica structures were obtained using low H_2O/Si ratios, whereas higher porosity was produced from a phase-separated sol-gel system with high H_2O/Si ratios. This tailoring process facilitated further condensation reactions and crosslinking of silica chains, leading to stronger silica matrices which were more resistant to densification.

The second part of this work is focused on improvement of the hydrostability of ES40-derived silica membrane materials by adjusting the reactant ratios of sol-gel synthesis process, as the low resistance of silica membranes to water vapor attack, which induce enlargement of the pore size followed by failure in salt rejection, can be detrimental to desalination performance. Investigations were carried out on the effects of reactant ratios on the microstructure of the silica matrices and their hydrothermal stability under harsh conditions (550 $°C$, 75 mol% vapour). The most hydrothermally stable matrix was obtained by decreasing the ethanol ratio whilst increasing water

and acid ratios. The improved hydrothermal stability was attributed to the further transition of silanol to siloxane groups on one hand and the formation of a more openly branched silica network on the other.

Further work was conducted on the preparation of ES40 derived interlayer-free silica membranes using RTP on the optimized reactant ratios as determined from above investigations. RTP involves a rapid heating rate and a short period of high temperature exposure up to 1 hour. This thesis shows for the first time the preparation of interlayer-free silica membranes by RTP. A major advantage of this novel preparation method is that the final membranes were coated with 2 silica layers only and were prepared in less than 3 hours, a considerable and significant reduction from 10-14 days for TEOS silica membranes. A comparison of the structure properties of silica materials produced by RTP and conventional thermal processing (CTP) found that the silica produced from RTP has more siloxane bridges and larger porosity, which can potentially deliver the corresponding membranes enhanced hydrostability and water fluxes.

The preparation feasibility of membranes was dependent on the pH of the sol-gel. The best membranes were prepared with ES40 sols with pH 4, which adhered well to substrates during the RTP calcination step. Water fluxes reached 17.8 kg m^{-2} h^{-1} for seawater (NaCl 3.5 wt%) at 60 ℃ whilst reaching salt rejections 95–99%. The long term stability tests showed stable water flux and salt rejection until ~300 hours. This is a major improvement from TEOS silica membranes which tend to fail within a few hours. In order to further improve the hydrostability, the effect of H$_2$O/Si, EtOH/Si and pH of the sol-gel solutions on silica xerogel properties and membrane performance was carried out. The prepared membranes gave good water flux (7 kg m^{-2} h^{-1}) and excellent salt rejection (>99%) for seawater desalination. In addition, long term testing at room temperature for 3.5 wt% saline solutions showed that the ES40 membrane was stable for 800 hours, whilst delivering 99% salt rejection. These results strongly suggested that high quality interlayer-free membranes were successfully prepared using RTP from ES40 precursor for the first time, delivering performance well above the current state of art.

Declaration by author

This thesis is composed of my original work, and contains no material previously published or written by another person except where due reference has been made in the text. I have clearly stated the contribution by others to jointly-authored works that I have included in my thesis.

I have clearly stated the contribution of others to my thesis as a whole, including statistical assistance, survey design, data analysis, significant technical procedures, professional editorial advice, and any other original research work used or reported in my thesis. The content of my thesis is the result of work I have carried out since the commencement of my research higher degree candidature and does not include a substantial part of work that has been submitted to qualify for the award of any other degree or diploma in any university or other tertiary institution. I have clearly stated which parts of my thesis, if any, have been submitted to qualify for another award.

I acknowledge that an electronic copy of my thesis must be lodged with the University Library and, subject to the policy and procedures of The University of Queensland, the thesis be made available for research and study in accordance with the Copyright Act 1968 unless a period of embargo has been approved by the Dean of the Graduate School.

I acknowledge that copyright of all material contained in my thesis resides with the copyright holder(s) of that material. Where appropriate I have obtained copyright permission from the copyright holder to reproduce material in this thesis.

Publications during candidature

Peer-reviewed papers

S. Wang, D.K. Wang, S. Smart, J.C.D. da Costa, Ternary Phase-Separation Investigation of Sol-Gel Derived Silica from Ethyl Silicate 40, Sci. Rep., 5, 2015, 1.

S. Wang, D.K. Wang, K.S. Jack, S. Smart, J.C.D. da Costa, Improved hydrothermal stability of silica materials prepared from ethyl silicate 40, RSC Adv., 2015, 5, 6092.

Conference abstracts

S. Wang, D.K. Wang, S. Smart, J.C.D. da Costa, Improved hydrothermal stability of ES40-derived silica matrices for molecular sieving silica membranes, International Conference of Inorganic Membrane 2014, Brisbane, Australia, 6-9 July. (Poster presentation)

S. Wang, D.K. Wang, S. Smart, J.C.D. da Costa, Hydrothermally stable ES40-derived silica membranes for desalination application" on the 9th Conference of Aseanian Membrane Society in July 2015. (Oral presentation)

Publications included in this thesis

1. S. Wang, D.K. Wang, S. Smart, J.C.D. da Costa, Ternary Phase-Separation Investigation of Sol-Gel Derived Silica from Ethyl Silicate 40, Sci. Rep., 5, 2015, 1. – incorporated as Chapter 3.

Contributor	Statement of contribution
Author Shengnan Wang (Candidate)	Designed experiments (50%) Analysed and interpreted data (70%) Wrote and edited paper (70%)
Author David K Wang	Designed experiments (50%) Analysed and interpreted data (10%) Wrote and edited paper (10%)
Author Simon Smart	Analysed and interpreted data (10%) Wrote and edited paper (10%)
Author João C. Diniz da Costa	Analysed and interpreted data (10%) Wrote and edited paper (10%)

2. S. Wang, D.K. Wang, K.S. Jack, S. Smart, J.C.D. da Costa, Improved hydrothermal stability of silica materials prepared from ethyl silicate 40, RSC Adv., 2015, 5, 6092. – incorporated as Chapter 4.

Contributor	Statement of contribution
Author Shengnan Wang (Candidate)	Designed experiments (50%)
	Analysed and interpreted data (70%)
	Wrote and edited paper (70%)
Author David K Wang	Designed experiments (50%)
	Analysed and interpreted data (10%)
	Wrote and edited paper (10%)
Author Kevin S Jack	Analysed and interpreted data (5%)
	Wrote and edited paper (5%)
Author Simon Smart	Analysed and interpreted data (5%)
	Wrote and edited paper (5%)
Author João C. Diniz da Costa	Analysed and interpreted data (10%)
	Wrote and edited paper (10%)

<u>Contributions by others to the thesis</u>

Contributions by Professor João C. Diniz da Costa, Dr. David K. Wang and Dr. Simon Smart in conception and design of the project, interpretation of data, revision or editorial of the draft.

Contributions by Dr Julius Motuzas in TGA characterisation of membrane materials and SEM imaging of membranes in Chapter 5 and 6.

Contributions by Dr Benjamin Ballinger in proof reading abstract and Chapter 1 and 2.

<u>Statement of parts of the thesis submitted to qualify for the award of another degree</u>

None

Acknowledgements

First of all, I wish to express my greatest appreciation to my supervisors Professor João C. Diniz da Costa, Dr David K Wang and Dr Simon Smart for their endless guidance, assistance, patience and encouragement throughout my PhD. I would not have been able to complete this work without their continuous and selfless support. Special thanks to Professor Victor Rudolph and Jason Stokes for their valuable comments and suggestions during milestone review as panel members.

Thanks to our previous and present Post doctors and colleagues in FIM^2LAB: Dr Julius Motuzas, Dana Lee Martens, Christelle Yacou, Yingjun Song, Gianni Olguin Contreras, Diego Ruben Schmeda Lopez, Guozhao Ji, Yen Chua, Nor Aida Zubir, Benjamin Ballinger, Liang Liu, Muthia Elma, Wenjing Wang, Weng Fu, Siti Nurehan Abd Jalil and Huihuang Chen for their professional advices and friendliness in our lab.

I would like to expand my gratitude to my friends and office mates Luhong Zhang, Jingwen Zhu, Yonghong Zeng and Ming Li who are always supportive and encouraging. Their accompanying as well as positive attitude at work have markedly comforted and inspired me in the school life.

I wish to acknowledge The University of Queensland and Australian Research Council for their financial support.

Finally, I wish to thank my parents for their unconditional love and my best friends Minchao Zhang, Xuejiao Zhang and Xue Wang for their understanding. Thanks for enlightening me every time when I feel depressed. I am more than lucky to have them as my family and friends.

Australian and New Zealand Standard Research Classifications (ANZSRC)

ANZSRC code: 090404, Membrane and Separation, 70%
ANZSRC code: 090410, Water Treatment Processes, 30%

Fields of Research (FoR) Classification

FoR code: 0904, Chemical Engineering, 100%

TABLE OF CONTENT

LIST OF FIGURES

LIST OF SUPPLEMENTARY FIGURES

LIST OF TABLES

1 INTRODUCTION

1.1 Background

Water scarcity has become one of the major problems for contemporary society due to population explosion, industrialization and contamination of natural water resources. Recent statistics show that over one-third (41%) of the world population live in areas suffering from water scarcity, and the proportion is predicted to increase to approximately two-thirds by 2025 [1]. Therefore, this global problem associated with water shortages motivates the development of technological solutions for the supply of potable water. Seawater desalination is a promising solution as it can offer high-quality water steadily and unlimitedly without tapping into the natural freshwater ecosystem due to the vast amount of seawater on earth [2]. Therefore, technical solutions have stimulated a rapid increase in the construction of seawater desalination plants in the past few decades in order to supplement water supply in water-stressed countries. It is expected that the global water production by desalination is likely to exceed 38 billion m^3 per year by 2016, which is double of that in 2008 [2, 3].

Desalination processes are generally divided into thermal or membrane-based processes depending on the mechanism of separation [4]. Thermal desalination process, where the saline solution is heated to promote evaporation and then the water vapor is condensed to produce fresh water, has been used for hundreds of years though large-scale plant did not start operating until the 1950s, when the first seawater distillation plant was opened in Kuwait [4]. This spurred a number of activities in countries in the Middle East to implement thermal seawater desalination based on the multi-effect distillation process, followed by an advanced thermal process called multi-stage flash distillation [5]. These plants are still in operation to date, producing almost half of the world's desalination capacity [6]. The main drawback of thermal desalination is that it consumes substantial amounts of energy during operation, thus is very costly and also results in a large emission of greenhouse gases [7-9]. Thermal processes remain the primary technology of choice in the oil-rich Middle Eastern countries, where energy prices are low. However, in the regions where fossil fuel resources are lacking and energy costs are significantly higher, the production of potable water is preferred by membrane-based desalination technologies as they are less energy intensive.

Membranes are semi-permeable filters, which retain salt whilst allowing water molecules to pass through, thus consuming much less energy than thermal desalination [7, 10]. The energy

requirements for seawater desalination using membrane based technologies (2–6 kW h m^{-3}) are less than half of that for thermal-based technologies (7–14 kW h m^{-3}) [7, 8, 11]. In the countries outside of the Middle East, membrane based desalination processes, in particular reverse osmosis, has rapidly developed since late 1960s [12] when the first successful reverse osmosis plant was installed, and has become the most commonly applied technology for desalinating seawater [10]. Large-scale seawater reverse osmosis desalination plants have been constructed all around the world, including Spain [13], Israel, the United States [14, 15], Jordan, Algeria, Chile and Australia [4]. Israel opened the world's largest seawater reverse osmosis desalination plant in 2005, offering production capacity of 330,000 m^3 day^{-1} [16]. The world's largest brackish water desalination plant was built in Jordan in 2006 with a maximum capacity of over 150,000 m^3 day^{-1} [17]. It is reported that in 2001, reverse osmosis accounted for 51% of new installed desalination capacity, which further increased to 75% in 2003 [18]. Membrane based desalination plants represent 80% of the worldwide desalination plants, and in the United States membrane processes represent 84% of the country's desalination capacity [4]. The membrane based desalination technology has emerged as the dominant choice in future desalination plant constructions.

Though the energy consumption of reverse osmosis is much lower than conventional thermal desalination process, the major cost in reverse osmosis is due to the high pressure required to overcome the high osmotic pressure of seawater during operation [19]. The high pressure requirement reaches over 40% of the total energy consumption [1, 20]. Reducing energy consumption is significant in reducing both the total cost of desalination from an economic standpoint and greenhouse gas emissions from an environmental perspective [21]. Thus, research and development are continuously devoted to develop techniques of low-grade energy consumption and low capital cost. Nevertheless, reverse osmosis is currently the most mature technology, and other novel membrane technologies are required to further improve the efficiency of desalination processes.

Membrane distillation and pervaporation processes have been considered as the alternatives to the conventional energy-intensive seawater desalination technologies. Although these technologies still require heat to operate efficiently, the operating temperatures are relatively low so sourcing industrial waste heat or solar panel heat makes these technologies attractive. Further, operating pressures are much lower than pressure-driven membrane separation process such as reverse osmosis, adding another operational benefit. Although the commercial application of pervaporation has been constrained by low water fluxes, pervaporation membranes have greatly improved in the last decade, with water fluxes increasing by one order of magnitude. Of particular attention, there

are a number of literature gaps related to silica membranes for desalination. This is an area of research that warrants further investigation, and forms the basis of this research thesis.

1.2 Motivation and gaps in literature that this research addresses

The application of pervaporation membranes in desalination is an emerging technology and still requires further investigation to reveal its full potential. The latest improvements in silica derived membranes are a proof of the potential of this type of inorganic membranes for desalination application. The major motivation of this research is to produce potable water from seawater desalination using interlayer-free ES40 derived silica membranes fabricated by rapid thermal processing (RTP) to address the water scarcity problem. There are several research and technical challenges relating to this type of membrane that have not yet been overcome.

The first gap in literature is related to membrane material preparation using an ES40 sol-gel process. ES40 membranes have a very few studies in literature compared to the extensively studied TEOS sol-gel process. There is a need to fundamentally understand the ES40 sol-gel process, and subsequent structural (surface area, pore volume, pore size and pore size distribution) formation, together with the functional (i.e. silanol and siloxane) groups evolution of the resultant silica. To this end, this thesis will systematically investigate how the reactant ratios (ES40, water and ethanol) and reaction conditions (pH and temperature) affect the physicochemical properties and hydrostability of the final silica product. These studies will form the bases for the preparation of interlayer-free ES40 derived silica membranes for desalination application.

A second gap is to reduce the capital cost for silica membrane fabrication by producing interlayer-free membrane using an RTP method. In general, an effective membrane requires interlayers and several top layers, which are coated and calcined sequentially with slow heating rate (1~2 °C min^{-1}), thus requiring up to 10-14 days of production and high energy consumption. The high production costs make silica membranes economically uncompetitive against other types of membranes for desalination application. Whereas, by adopting interlayer-free membrane using an RTP method, the silica sols for the separation layer are dip-coated directly on substrates with large size pore sizes (up to 0.5 μm) instead of smooth interlayers with medium pore sizes (up to 0.05 μm), and silica membranes are produced in less than 1% of the time that required by the conventional thermal processing (CTP) method. It is postulated in this thesis that the formation of interlayer-free silica films on large pore size substrates by the RTP method can be achieved by a careful modulation of the ES40 sol-gel method. As a partially-condensed silica precursor ES40 can form a strong silica

backbone structure which may be able to cope with thermal stress and expansion better than TEOS derived silica membranes. Moreover, the membranes are expected to be fully tested in a desalination set up under various conditions of temperature and salt concentration to further elucidate the structural and performance stability of the interlayer-free RTP silica membranes.

1.3 Key contributions to this field

The most important novel features of this work are the development of interlayer-free silica membranes by the RTP method for desalination application, in tandem with ES40 sol-gel synthesis. There are four key contributions to knowledge which are listed below:

The first contribution is the fundamental study of the ES40 sol-gel method, elucidating the miscible and non-miscible regions in a ternary phase diagram. A key finding of this work is related to the formation of dense and porous silica from miscible and non-miscible regions of ES40 sol-gel solution, respectively.

A second contribution is related to a systematic study where the high water/Si and acid/Si ratios and low ethanol/Si ratios delivered microporous features such as higher surface areas and pore volumes. A key finding is the formation of large silica particle clusters as revealed by small angle X-Ray scattering, structures of which were more hydrostable when exposed to harsh conditions (550 ℃ and 75 mol% water vapor).

A third contribution is the first demonstration of the preparation of interlayer-free silica membranes by an RTP method. The membranes proved to have high salt rejection in desalination application. A key finding is a significant reduction of the fabrication time, equivalent to 1% of that for a conventionally prepared silica membrane.

A fourth contribution is associated with the flexibility of the ES40 sol-gel film formation, where the membranes were synthesized below or above the silica isoelectric point (pH 2). A key finding is that by changing the ES40 sol-gel conditions, basic (pH 4) and acidic (pH 1) conditions, films were very porous and less porous, respectively, though salt rejection remained high in excess of 95%. The membranes proved to be hydrostable up to 120 h or 800 h depending on the initial sol-gel conditions.

1.4 Thesis structure

Chapter 1 – Introduction

A brief description of the desalination processes is given including a discussion on the gaps of silica membranes in pervaporation processes. The motivation and postulation of this thesis are stated.

Chapter 2 – Literature review

Review of major membrane technologies currently employed in desalination, including the type of membranes and performance at various operating conditions. Subsequently, the review is focused on silica membranes and sol-gel synthesis methods, followed by film formation by dip coating and calcination methods. A summary is given based on discussions and gaps in literature.

Chapter 3 – Phase separated sol gel process of ES40

This chapter focuses on mapping the ternary diagram of ES40/EtOH/H_2O for sol-gel processing, which has not previously been studied or reported. It shows a smaller miscible area than the conventional silica precursor TEOS. It aims to understand the specific role played by the ES40 silica precursor, the concentration of water (hydrolysing agent) and ethanol (solvent). This systematic study, supported by material characterisation (N_2 sorption, TGA and FTIR), provides a fundamental understanding of the ES40 sol-gel method. The outcomes of this study are used in subsequent chapters. This work has now been published in Scientific Reports.

Chapter 4 – Influence of sol gel conditions on hydrothermal stability of ES40-derived silica xerogels

This work involves the fundamental physicochemical characterization of ES40-derived silica xerogels prepared from different $Si:EtOH:H_2O:HNO_3$ ratios according to the ternary diagram from Chapter 3. The prepared sols were synthesized to study the influence of each parameter on the resultant structure based on characterisation using N_2 adsorption, FTIR, SAXS and ^{29}Si NMR. The dried sols (xerogels) were hydrothermally studied under harsh conditions at 550 ℃ with 75 mol% vapor for 20 h. This work has been published in RSC Advances.

Chapter 5 – RTP Interlayer free ES40 derived silica membranes for desalination (pH series)

In this chapter, interlayer-free ES40 derived membranes were prepared by the RTP method. The membranes proved to be suitable for desalination application. A series of ES40 sol-gels were developed and fully characterised by changing their pH where best membranes were stable up to

120 h. Subsequently, the Si:EtOH ratio was modified, demonstrating that the stability of the membranes improved up to 300 h. A fundamental study on the effects of RTP on silica structural and functional formation was carried out by N_2 sorption, FTIR, SEM and TGA analyses. This work is currently under review in the Journal of Membrane Science.

Chapter 6 – RTP Interlayer free ES40-derived silica membranes for desalination (water series)

This chapter investigates the effect of the H_2O:Si ratio in the formation and performance of interlayer-free RTP membranes for desalination application. An optimal ratio was developed where membrane stability was improved up to 800 h. A fundamental study on the effects of RTP on silica structural and functional formation was also carried out by N_2 sorption, FTIR, SEM and TGA analyses.

Chapter 7 – Conclusions and Recommendations

Major conclusions and recommendations for future work are given in this final Chapter.

References

[1] R.F. Service, Desalination Freshens Up, Science, 313 (2006) 1088-1090.

[2] M. Elimelech, W.A. Phillip, The Future of Seawater Desalination: Energy, Technology, and the Environment, Science, 333 (2011) 712-717.

[3] Q. Schiermeier, Purification with a pinch of salt, Nature, 452 (2008) 260-261.

[4] L.F. Greenlee, D.F. Lawler, B.D. Freeman, B. Marrot, P. Moulin, Reverse osmosis desalination: Water sources, technology, and today's challenges, Water Res., 43 (2009) 2317-2348.

[5] B. Van der Bruggen, C. Vandecasteele, Distillation vs. membrane filtration: Overview of process evolutions in seawater desalination, Desalination, 143 (2002) 207-218.

[6] L. Henthorne, Desalination today, Southwest Hydrology, (2003) pp. 12-13.

[7] R. Semiat, Energy Issues in Desalination Processes, Environ. Sci. Technol., 42 (2008) 8193-8201.

[8] A. Subramani, M. Badruzzaman, J. Oppenheimer, J.G. Jacangelo, Energy minimization strategies and renewable energy utilization for desalination: A review, Water Res., 45 (2011) 1907-1920.

[9] R.G. Raluy, L. Serra, J. Uche, Life cycle assessment of desalination technologies integrated with renewable energies, Desalination, 183 (2005) 81-93.

[10] C. Fritzmann, J. Lowenberg, T. Wintgens, T. Melin, State-of-the-art of reverse osmosis desalination, Desalination, 216 (2007) 1-76.

[11] R. Semiat, Energy issues in desalination processes, Environ. Sci. Technol., 42 (2008) 8193-8201.

[12] S. Loeb, S. Sourirajan, Sea Water Demineralization by Means of an Osmotic Membrane, in: Saline Water Conversion II, AMERICAN CHEMICAL SOCIETY, 1963, pp. 117-132.

[13] G.L.M. von Medeazza, "Direct" and socially-induced environmental impacts of desalination, Desalination, 185 (2005) 57-70.

[14] Y. Dreizin, A. Tenne, D. Hoffman, Integrating large scale seawater desalination plants within Israel's water supply system, Desalination, 220 (2008) 132-149.

[15] A. Tal, Seeking Sustainability: Israel's Evolving Water Management Strategy, Science, 313 (2006) 1081-1084.

[16] B. Sauvet-Goichon, Ashkelon desalination plant - A successful challenge, Desalination, 203 (2007) 75-81.

[17] M.S. Mohsen, Water strategies and potential of desalination in Jordan, Desalination, 203 (2007) 27-46.

[18] P. Wolfe, Fujairah Marks Major Milestone for Desalination in Middle East, Water and Wastewater International, (2005)

Available from: http://www.waterworld.com/articles/wwi/print/volume-20/issue-21/regional-focus/fujairah-marks-major-milestone-for-desalination-in-middle-east.html (accessed 08.03.2016).

[19] R.L. McGinnis, M. Elimelech, Global Challenges in Energy and Water Supply: The Promise of Engineered Osmosis, Environ. Sci. Technol., 42 (2008) 8625-8629.

[20] L. Souari, M. Hassairi, Sea water desalination by reverse osmosis: the true needs for energy, Desalination, 206 (2007) 465-473.

[21] C. Charcosset, A review of membrane processes and renewable energies for desalination, Desalination, 245 (2009) 214-231.

2 LITERATURE REVIEW

2.1 Abstract

This chapter presents a literature review on desalination and membranes. It starts with a brief review of desalination processes and their general features, leading to the utilization of membranes. Organic and inorganic membranes are then reviewed in the context of desalination, including their performance in terms of water fluxes and salt rejection under varying testing conditions, together with their potential for further research and development, particularly the potential of pervaporation inorganic membranes. The review is subsequently focused on silica derived membrane synthesis methods with an introduction to the theory and principles applicable to sol-gel chemistry and methods, membrane preparation and calcination methods.

2.2 Membrane related technologies for desalination

2.2.1 Reverse osmosis (RO)

RO was developed in the 1970's and since then has been widely applied for desalination of various concentrations of salty water. Nowadays, RO is the dominant water purification technique for desalination with a large number of plants installed all around the world including the United States, Middle East, China and Australia among many other countries. RO works by using a semipermeable membrane which allows water to pass through via solution diffusion transport while rejecting the diffusion of salts. In a natural osmosis process, osmotic pressure arises when the concentration of the solution on one side is unequal to that on the other side of the membrane and the solvent (i.e. water in desalination) moves spontaneously from the low concentration to high concentration solution aiming to equalize the concentration of each side of the membrane and minimize the free energy of the system [1, 2]. Whereas in the RO process, an extra pressure, which is strong enough to overcome the osmotic pressure difference, is exerted to reverse the direction of water flow and results in the production of pure water on one side.
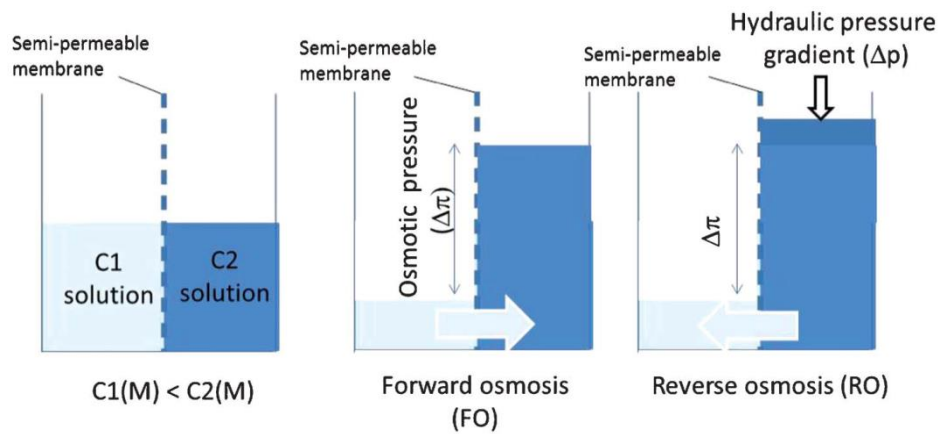
Figure 2.1 Schematic of FO and RO processes. C1(M) and C2(M) are the solution concentration in molarity. C2 solution is the draw solution, containing the draw solutes (or osmotic agents) [2].

By being the most established industrial membrane process for desalination, reverse osmosis preference is due to several reasons as follows:

- It can diminish 99% of the solute and the permeate water is ready to use after this process.
- It is environmentally friendly as no toxic chemicals is used or produced during this process.
- RO water production cost has greatly reduced due to the development of membrane materials.

However, RO requires very high operating pressures (6 MPa to 8 MPa) for seawater desalination in order to overcome osmotic pressure and drive the water to pass through the membrane. High pressures are closely related to high energy consumption which translates into high operating costs. Further, high pressures require mechanically robust membrane modules and associate pipelines, which increase plant capital costs. On a positive note, the lifespan of the RO membranes are around 5 years [3]. Although replacing the membranes attracts extra costs, the lifespan of 5 years is considered to be excellent in terms of industrial operations.

2.2.2 Forward osmosis (FO)

FO has been developed over the past 70 years [4], andalso uses semipermeable membranes, similar to RO. However, FO process does not require external high pressures, as it takes the advantage of the natural osmotic flow by using a highly concentrated draw solution. Therefore, as shown in Figure 2.1, due to the high osmotic pressure generated from uneven concentration, water in seawater feed side is pulled to the more concentrated draw solution. After eliminating the solutes in

the draw solution, the final water product is obtained. The solutes are desired to be nontoxic, neutral pH, stable and highly soluble in water to provide high osmotic pressure thus driving force, and can be easily removed from water through simple processing. Volatiles such as ammonium bicarbonate [5], ammonia and carbon dioxide mixtures (NH_3/CO_2) [6] can be used as solutes in draw solution, as they can be conveniently separated by heating and then recycled. Recently, a number of draw solutes have been reported including sugars (glucose, fructose and sucrose) [7] and fertilizers (KCl, $NaNO_3$, KNO_3, $Ca(NO_3)_2$, $NH_4H_2PO_4$, $(NH_4)_2SO_4$) [8].

FO desalination process has several advantages. As the driving force is osmotic pressure in FO, instead of external hydraulic pressure as in RO, FO is less energy intensive, more economically efficient and has lower tendency of membrane fouling [9-11]. The osmotic pressure in FO can provide much greater driving force than the hydraulic pressure in RO, thus may offer higher water flux [11]. Moreover, another outstanding character of FO is viable in a wider range than RO, as it can handle more concentrated saline solutions. On the other hand, the drawbacks of FO are the use of highly concentrated draw solution is imperative in the process, which adds extra cost. Also, although the solute can be recovered and reused, more efforts need to be made to separate the solute and water, which attracts increase energy requirement and capital cost.

2.2.3 Membrane distillation (MD)

MD is a thermal driven process. The temperature difference across the membrane generates vapour pressure gradient, which can drive the vapour molecules transfer through the membrane. A schematic of MD process shown in Figure 2.2 (B), the pore of the membrane allows the formation of a meniscal liquid/vapor interface, from where the water vapor can diffuse through the membrane, while the non-volatile salt is retained on the feed side. The fresh water can be collected on the permeate side by condensation of water vapour. To increase the efficiency of desalination, water on the permeate side is removed from the system during operating as direct contact MD, air gap MD, vacuum MD and sweeping gas MD [12, 13]. Among these, vacuum membrane distillation is operated by maintaining the permeate side at vacuum to enhance the driving force. It is deemed to be the best option when the volatiles need to be eliminated from the feed side. In general, the membranes used in the MD process must be porous and hydrophobic to avoid wetting the pores by liquid [14, 15]. No capillary condensation should happen inside the pores during operation and only vapour can pass through the pores.
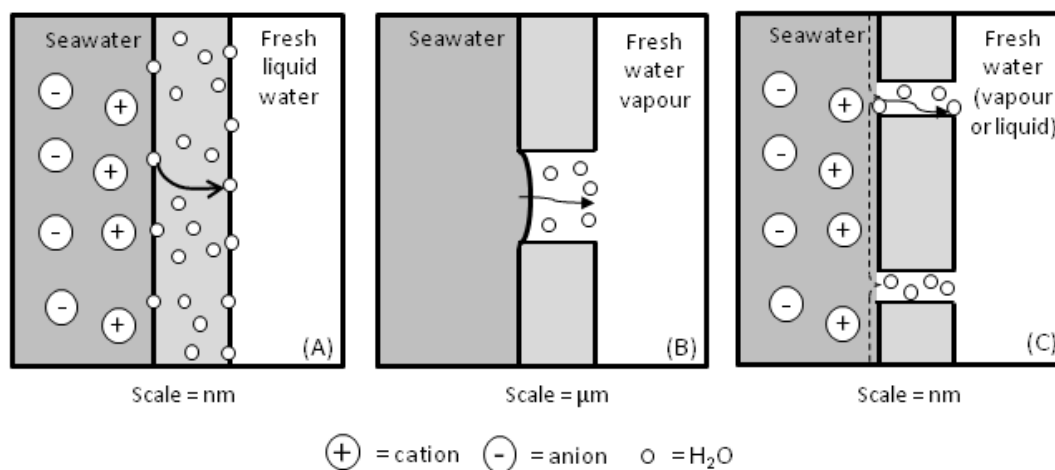
Figure 2.2 Schematics of reverse osmosis (A), membrane distillation (B) and pervaporation (C) desalination processes at the scale by which governing separation mechanisms operate [16].

Currently, MD is considered to be an alternative to the existing widely used desalination RO process. It offers several advantages such as reduced operation space, milder operating conditions and less tendency of membrane fouling [17]. MD can achieve 100% salt rejection at atmospheric pressure and low temperature. Since it is not a pressure driven process as RO, the theoretical potential of fouling is lower. However, MD is susceptible to scaling by calcium carbonate and calcium sulphates [18], which is another form of membrane fouling. Further, there is a need to condense the water vapour which diffuses from the feed side to the permeate side. Therefore, MD processes are likely to use more energy than RO processes, as condensation consumes more energy than pumping seawater to high pressures.

The application of MD is still limited in industry because of its low water flux and energy efficiency. As MD is a thermal driven process, by increasing the temperature in the feed side likewise increases the vapour pressure difference from the feed side to the permeate side, thus increasing water fluxes. Hence, the problem of low energy efficiency can be solved by tapping into using waste heat or other heat sources. For instance, Kim et al. [19] presented a solar-assisted MD configuration, where solar energy was collected during solar-peak hours and utilized to maintain the feed seawater temperature. The annual solar fraction was reported to be 77%. Heat recovery was further applied in this system, which means to employ the heat from permeate and brine streams to heat feed water. It was observed that the thermal energy consumption reduced by 43% compared to conventional designs, and thus highlighting the technical and economical feasibility of MD desalination.

2.2.4 Pervaporation (PV)

PV is also a thermally driven process similar to MD, and commonly used for organic dehydration [20]. Contrary to MD process, where the membrane is merely used as a device to facilitate the formation of meniscal liquid/vapor interface, the properties of PV membrane material play a significant role in separation. In PV, separation is achieved by the preferential transport of one of the components in the feed solution due to its higher affinity to the membrane [11]. While hydrophobic membrane is applicable in MD to produce meniscus interface, hydrophilic membranes are favourable in PV. By using hydrophilic membranes, water is transport through the membrane by the sorption-diffusion mechanism [21]. Firstly, water in the solution is preferentially adsorbed on the membrane surface, followed by selective access to the pore entrance and diffusion through the membrane. Vacuum is usually employed on the permeate side while atmospheric pressure is maintained on the feed side to create the driving force. The permeate water then evaporates due to a low pressure on the permeate side and desorbs from the membrane. Finally, the permeate water vapor is condensed in a cold atmosphere downstream. The pressure on the permeate side is then kept at low pressure by a vacuum pump followed by condensing the water vapor into liquid, thus the driving force is maintained during desalination via PV process. The rejection of pervaporation for desalination is expected to be close to 100% [11, 22] since hydrated salt ions are non-volatile and only free water molecules can transport and then condense in the permeate collector.

2.3 Membrane process performance and discussion

The current gold standard membrane-based system for desalination is reverse osmosis (RO) [23-25]. RO membranes have undergone large development in the 1980s and 1990s which has yielded significant technological improvements. This technology has been transferred to the industry and is currently considered a mature technology. It is therefore envisaged that RO membrane improvements are going to be minor, as major breakthroughs occurred 30 years ago. Table 2.1 lists the membrane types, testing conditions and performance of RO membranes. Both organic and inorganic membranes have been prepared and tested under various conditions. The best RO membranes are polyamide membranes which have been extensively used in desalination plants, and newly researched RO membranes have achieved high fluxes of ~42 kg m^{-2} h^{-1} for processing seawater whilst delivering very high salt rejections >99% [26]. Other recent works have reported relatively similar performances using novel hybrid organic-inorganic membranes, yet these were tested at a much lower salt concentration (0.2 wt%) which is significantly below the typical salt

concentration of seawater (3.5 wt%). It is also observed novel RO membranes based on mixed matrix membranes (MMM), containing both polymer and inorganic phase, where the latter included nano-silicas and zeolites.

Table 2.1– RO membranes, testing conditions and performance.

Membrane materials	Testing conditions	Feed conc.	Water flux (kg m^{-2} h^{-1})	Rejection (%)	Stability test	Ref.
Silica-polyamide nanocomposite	1.72 MPa	2000 ppm	9.0/ 40.8	90.7/ 71.7	N/A	[27]
Organosilica membranes	25 ℃ 1.15 MPa	2000 ppm	14	95	N/A	[28]
Thin-film nanocomposite membrane containing MCM-41 silica nanoparticles	25 ℃ 2.07 MPa	2000 ppm	46.6	97.9	N/A	[29]
Nanosilica-polyamide thin film composite	25 ℃ 1.6 MPa	2000 ppm	53	96	N/A	[30]
Thin film nanocomposite RO membranes loaded with silicate-1 nanozeolites	25 ℃ 1.6 MPa	2000 ppm	66.6	96.4	Acid stability	[31]
Organosilica	25-90 ℃ 1.5 MPa	2000 ppm	1.9×10^{-7} m^3/(m^2 s)	98	N/A	[32]
Polyamide membrane with hydrophilic additive	25 ℃ 5.52 MPa	3.28 wt%	41.7	99.41	N/A	[26]
MFI-type zeolite	25-90 ℃ 0.7 MPa	0.3 wt%	30	93	90 days	[33]
Polyamide membrane with SiO$_2$ incorporation	28 ℃ 4.4 MPa	11000 ppm	50	98	N/A	[34]

Akin to RO, FO processes are attracting major interest from the research community lately, and a list of FO membranes, testing conditions and performance is given in Table 2.2. FO membranes are generally polymeric, though there are some initial work reported on MMM and inorganic membranes. The results are varied, though none have shown satisfying results for seawater (NaCl 3.5 wt%) processing. FO is a simple process, not requiring pumps for high pressure operation, and therefore attractive for industrial operations. Hence, FO uses the osmotic pressure to draw water

from the feed side to the permeate side, also known as the draw side. FO membranes have also been reported for alcohol dehydration [35] and water treatment [36, 37]. In principle, FO can be used for desalination although the draw solution cannot contain NaCl, possibly a sugar solution to increase the osmotic pressure for water to diffuse from the seawater feed side to the draw solution (permeate) side of the membrane. The problem here is that there is still a need for a second step to separate water from the draw solute, possibly using RO membranes, which increases capital and operating costs. Therefore, FO process for desalination may not be attractive.

Table 2.2 – FO membranes, testing conditions and performance.

Membrane materials	Testing conditions	Feed (draw) conc.	Water flux (kg m^{-2} h^{-1})	Rejection (%)	Stability test	Ref.
Polybenzimidazole (PBI)	22.5 ℃	DI water (2.0 M)	3.84	97.3	N/A	[38]
PBI	23 ℃	DI water (5.0 M)	32.4	99.5	N/A	[39]
PBI-PES	23 ℃	DI water (5.0 M)	24.2	90	N/A	[40]
Cellulose acetate	22 ℃	DI water (5.0 M)	48.2	86.5	N/A	[41]
Polyamide	22 ℃	Seawater (2.0 M)	13.5	91.4	N/A	[42]
Polyamide	23 ℃	Seawater (2.0 M)	17	91	N/A	[43]
Microporous silica xerogels	23 ℃	DI water (2.0 M)	60.3	92	N/A	[44]
Zeolite-polyamide nanocomposite	20 ℃	DI water (1.0 M)	25.7	95.6	N/A	[45]

The less common membrane distillation (MD) process [46, 47] has also been employed for desalination application. Table 2.3 displays representative results for MD membranes, testing conditions and performance. This process has been dominated by hydrophobic polymeric membranes for many years, to avoid pore wetting. With the advent of nanotechnology there has been a resurgence of new inorganic materials and MMM membranes tested in MD processes. One example in carbon nanotube and graphene oxide membranes delivering high water fluxes of 36.8

and 97 kg m^{-2} h^{-1}, respectively, together with high salt rejections >99%, though testing conditions of temperature and feed salt concentration were varied [56, 58].

Table 2.3 – MD membranes, testing conditions and performance.

Membrane materials	Testing conditions	Feed conc.	Water flux (kg m^{-2} h^{-1})	Rejection (%)	Stability test	Ref.
Carbon nanotube/ Polypropylene composite	80 ℃	10 mg L^{-1}	19.38	99	N/A	[48]
Polyvinylidene fluoride (PVDF)	30-80 ℃	3.5 wt%	15.2	99.98	40 h	[49]
PTFE hollow fiber	80 ℃	30 g/L	17.2	99.9	N/A	[50]
Nanoporous organosilica	60 ℃	10-150 g/L	13	99.9	N/A	[51]
Titanium oxide nanotubes/polyethersulfone	65 ℃	7000 ppm	15.2	98	N/A	[52]
Microporous PVDF	25-75 ℃	30000 ppm	12	99	N/A	[53]
PVDF-PTFE nanofiber	40-70 ℃	3.5 wt%	18.5	99.9	15 h	[54]
Titania ceramic membranes	70-90 ℃	0-2.0 M	3.69	99	N/A	[55]
Carbon nanotube	70 ℃	10000 ppm	36.8	99.9	60 days	[56]
PVDF hollow fiber	90 ℃	7.0 wt%	6.4	99.9	240 h	[57]
Graphene oxide	80 ℃	3500/34000 mg/L	97/83	99.9	90 days	[58]
Carbon-silica nanocomposite	25-60 ℃	0-35 g/L	12	99	N/A	[59]
Polyethersulfone grafting TEOS	35-50 ℃	2 wt%	10.44	99.7	N/A	[60]

Table 2.4 – Pervaporation membranes, testing conditions and performance.

Membrane materials	Testing conditions	Feed conc.	Water flux (kg m^{-2} h^{-1})	Rejection (%)	Stability test	Ref.
Porous alumina and silica membranes	25 ℃ 7 bar	3.5 wt%	1.8	98	5 h	[61]
Triethylammonium bromide Carbonised template silica	25 ℃ 1 bar	3.5 wt%	3	97	N/A	[62]
Hybrid carbon silica	1 bar 25 ℃	0.3-3.5 wt%	3.7	98.5	12 h	[63]
Acid catalysed cobalt oxide silica	1 bar 25 ℃	1 wt%	1.8	99.9	570 h	[64]
MFI zeolite	1 bar 75 ℃	0.3 wt%	11.5	99	560 h	[65]
Zeolite	1 atm 93 ℃	100 mg/L	2.5	97.5	N/A	[66]
Zeolite clinoptilolite-phosphate composite	1 atm 95 ℃	1400 ppm	15	95	N/A	[67]
Polysulfone composite with Poly(vinyl alcohol) coating	1 atm 70 ℃	30000 ppm	7.4	99.9	N/A	[68]
Acid-base catalysed cobalt oxide silica	1 atm 60 ℃	3.5 wt%	31.5	90	N/A	[69]
P123 Carbonised template silica	1 atm 60 ℃	0.3 wt%	8.5	99.5	250 h	[70]
Cellulose	1 atm 25 ℃	40 g/L	5.97	99.7	N/A	[71]
Silica membrane	1 atm 25 ℃	40000 ppm	2.6	99.9	N/A	[72]
Mesoporous TiO$_2$ membrane	1 atm 75 ℃	0.3 wt%	10.5	99	350 h	[73]
Poly(vinyl alcohol) with zeolite loading	30 mbar 40 ℃	3.5 wt%	3.45	97.6	N/A	[74]

Pervaporation (PV) is also a low grade energy technique as it operates relatively well at low feed temperatures (<90 ℃) and generally only vacuum is required at the permeate side. PV membranes

as summarized in Table 2.4 are mainly polymeric, though recently there have been a limited number of papers using a variety of ceramic type membranes, including silica, titania and zeolites. Water fluxes are generally low, though there has been a current trend of flux improvement towards values of or in excess of $10 \, kg \, m^{-2} \, h^{-1}$. Novel inorganic membranes have been reported using hybrid materials (i.e. silica and carbon) and generally have microporous structures [62, 63, 70], though titania membranes with mesoporous structures are also applied in membranes [73]. Salt rejections are generally high >95%.

All of these technologies are viable, albeit at different scales, and their utilisation depends on production volume, energy consumption and feed water characteristics. In terms of research, RO offers marginal improvements whilst FO industrial application for desalination is questionable. MD and PV are very similar processes, and novel PV membranes are now attracting the interest of the research community. Though the most accepted application of PV membrane process is water/solvent separation, its potential for desalination has emerged and been proven by many studies as summarized in Table 2.4. Similar to MD, pervaporation is also a low-grade energy technique as it operates well at low feed temperatures (<90 °C) though it requires a system to maintain the water vapour pressure low and a condenser in the permeate side. As a result, PV has higher energy consumption than the high pressure required for the RO process. However, RO cannot process brines or sea waters with NaCl concentration higher than 5% as osmotic pressures become too prohibitive due to limitation of pressure loading on engineering equipment. Contrary to this, PV membranes can process even higher brine concentrations of 15% and there are a number of opportunities for processing salty waters in dry areas around the world, in addition of dewatering mineral brines such as lithium and potash brines. Although PV desalination application is still at its infancy, promising results have emerged that warrant further research focusing on preparation of membranes that offering high water fluxes. For instance, improvements in water flux have been realised in the last 10 years, as initial values for silica derived membranes have increased from ~1 to $10 \, kg \, m^{-2} \, h^{-1}$. These improvements were attributed to novel silica or mixed (metal oxide or carbon) silica films. This is an area that is not well explored in the literature and further research is warranted. There are potential improvements envisaged by changing silica precursors, sol-gel process and membrane fabrication to advance knowledge in this area. This is one of main gaps in literature, and forms the basis of research in this thesis.

2.4 Silica sol-gel

2.4.1 Sol gel reaction and synthesis

The synthesis of ceramic membranes by sol-gel process was first reported by Burggraaf and co-workers in 1984 [75] and received extensive attention. Later, the sol-gel method was applied by Asaeda and Burggraaf groups to prepare microporous silica membranes in 1986 [76-78]. Since then, sol-gel method has been widely used to prepare microporous inorganic membranes [79-84].

In a typical homogeneous sol-gel process, a silica alkoxide precursor (for example, TEOS) undergoes hydrolysis and condensation reactions in the presence of a mineral acid or base as a catalyst to produce a microporous silica matrix. The following general reactions describe the typical sol-gel process:

Hydrolysis reaction:

$$\equiv Si-OR \ + H_2O \ \underset{\text{Esterification}}{\overset{\text{Hydrolysis}}{\rightleftharpoons}} \ \equiv Si-OH \ + \ R-OH \tag{Eq. 1}$$
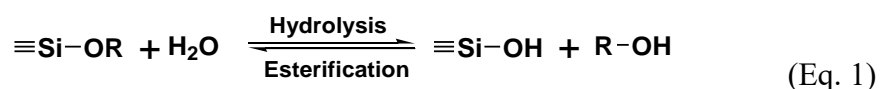
Polymerisation/Condensation reaction:

$$\equiv Si-OR \ + \ HO-Si\equiv \ \underset{\text{Alcoholysis}}{\overset{\text{Alcohol Condensation}}{\rightleftharpoons}} \ \equiv Si-O-Si\equiv \ + \ R-OH \tag{Eq. 2}$$

$$\equiv Si-OH \ + \ HO-Si\equiv \ \underset{\text{Siloxane Hydrolysis}}{\overset{\text{Water Condensation}}{\rightleftharpoons}} \ \equiv Si-O-Si\equiv \ + \ H_2O \tag{Eq. 3}$$
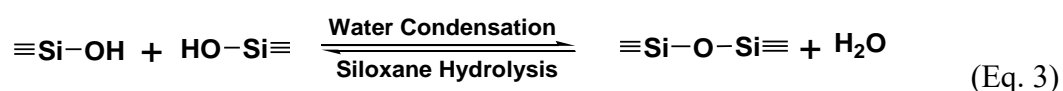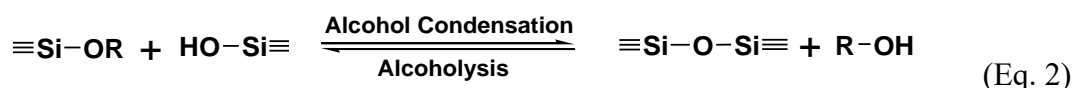
Firstly, hydrolysis reaction occurs (Eq. 1). During this process, the alkoxy groups of silica precursor are hydrolyzed by water to hydroxyl groups via silanol bonds (Si–OH) and the alcohol as byproducts. This is followed by condensation reactions, where the silanol bonds further react with either an alkoxy group (alcohol condensation; Eq. 2) or another silanol group (water condensation; Eq. 3) to produce siloxane bonds (Si–O–Si) and the by-products alcohol (ROH) or water, respectively. Since alkoxysilanes are insoluble in water, a mutual co-solvent, such as alcohol is usually used to form a homogeneous sol solution [85, 86].

The sol-gel synthesis conditions, including the type and concentrations of alkoxysilane, catalyst, co-solvent (water and alcohol), temperature and reaction time can significantly affect the degree of hydrolysis of a monomer, the extent of branching, and the rates and mechanisms of hydrolysis and

condensation reactions [85, 87]. Under different preparation conditions, the morphology of the resultant silica polymeric chains in the sol can be predominately linear, highly branched, or various degree of both polymeric species. Weakly branched sols are relatively easy to densify, thus after drying and calcination, microporous structure with pore sizes of 2-4 Å is obtained [88]. In contrast, highly condensed silica sols densify into small clusters with larger (> 2 nm) intercluster pores forming mesoporous structures [88]. It has been shown by many studies that using a base catalyst or increasing water content in the sol-gel process can increase the proportion of mesopores due to the formation of highly branched silica chains [89]. On the other hand, silica matrix synthesized under very acidic conditions and low H_2O/silica ratios are microporous. The structure of the membrane and the resultant gas permeation and separation properties are thus highly controllable by adjusting the synthesis conditions. The drying conditions are also very important in deciding the final pore structure and properties of the silica gels and membranes [79, 84, 90]. Due to the differences in drying rate, the properties of the bulk xerogels and membranes are generally incongruent. However, as confirmed by Nair et al. the properties of the gel can give a qualitative indication of the thin film membrane structure [91].

2.4.2 Sol gel pH effects

In most cases, the polymeric sol of microporous silica membranes is prepared from acid catalyzed sol-gel process, since acid catalysis favors the formation of long-chained weakly-branched silica. In the case of acid catalyzed reaction, the hydrolysis proceeds through electrophilic attack of the H^+ ion [92]. This causes a decrease in reactivity as the number of –OR groups on the Si decreases with the progress of hydrolysis. Complete hydrolysis of silicon to $Si(OH)_4$ is thus limited and the condensation reaction will start before the hydrolysis has been completed. Acid-catalyzed condensation is believed to take place via protonated silanol species [85]. Since Si–O groups are strongly electron withdrawing (even stronger than –OH groups), the preferred reaction sites for condensation are the most basic silanol bonds on monomers or weakly branched oligomers [86]. As a result of this, an acid catalyzed sol creates long chains of siloxane bonds, forming a weakly branched polymer.

Conversely, base catalysis favors the formation of highly branched silica. In the case of base catalyzed reaction, the hydrolysis proceeds through the nucleophilic substitution of OH$^-$ ion, which leads to an increase in reactivity as the number of –OR groups decrease with the hydrolysis process [85]. The preferred reaction sites for condensation are the most acidic (most likely deprotonated) silanol bonds of the Q^3 Si atoms [86], where n (0, 1, 2, 3 or 4) in Q^n represents the number of Si–O–

Si linkages. Besides, alcoholysis (reverse of Eq. 2.2) is much faster under base catalysis than acid catalysis and favors reaction of Q^1 silica groups. In this way a base catalyzed sol can contain significant amounts of silica monomers constantly forming and reforming. This process is known as Ostwald ripening, which allows the structure to settle into its most thermodynamically favored configuration with as many siloxane bonds as possible, thereby creating a highly branched silica network [88].

Other important sol-gel synthesis effects include H_2O:Si ratio. Condensation reactions are inhibited by preparing sols with low H_2O:Si ratio [93], which leads to weakly branched polymeric sols system and therefore forming materials with micropores of molecular dimension. Silica becomes extremely microporous under low pH and low H_2O:silica ratios [89] because hydrolysis reaction is slow, hence, the propensity to form shorter and weakly branched structure is much greater under this condition. Nevertheless, the ability of the polymers to pack and rearrange while gel shrinkage occurs at the drying stage is also very important in the final structural properties of the membrane. For examples, the textural of silica gels could also be controlled by the extent of gel shrinkage and collapse of the gel network. It has been reported that porosity, surface area and pore size could increase monotonically with aging time employed to grow the fractal species prior to film deposition [94].

2.4.3 Silica Hydrostability

A major drawback of silica membranes is that they are not hydrothermally stable due to its hydrophilic surface. It has been reported by many groups that after treatment with steam or low grade heating, both permeance and selectivity of silica membranes showed great degree of reduction [95-100], which hinders their industrial application. The mechanism of material instability is not trivial. Firstly, the H_2O molecules are attracted to the hydrophilic silica surfaces decorated with silanol groups promoting rehydration and recondensation of neighbouring siloxane bonds, which leads to reconstruction of the matrix [101]. Duke et al. [102] proposed that the mobile silica produced by rehydration of siloxane groups during reconstruction prefer to move from the larger pores towards the smaller pores due to a lower surface energy. Thus after recondensation reactions, the smaller pores are blocked while larger pores are widened, leading to a loss in membrane performance (lower salt rejection) as reported by Duke and co-workers for wet gas streams.

Several strategies have been employed and reported to improve the hydrothermal stability of silica

membranes with various degree of success. In carbon templating method [103-105], organic precursors or surfactant were employed to introduce carbon templates into the silica matrix. Organic precursors, which including terminal alkyl groups, such as $\equiv$Si–CH_3 or organic bridges, such as Si–CH_2–CH_2–Si in their structure, can offer increased hydrophobicity to the surface of the matrix. As a result, water adsorbed on the surface is reduced and thus restructuring of the silica matrix is minimised. Contrary to the strategies of organosilica precursors, carbon templating by surfactant incorporation of non-covalently bonded in the silica matrix has also been reported [106]. Surfactant templates were introduced during the sol-gel process and then calcined under vacuum or inert conditions to preserve the carbon remains in the silica matrix, which can limit the rehydration and recondensation reaction of siloxane bonds and consequently increase their hydrothermal stability [102]. Although the carbon templating is a very effective way, it cannot be applied at high temperatures or in oxidising conditions where chemical changes can occur in the carbon moieties in the matrix [107, 108].

Metal doping is another method to improve the hydrothermal stability of silica membranes. In this method, metal can be introduced into silica matrix by packing transition metals, such as Ni [109], Co [110-116] and Nb [117-120] in the silica matrix or by adding another ceramic component, such as Ti, Al and Zr to form mixed-matrix oxides [121-123]. It has been reported that the improvement in hydrothermal stability by combining with other ceramics (such as Zr and Ti) is due to the formation of Si–O–M bonds, which are less susceptible to hydrolysis [123, 124]. On the other hand, the improvement in the stability by transition metals is believed to be the result of a reinforcing effect induced by metals or metal oxides particles encapsulated in the silica network, for example, in the case of Ni/NiO nanoparticles [109]. The downside of using this method is the possibility of metal leaching into the permeate water and the use of expensive metal as a starting material.

A further strategy is to change the silica precursor. One example is ES40, an oligomer of ethyl polysilicate from partially pre-hydrolysed TEOS as shown in Figure 2.3. ES40 is composed of a mixture of linear, branched and cyclic ethyl polysilicate and has five silicon atoms in average thus can produce 40 wt% SiO_2 after sol-gel process [125, 126]. It is manufactured from industrial alcohol containing water, while TEOS is manufactured using absolute alcohol and the silica content is only 28 wt% [127]. Therefore, ES40 is more favorable in industrial applications due to its lower price and higher silica content compared to TEOS, and it has been investigated by many groups [125-130]. Mrowiec-Białon and coworkers used ES40 instead of TEOS in the synthesis of heteropolyacid-silica composite catalysts and produced a preferable structure with larger surface areas and pore volume than their TEOS counterparts [131]. The presence of larger porosity in the

case of ES40 can be explained by the fact that, due to the greater degree of random crosslinking between the comparatively larger precursor molecules, there is more steric hindrance effect in the ES40-derived sol-gel product and thus prevented further densification during the thermal process. As a result, a more open silica network is formed. In another work, ES40 xerogels and aerogels were analysed by ^{29}Si NMR and small-angle X-ray scattering method, showing a high concentration of Q^3 and Q^4 species indicating a further degree of crosslinking and siloxane bridges [132]. In these reports, the reduction of silanol formation provides research opportunities to improve the hydrostability of silica membranes.
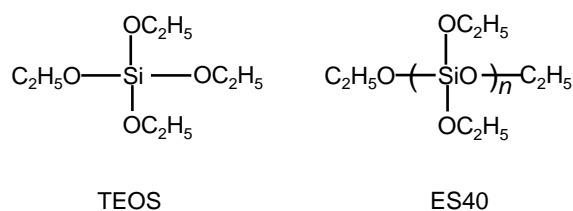
Figure 2.3 Chemical structures of TEOS and the ES40.

2.5 Silica membranes

2.5.1 Asymmetric membranes

Asymmetric membranes are prepared based on the principle of stacking smaller colloids (γ-alumina) on top of larger colloids (α-alumina), a membrane's support. As shown in Figure 2.4, this preparation method produces layers in a way that its pore size is reduced from the bottom to the top layer, thus reducing flux resistance of diffusing molecules due to its large pores while providing integrity to the microporous thin-films [133]. Silica membranes are generally prepared as asymmetric membranes, which is generally composed of a thicker porous support, interlayers and top thin-film silica. The porous support is required to provide the mechanical stability and integrity to the microporous thin films [79]. The support should have the following three characters: (i) small pore size, (ii) low surface roughness, and (iii) low void defect concentration. The small pore sizes are required to avoid infiltration of the microporous ceramic into the support pores, thus minimizing the effective thickness of the microporous membrane layer [82]. This ensures the formation of a thin uniform microporous ceramic layer. In the case of large pores and voids, when they are emptied by evaporation by the coating of silica thin-films, the wall between adjoining pores is

subjected to uneven stress that can cause cracking [93]. Micro-cracks are serious membrane surface defects which tend to render membranes ineffective in separation processes.
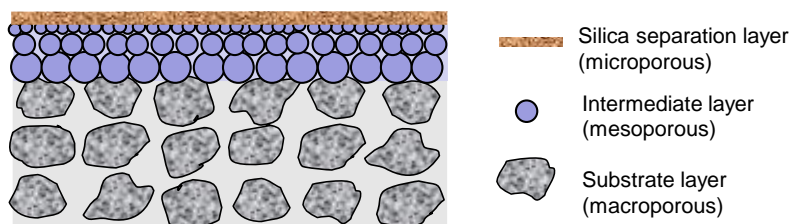
Figure 2.4 Schematic of a silica asymmetric membrane.

Alumina supports are most suitable for silica membrane preparation [134]. The problem here is that the pore size of α-alumina substrates can be quite large; up to 0.5 μm. These pores are too large for the coating of thin-film silica films, which are generally < 55 nm in thickness for each layer [115]. Therefore, substrates do not have ideal surfaces for silica thin-film deposition, thus requiring interlayers, which are traditionally prepared with γ-alumina. The role of the interlayer is to provide a smooth surface with smaller pores and homogeneous pore size distribution. This approach is known to reduce defects in the final silica membranes. Further, silica membranes are prepared with several thin-film layers to cover any minor defect that may occur during the deposition of each silica layer. Therefore, only a multi-layered system can provide a substrate which is sufficiently smooth and flawless to serve as a support on which an almost defect free microporous membrane can be made [135].

Recently, Elma and co-workers [70] reported for the first time the production of interlayer-free silica membranes using TEOS as a silica precursor. This was only possible by incorporating tri-block copolymers in the silica sol-gel, which allowed for the controlled depth penetration of the sol into the porous substrate followed by carbonization treatment to form functional carbon silica membranes. In a similar interlayer-free recent development, Liu et al. [136] modified the TEOS sol-gel synthesis by adding larger silica colloids or 'seeds' to a sol-gel solution which prevented the infiltration of the sol-gel into porous substrates. In these works, a clear advantage of interlayer-free technique is the reduction of membrane fabrication time and costs. Since, there are only two papers dealing with interlayer-free membranes in the literature, this is a research and knowledge gap that is in need to be addressed.

2.5.2 Membrane preparation

Silica membranes are generally prepared using chemical vapour deposition (CVD) or the dip coating methods. Although delivering high quality silica films, CVD has been limited to small surface areas and technically challenging to scale up. The dip coating is the most common method used to deposit microporous layer on a porous support. It is a technically simple and easy coating method, though requiring a significant fundamental understanding of the sol-gel and coating parameters. In this method the support substrate is vertically dipped into a solution and withdrawn without creating surface tears or non-uniform films [79, 82, 84, 90]. The thickness of the layer formed is controlled by manipulating dipping time, withdrawal speed and the sol viscosity [137-140].

There are several models describing the formation of thin films, though the most discussed model of predicted behaviour in silica sol-gel film formation was proposed by Brinker et al. [137]. In this model as schematically shown in Figure 2.5, the concentration of the deposited film increases 18-36 folds due to evaporation. Consequently, this causes the precursors to come into close proximity with each other resulting in closer aggregation, then gelation and drying with significant reorganisation of the film matrix. During this process, chemical reaction rates increase considerably until gelation occurs and the film matrix continues to evolve during drying, aging and thermal treatment. The evaporation process is almost instantaneous due the nano dimensions of the thin film. Subsequently, the dip coated supports are usually dried under controlled conditions, first to evaporate any solvent remaining in the pores of the layer formed and the support layer, and then calcined at the required temperature.
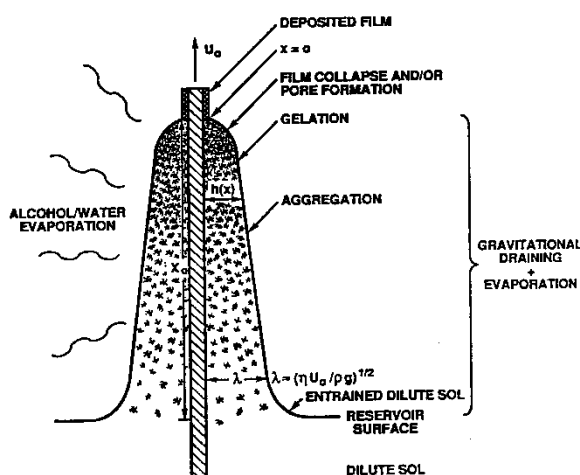
Figure 2.5 Schematic of the steady state sol gel dip coating process [137].

The calcination method that is generally reported in literature for silica membranes involves increasing the temperature slowly from room temperature up to 600 or 650 ℃, maintaining at the high temperature for 1 to 4 hours (dwell-time), and then reducing to room temperature. The ramping and cooling down rates are generally between 0.5 to 1 ℃ min^{-1}. This is known as conventional thermal processing (CTP), which has been extensively used for the preparation of silica derived membranes regardless of the research applications [51, 64, 69, 119, 136, 141]. CTP technique uses very slow ramping and cooling down rates as rapid changes in temperature may cause thermal stresses, thus resulting in the undesirable effect of cracking films during the calcination method. As membranes generally have 2 interlayers, and 4 to 6 silica layers, where each layer is dip-coated and calcined each time, CTP derived silica membranes may take from 10 to 14 days to prepare. This is seen as a major bottleneck for manufacturing of silica membranes because of adding several processing stages and increasing processing costs.

In 2010, Schillo et al. [142] reported for the first time a rapid thermal processing (RTP) technique using tungsten-halogen lamps with heating rates of > 100 ℃ s^{-1}. The RTP was applied for the fabrication of thin γ-alumina membrane layers and did not induce layer cracking. In 2012, Kappert et al. [143] also reported success for TEOS derived silica membranes using rapid heating rates whereby the coated membrane was either placed directly into a preheated furnace or was placed on a hot plate. Yet, despite these promising results, CTP still dominates the research landscape and significant work is still required to establish RTP as a credible alternative synthesis route [144]. In these initial studies, small scale flat membrane geometries to ensure homogenous heating rates was used whilst scale up production was perceived as technically challenging.

The first report on scale up RTP silica membranes was published in 2013 by Wang et al. [144]. The authors prepared RTP silica derived membranes doped with cobalt oxide in tubular geometries, which was achieved by changing the silica precursor from TEOS to ES40. The first RTP report was a hybrid RTP couple with intermittent CTP technique, where membranes were produced in 2 days on top of interlayer supports. Subsequent work by the same authors published in the same area in 2014 [145] has shown improvements using ES40 silica sol-gel via RTP only. Both of these RTP studies reported that the integrity of the silica thin film was attributed to the robustness of ES40-derived matrices, and thus was able to achieve high quality membranes with good gas separation efficiency. Despite the supports used to prepare the membranes in these works contained γ–alumina interlayers, the studies not only demonstrated the versatility of RTP techniques but also the scale-up potential of the membrane processing technology. This is another research area where development

in the RTP technology is highly required to further bridge the knowledge gaps in the literature for industrial deployment.

2.6 Summary

Water scarcity is a major global problem which is driving research and development for desalination technology. The outdated thermal technologies are now loosing desalination market to the new membrane technology spearheaded by RO membranes. Less conventional membrane technologies are now gathering pace as evidenced by improvements in FO and MD/PV technologies. FO still requires further downstream processing to separate water from sugars or other draw agents, hence is not as promising as PV for desalination. PV membranes can be either polymeric or inorganic, whilst the former does not offer significant improvements. Inorganic membranes reported thus far are mainly silica and zeolite membranes, or hybrid silica with carbon or metal oxides. The water fluxes of zeolite membranes are still too low for any desalination application. However, PV silica derived membranes have been improving with water fluxes increasing by one order of magnitude in the last 10 years. This is an area that offers significant improvements for further development, and thus presents a research gap in the literature. It is expected that novel silica structures, or silica membrane preparation processes can open an opportunity of innovation and research gains.

Lately, there have been two very recent developments in silica membranes, namely: (i) rapid thermal processing (RTP) and (ii) interlayer-free silica membranes. Silica derived membranes are generally prepared via a conventional thermal processing (CTP), where the calcination process follows a very slow ramping and cooling rates (≤ 1 °C min^{-1}) to avoid thermal stress, which leads to membrane defects and thus render the membranes ineffective in separation processes. In terms of silica membranes for separation processes, there are only three papers reporting the use of RTP method in literature, where the silica films were coated on supports containing interlayers. The RTP method was only possible by replacing TEOS with ES40 (with cobalt oxide doping) as the silica precursor. A major advantage of the RTP method is the reduction of silica membrane fabrication time, from 10-14 days to less than 1 day. Likewise, there are only two papers interlayer-free silica membranes using TEOS and cobalt oxide or triblock copolymers. Hence, another gap in knowledge is the production of interlayer-free silica membranes using the RTP method, which could significantly lower the production time to a few hours only.

ES40 is a better silica precursor for the RTP method due to its partially-condensed silica backbone chains, thus much stronger to cope with the thermal stresses than the TEOS. Based on the growing interest on ES40-derived xerogels and composite membranes, it opens up a new research avenue into the investigation in the synthesis of robust silica membranes using ES40 via RTP technique. Since this area is still at its infancy and there is currently no work being carried out on the pure ES40 membranes, there is still a vast amount of knowledge required to be gained and understood on ES40 sol-gel methods. Hence, the study of structure-property-performance relationship of ES40-derived xerogels and membranes is novel with enormous potentials in tailoring and improving the properties of membranes for desalination applications. Therefore, it is postulated that interlayer-free silica membranes with high desalination performance can be prepared by the RTP method using ES40 as precursor.

Reference

[1] M. Soltanieh, W.N. Gill, Review of reverse osmosis membranes and transport models, Chemical Engineering Communications, 12 (1981) 279-363.

[2] M.G. Buonomenna, Membrane processes for a sustainable industrial growth, RSC Adv., 3 (2013) 5694-5740.

[3] L.F. Greenlee, D.F. Lawler, B.D. Freeman, B. Marrot, P. Moulin, Reverse osmosis desalination: Water sources, technology, and today's challenges, Water Res., 43 (2009) 2317-2348.

[4] R. Semiat, Energy Issues in Desalination Processes, Environ. Sci. Technol., 42 (2008) 8193-8201.

[5] P. Liu, B. Gao, H.K. Shon, D. Ma, H. Rong, P. Zhao, S. Zhao, Q. Yue, Q. Li, Water flux behavior of blended solutions of ammonium bicarbonate mixed with eight salts respectively as draw solutions in forward osmosis, Desalination, 353 (2014) 39-47.

[6] J.R. McCutcheon, R.L. McGinnis, M. Elimelech, Desalination by ammonia-carbon dioxide forward osmosis: Influence of draw and feed solution concentrations on process performance, J. Membr. Sci., 278 (2006) 114-123.

[7] L. Liu, M. Wang, D. Wang, C. Gao, Current Patents of Forward Osmosis Membrane Process, Recent Patents on Chemical Engineering, 2 (2009) 76-82.

[8] A. Achilli, T.Y. Cath, A.E. Childress, Selection of inorganic-based draw solutions for forward osmosis applications, J. Membr. Sci., 364 (2010) 233-241.

[9] N. Akther, A. Sodiq, A. Giwa, S. Daer, H.A. Arafat, S.W. Hasan, Recent advancements in forward osmosis desalination: A review, Chem Eng J, 281 (2015) 502-522.

[10] M. Qasim, N.A. Darwish, S. Sarp, N. Hilal, Water desalination by forward (direct) osmosis phenomenon: A comprehensive review, Desalination, 374 (2015) 47-69.

[11] A. Subramani, J.G. Jacangelo, Emerging desalination technologies for water treatment: A critical review, Water Res., 75 (2015) 164-187.

[12] A.M. Alklaibi, N. Lior, Membrane-distillation desalination: Status and potential, Desalination, 171 (2005) 111-131.

[13] M. Khayet, Membranes and theoretical modeling of membrane distillation: A review, Adv. Colloid Interface Sci., 164 (2011) 56-88.

[14] M. Tomaszewska, Membrane Distillation - Examples of Applications in Technology and Environmental Protection, Polish J. Environ. Studies, 9 (2000) 27-36.

[15] A. Alkhudhiri, N. Darwish, N. Hilal, Membrane distillation: A comprehensive review, Desalination, 287 (2012) 2-18.

[16] M.C. Duke, J. O'Brien-Abraham, N. Milne, B. Zhu, J.Y.S. Lin, J.C. Diniz da Costa, Seawater desalination performance of MFI type membranes made by secondary growth, Sep. Purif. Technol, 68 (2009) 343-350.

[17] K.W. Lawson, D.R. Lloyd, Membrane distillation, J. Membr. Sci., 124 (1997) 1-25.

[18] D.M. Warsinger, J. Swarninathan, E. Guillen-Burrieza, H.A. Arafat, J.H. Lienhard, Scaling and fouling in membrane distillation for desalination applications: A review, Desalination, 356 (2015) 294-313.

[19] Y.D. Kim, K. Thu, N. Ghaffour, K. Choon Ng, Performance investigation of a solar-assisted direct contact membrane distillation system, J. Membr. Sci., 427 (2013) 345-364.

[20] B. Bolto, M. Hoang, Z. Xie, A review of membrane selection for the dehydration of aqueous ethanol by pervaporation, Chemical Engineering and Processing: Process Intensification, 50 (2011) 227-235.

[21] S. Daer, J. Kharraz, A. Giwa, S.W. Hasan, Recent applications of nanomaterials in water desalination: A critical review and future opportunities, Desalination, 367 (2015) 37-48.

[22] Y.P. Kuznetsov, E.V. Kruchinina, Y.G. Baklagina, A.K. Khripunov, O.A. Tulupova, Deep desalination of water by evaporation through polymeric membranes, Russ J Appl Chem+, 80 (2007) 790-798.

[23] J.T. Duan, E. Litwiller, I. Pinnau, Preparation and water desalination properties of POSS-polyamide nanocomposite reverse osmosis membranes, J. Membr. Sci., 473 (2015) 157-164.

[24] S.T.V. Sim, W.B. Krantz, T.H. Chong, A.G. Fane, Online monitor for the reverse osmosis spiral wound module - Development of the canary cell, Desalination, 368 (2015) 48-59.

[25] A. Subramani, J.G. Jacangelo, Treatment technologies for reverse osmosis concentrate volume minimization: A review, Sep. Purif. Technol, 122 (2014) 472-489.

[26] L. Zhao, W.S.W. Ho, Novel reverse osmosis membranes incorporated with a hydrophilic additive for seawater desalination, J. Membr. Sci., 455 (2014) 44-54.

[27] G.L. Jadav, P.S. Singh, Synthesis of novel silica-polyamide nanocomposite membrane with enhanced properties, J. Membr. Sci., 328 (2009) 257-267.

[28] R. Xu, J. Wang, M. Kanezashi, T. Yoshioka, T. Tsuru, Development of robust organosilica membranes for reverse osmosis, Langmuir, 27 (2011) 13996-13999.

[29] J. Yin, E.S. Kim, J. Yang, B.L. Deng, Fabrication of a novel thin-film nanocomposite (TFN) membrane containing MCM-41 silica nanoparticles (NPs) for water purification, J. Membr. Sci., 423 (2012) 238-246.

[30] M.R. Bao, G.R. Zhu, L. Wang, M. Wang, C.J. Gao, Preparation of monodispersed spherical mesoporous nanosilica-polyamide thin film composite reverse osmosis membranes via interfacial polymerization, Desalination, 309 (2013) 261-266.

[31] H. Huang, X.Y. Qu, X.S. Ji, X. Gao, L. Zhang, H.L. Chen, L. Hou, Acid and multivalent ion resistance of thin film nanocomposite RO membranes loaded with silicalite-1 nanozeolites, J Mater Chem A, 1 (2013) 11343-11349.

[32] R. Xu, J. Wang, M. Kanezashi, T. Yoshioka, T. Tsuru, Reverse osmosis performance of organosilica membranes and comparison with the pervaporation and gas permeation properties, AIChE Journal, 59 (2013) 1298-1307.

[33] B. Zhu, Z. Hong, N. Milne, C.M. Doherty, L.D. Zou, Y.S. Lin, A.J. Hill, X.H. Gu, M. Duke, Desalination of seawater ion complexes by MFI-type zeolite membranes: Temperature and long term stability, J. Membr. Sci., 453 (2014) 126-135.

[34] A. Peyki, A. Rahimpour, M. Jahanshahi, Preparation and characterization of thin film composite reverse osmosis membranes incorporated with hydrophilic SiO_2 nanoparticles, Desalination, 368 (2015) 152-158.

[35] X.W. Zhang, Z.Y. Ning, D.K. Wang, J.C.D. da Costa, A novel ethanol dehydration process by forward osmosis, Chem Eng J, 232 (2013) 397-404.

[36] H.M. Zhang, Y.J. Ma, T. Jiang, G.Y. Zhang, F.L. Yang, Influence of activated sludge properties on flux behavior in osmosis membrane bioreactor (OMBR), J. Membr. Sci., 390 (2012) 270-276.

[37] J.S. Zhang, W.L.C. Loong, S.R. Chou, C.Y. Tang, R. Wang, A.G. Fane, Membrane biofouling and scaling in forward osmosis membrane bioreactor, J. Membr. Sci., 403 (2012) 8-14.

[38] K.Y. Wang, T.-S. Chung, J.-J. Qin, Polybenzimidazole (PBI) nanofiltration hollow fiber membranes applied in forward osmosis process, J. Membr. Sci., 300 (2007) 6-12.

[39] K.Y. Wang, Q. Yang, T.-S. Chung, R. Rajagopalan, Enhanced forward osmosis from chemically modified polybenzimidazole (PBI) nanofiltration hollow fiber membranes with a thin wall, Chem Eng Sci, 64 (2009) 1577-1584.

[40] Q. Yang, K.Y. Wang, T.-S. Chung, Dual-Layer Hollow Fibers with Enhanced Flux As Novel Forward Osmosis Membranes for Water Production, Environ Sci Technol, 43 (2009) 2800-2805.

[41] K.Y. Wang, R.C. Ong, T.-S. Chung, Double-Skinned Forward Osmosis Membranes for Reducing Internal Concentration Polarization within the Porous Sublayer, Ind Eng Chem Res, 49 (2010) 4824-4831.

[42] N. Widjojo, T.-S. Chung, M. Weber, C. Maletzko, V. Warzelhan, The role of sulphonated polymer and macrovoid-free structure in the support layer for thin-film composite (TFC) forward osmosis (FO) membranes, J Membr Sci, 383 (2011) 214-223.

[43] G. Han, T.-S. Chung, M. Toriida, S. Tamai, Thin-film composite forward osmosis membranes with novel hydrophilic supports for desalination, J Membr Sci, 423–424 (2012) 543-555.

[44] S. You, C. Tang, C. Yu, X. Wang, J. Zhang, J. Han, Y. Gan, N. Ren, Forward Osmosis with a Novel Thin-Film Inorganic Membrane, Environ Sci Technol, 47 (2013) 8733-8742.

[45] N. Ma, J. Wei, R.H. Liao, C.Y.Y. Tang, Zeolite-polyamide thin film nanocomposite membranes: Towards enhanced performance for forward osmosis, J Membr Sci, 405 (2012) 149-157.

[46] E.K. Summers, H.A. Arafat, J.H. Lienhard, Energy efficiency comparison of single-stage membrane distillation (MD) desalination cycles in different configurations, Desalination, 290 (2012) 54-66.

[47] D.Y. Hou, J. Wang, D. Qu, Z.K. Luan, X.J. Ren, Fabrication and characterization of hydrophobic PVDF hollow fiber membranes for desalination through direct contact membrane distillation, Sep. Purif. Technol, 69 (2009) 78-86.

[48] K. Gethard, O. Sae-Khow, S. Mitra, Water Desalination Using Carbon-Nanotube-Enhanced Membrane Distillation, ACS Appl Mater Interfaces, 3 (2011) 110-114.

[49] J.A. Prince, V. Anbharasi, T.S. Shanmugasundaram, G. Singh, Preparation and characterization of novel triple layer hydrophilic–hydrophobic composite membrane for desalination using air gap membrane distillation, Sep. Purif. Technol, 118 (2013) 598-603.

[50] H. Zhu, H. Wang, F. Wang, Y. Guo, H. Zhang, J. Chen, Preparation and properties of PTFE hollow fiber membranes for desalination through vacuum membrane distillation, J Membr Sci, 446 (2013) 145-153.

[51] Y.T. Chua, C.X.C. Lin, F. Kleitz, X.S. Zhao, S. Smart, Nanoporous organosilica membrane for water desalination, Chem Commun, 49 (2013) 4534-4536.

[52] H. Abdallah, A.F. Moustafa, A.A. AlAnezi, H.E.M. El-Sayed, Performance of a newly developed titanium oxide nanotubes/polyethersulfone blend membrane for water desalination using vacuum membrane distillation, Desalination, 346 (2014) 30-36.

[53] S. Devi, P. Ray, K. Singh, P.S. Singh, Preparation and characterization of highly micro-porous PVDF membranes for desalination of saline water through vacuum membrane distillation, Desalination, 346 (2014) 9-18.

[54] Z.-Q. Dong, X.-h. Ma, Z.-L. Xu, W.-T. You, F.-b. Li, Superhydrophobic PVDF–PTFE electrospun nanofibrous membranes for desalination by vacuum membrane distillation, Desalination, 347 (2014) 175-183.

[55] J. Kujawa, S. Cerneaux, S. Koter, W. Kujawski, Highly Efficient Hydrophobic Titania Ceramic Membranes for Water Desalination, Acs Appl Mater Interfaces, 6 (2014) 14223-14230.

[56] S. Roy, M. Bhadra, S. Mitra, Enhanced desalination via functionalized carbon nanotube immobilized membrane in direct contact membrane distillation, Sep. Purif. Technol, 136 (2014) 58-65.

[57] L. Lin, H. Geng, Y. An, P. Li, H. Chang, Preparation and properties of PVDF hollow fiber membrane for desalination using air gap membrane distillation, Desalination, 367 (2015) 145-153.

[58] M. Bhadra, S. Roy, S. Mitra, Desalination across a graphene oxide membrane via direct contact membrane distillation, Desalination, 378 (2016) 37-43.

[59] Y.T. Chua, C.X.C. Lin, F. Kleitz, S. Smart, Synthesis of mesoporous carbon-silica nanocomposite water-treatment membranes using a triconstituent co-assembly method, J Mater Chem A, 3 (2015) 10480-10491.

[60] A. Rastegarpanah, H.R. Mortaheb, Surface treatment of polyethersulfone membranes for applying in desalination by direct contact membrane distillation, Desalination, 377 (2016) 99-107.

[61] M.C. Duke, S. Mee, J.C.D. da Costa, Performance of porous inorganic membranes in non-osmotic desalination, Water Res, 41 (2007) 3998-4004.

[62] S. Wijaya, M.C. Duke, J.C. Diniz da Costa, Carbonised template silica membranes for desalination, Desalination, 236 (2009) 291-298.

[63] B.P. Ladewig, Y.H. Tan, C.X.C. Lin, K. Ladewig, J.C.D. da Costa, S. Smart, Preparation, Characterization and Performance of Templated Silica Membranes in Non-Osmotic Desalination, Materials, 4 (2011) 845-856.

[64] C.X.C. Lin, L.P. Ding, S. Smart, J.C. Diniz da Costa, Cobalt oxide silica membranes for desalination, J Colloid Interface Sci, 368 (2012) 70-76.

[65] M. Drobek, C. Yacou, J. Motuzas, A. Julbe, L. Ding, J.C. Diniz da Costa, Long term pervaporation desalination of tubular MFI zeolite membranes, J Membr Sci, 415–416 (2012) 816-823.

[66] P. Swenson, B. Tanchuk, A. Gupta, W. An, S.M. Kuznicki, Pervaporative desalination of water using natural zeolite membranes, Desalination, 285 (2012) 68-72.

[67] W. An, X. Zhou, X. Liu, P.W. Chai, T. Kuznicki, S.M. Kuznicki, Natural zeolite clinoptilolite-phosphate composite Membranes for water desalination by pervaporation, J Membr Sci, 470 (2014) 431-438.

[68] B. Liang, K. Pan, L. Li, E.P. Giannelis, B. Cao, High performance hydrophilic pervaporation composite membranes for water desalination, Desalination, 347 (2014) 199-206.

[69] M. Elma, D.K. Wang, C. Yacou, J. Motuzas, J.C. Diniz da Costa, High performance interlayer-free mesoporous cobalt oxide silica membranes for desalination applications, Desalination, 365 (2015) 308-315.

[70] M. Elma, D.K. Wang, C. Yacou, J.C. Diniz da Costa, Interlayer-free P123 carbonised template silica membranes for desalination with reduced salt concentration polarisation, J. Membr. Sci., 475 (2015) 376-383.

[71] M. Naim, M. Elewa, A. El-Shafei, A. Moneer, Desalination of simulated seawater by purge-air pervaporation using an innovative fabricated membrane, Water Sci. Technol., 72 (2015) 785-793.

[72] P.S. SINGH, S.G. CHAUDHRI, A.M. KANSARA, W. SCHWIEGER, T. SELVAM, S. REUSS, V.K. ASWAL, Cetyltrimethylammonium bromide–silica membrane for seawater desalination through pervaporation, Bull. Mater. Sci., 38 (2015) 565-572.

[73] C. Yacou, S. Smart, J.C. Diniz da Costa, Mesoporous TiO2 based membranes for water desalination and brine processing, Sep. Purif. Technol., 147 (2015) 166-171.

[74] F.U. Nigiz, N.D. Hilmioglu, Pervaporative desalination of seawater by using composite and blended poly(vinyl alcohol) membranes, Desalin and Water Treat, 57 (2016) 4749-4755.

[75] A.F.M. Leenaars, K. Keizer, A.J. Burggraaf, The preparation and characterization of alumina membranes with ultra-fine pores, J Mater Sci, 19 (1984) 1077-1088.

[76] M. Asaeda, L.D. Du, Separation of alcohol water gaseous-mixtures by thin ceramic membrane, Journal of Chemical Engineering of Japan, 19 (1986) 72-77.

[77] K. Keizer, R.J.R. Uhlhorn, R.J. Vanvuren, A.J. Burggraaf, Gas separation mechanisms in microporous modified gamma-Al_2O_3 membranes, J. Membr. Sci., 39 (1988) 285-300.

[78] R.J.R. Uhlhorn, M.H.B.J. Huis In't Veld, K. Keizer, A.J. Burggraaf, High permselectivities of microporous silica-modified γ-alumina membranes, J Mater Sci Lett, 8 (1989) 1135-1138.

[79] R.S.A. Delange, J.H.A. Hekkink, K. Keizer, A.J. Burggraaf, Formation and Characterization of Supported Microporous Ceramic Membranes Prepared by Sol-Gel Modification Techniques, J. Membr. Sci., 99 (1995) 57-75.

[80] B.N. Nair, T. Yamaguchi, T. Okubo, H. Suematsu, K. Keizer, S.I. Nakao, Sol-gel synthesis of molecular sieving silica membranes, J. Membr. Sci., 135 (1997) 237-243.

[81] C.J. Brinker, N.K. Raman, R. Sehgal, S.S. Prakash, L. Delattre, Sol-gel strategies for controlled porosity ceramic materials: Thin film and bulk, Mater Res Soc Symp P, 368 (1995) 329-343.

[82] Y.S. Lin, I. Kumakiri, B.N. Nair, H. Alsyouri, Microporous inorganic membranes, Sep Purif Rev, 31 (2002) 229-379.

[83] J.C.D. da Costa, G.Q. Lu, V. Rudolph, Y.S. Lin, Novel molecular sieve silica (MSS) membranes: characterisation and permeation of single-step and two-step sol-gel membranes, J. Membr. Sci., 198 (2002) 9-21.

[84] R.S.A. Delange, J.H.A. Hekkink, K. Keizer, A.J. Burggraaf, Permeation and Separation Studies on Microporous Sol-Gel Modified Ceramic Membranes, Microporous Mater, 4 (1995) 169-186.

[85] C.J. Brinker, G.W. Scherer, Sol-gel science: the physics and chemistry of sol-gel processing, Academic Press, Boston, 1990.

[86] C.J. Brinker, Hydrolysis and Condensation of Silicates - Effects on Structure, J Non-Cryst Solids, 100 (1988) 31-50.

[87] Y.S. Lin, I. Kumakiri, B.N. Nair, H. Alsyouri, Microporous inorganic membranes, Separ Purif Method, 31 (2002) 229-379.

[88] U. David, Robust Microporous Cobalt Oxide Doped Silica Membranes for High Temperature Industrial Coal Gasification Syngas Separation, in, 2011.

[89] K. Akamatsu, M. Nakane, T. Sugawara, T. Hattori, S. Nakao, Development of a membrane reactor for decomposing hydrogen sulfide into hydrogen using a high-performance amorphous silica membrane, J Membr Sci, 325 (2008) 16-19.

[90] R.S.A. Delange, K. Keizer, A.J. Burggraaf, Analysis and Theory of Gas-Transport in Microporous Sol-Gel Derived Ceramic Membranes, J Membr Sci, 104 (1995) 81-100.

[91] B.N. Nair, K. Keizer, H. Suematsu, Y. Suma, N. Kaneko, S. Ono, T. Okubo, S.I. Nakao, Synthesis of gas and vapor molecular sieving silica membranes and analysis of pore size and connectivity, Langmuir, 16 (2000) 4558-4562.

[92] R.J.R. Uhlhorn, K. Keizer, A.J. Burggraaf, Gas-Transport and Separation with Ceramic Membranes .2. Synthesis and Separation Properties of Microporous Membranes, J Membr Sci, 66 (1992) 271-287.

[93] J.C. Diniz Da Costa, Synthesis and characterisation of molecular sieve silica (MSS) membranes, in, 2000.

[94] C.J. Brinker, A.J. Hurd, P.R. Schunk, G.C. Frye, C.S. Ashley, Review of sol-gel thin-film formation, J Non-Cryst Solids, 147 (1992) 424-436.

[95] G.R. Gallaher, P.K.T. Liu, Characterization of Ceramic Membranes .1. Thermal and Hydrothermal Stabilities of Commercial 40 Angstrom Membranes, J Membr Sci, 92 (1994) 29-44.

[96] G.R. Gavalas, C.E. Megiris, S.W. Nam, Deposition of H2 Permselective SiO_2 Films, Chem Engin Sci, 44 (1989) 1829-1835.

[97] H. Imai, H. Morimoto, A. Tominaga, H. Hirashima, Structural changes in sol-gel derived SiO2 and TiO_2 films by exposure to water vapor, J Sol-Gel Sci Techn, 10 (1997) 45-54.

[98] R. Leboda, E. Mendyk, A. Gierak, V.A. Tertykh, Hydrothermal modification of silica gels (xerogels) .1. Effect of treatment temperature on their porous structure, Colloid Surface A, 105 (1995) 181-189.

[99] R. Leboda, E. Mendyk, A. Gierak, V.A. Tertykh, Hydrothermal modification of silica gels (xerogels) .2. Effect of the duration of treatment on their porous structure, Colloid Surface A, 105 (1995) 191-197.

[100] E. Mendyk, R. Leboda, A. Gierak, Properties of Hydrothermally Modified Silica-Gels - Effect of the Parameters of Porous Structure on the Course of the Modification Process, Mater Chem Phys, 20 (1988) 87-97.

[101] The chemistry of silica : solubility, polymerization, colloid and surface properties, and biochemistry / Ralph K. Iler, Wiley, New York, 1979.

[102] M.C. Duke, J.C.D. da Costa, D.D. Do, P.G. Gray, G.Q. Lu, Hydrothermally robust molecular sieve silica for wet gas separation, Adv Funct Mater, 16 (2006) 1215-1220.

[103] R.M. de Vos, W.F. Maier, H. Verweij, Hydrophobic silica membranes for gas separation, J Membr Sci, 158 (1999) 277-288.

[104] Q. Wei, Y.L. Wang, Z.R. Nie, C.X. Yu, Q.Y. Li, J.X. Zou, C.J. Li, Facile synthesis of hydrophobic microporous silica membranes and their resistance to humid atmosphere, Micropor Mesopor Mat, 111 (2008) 97-103.

[105] Y.F. Lu, R. Ganguli, C.A. Drewien, M.T. Anderson, C.J. Brinker, W.L. Gong, Y.X. Guo, H. Soyez, B. Dunn, M.H. Huang, J.I. Zink, Continuous formation of supported cubic and hexagonal mesoporous films by sol gel dip-coating, Nature, 389 (1997) 364-368.

[106] C.Y. Tsai, S.Y. Tam, Y.F. Lu, C.J. Brinker, Dual-layer asymmetric microporous silica membranes, J Membr Sci, 169 (2000) 255-268.

[107] M. Kanezashi, K. Yada, T. Yoshioka, T. Tsuru, Organic-inorganic hybrid silica membranes with controlled silica network size: Preparation and gas permeation characteristics, J Membr Sci, 348 (2010) 310-318.

[108] M. Kanezashi, K. Yada, T. Yoshioka, T. Tsuru, Design of Silica Networks for Development of Highly Permeable Hydrogen Separation Membranes with Hydrothermal Stability, J Am Chem Soc, 131 (2009) 414-+.

[109] Y.H. Ikuhara, H. Mori, T. Saito, Y. Iwamoto, High-temperature hydrogen adsorption properties of precursor-derived nickel nanoparticle-dispersed amorphous silica, J Am Ceram Soc, 90 (2007) 546-552.

[110] S. Battersby, M.C. Duke, S.M. Liu, V. Rudolph, J.C.D. da Costa, Metal doped silica membrane reactor: Operational effects of reaction and permeation for the water gas shift reaction, J Membr Sci, 316 (2008) 46-52.

[111] S. Battersby, B.P. Ladewig, M. Duke, V. Rudolph, J.C.D. da Costa, Membrane Reactor Modelling, Validation and Simulation for the WGS Reaction using Metal Doped Silica Membranes, Asia-Pac J Chem Eng, 5 (2010) 83-92.

[112] S. Battersby, S. Smart, B. Ladewig, S.M. Liu, M.C. Duke, V. Rudolph, J.C.D. da Costa, Hydrothermal stability of cobalt silica membranes in a water gas shift membrane reactor, Sep Purif Technol, 66 (2009) 299-305.

[113] S. Battersby, T. Tasaki, S. Smart, B. Ladewig, S.M. Liu, M.C. Duke, V. Rudolph, J.C.D. da Costa, Performance of cobalt silica membranes in gas mixture separation, J Membr Sci, 329 (2009) 91-98.

[114] R. Igi, T. Yoshioka, Y.H. Ikuhara, Y. Iwamoto, T. Tsuru, Characterization of co-doped silica for improved hydrothermal stability and application to hydrogen separation membranes at high temperatures, J Am Ceram Soc, 91 (2008) 2975-2981.

[115] D. Uhlmann, S.M. Liu, B.P. Ladewig, J.C.D. da Costa, Cobalt-doped silica membranes for gas separation, J Membr Sci, 326 (2009) 316-321.

[116] S. Fujisaki, K. Hataya, T. Saito, S. Arai, Y. Iwamoto, K. Kuroda, Nanostructural characterizations of hydrogen-permselective Si-Co-O membranes by transmission electron microscopy, J Mater Res, 24 (2009) 372-378.

[117] V. Boffa, D.H.A. Blank, J.E. ten Elshof, Hydrothermal stability of microporous silica and niobia-silica membranes, J Membr Sci, 319 (2008) 256-263.

[118] V. Boffa, H.L. Castricum, R. Garcia, R. Schmuhl, A.V. Petukhov, D.H.A. Blank, J.E. ten Elshof, Structure and Growth of Polymeric Niobia-Silica Mixed-Oxide Sols for Microporous Molecular Sieving Membranes: A SAXS Study, Chem Mater, 21 (2009) 1822-1828.

[119] V. Boffa, J.E. ten Elshof, R. Garcia, D.H.A. Blank, Microporous niobia-silica membranes: Influence of sol composition and structure on gas transport properties, Micropor Mesopor Mat, 118 (2009) 202-209.

[120] V. Boffa, J.E. ten Elshof, A.V. Petukhov, D.H.A. Blank, Microporous niobia-silica membrane with very low CO_2 permeability, Chemsuschem, 1 (2008) 437-443.

[121] G.P. Fotou, Y.S. Lin, S.E. Pratsinis, Hydrothermal Stability of Pure and Modified Microporous Silica Membranes, J Mater Sci, 30 (1995) 2803-2808.

[122] J. Sekulic, M.W.J. Luiten, J.E. ten Elshof, N.E. Benes, K. Keizer, Microporous silica and doped silica membrane for alcohol dehydration by pervaporation, Desalination, 148 (2002) 19-23.

[123] S. Araki, Y. Kiyohara, S. Imasaka, S. Tanaka, Y. Miyake, Preparation and pervaporation properties of silica-zirconia membranes, Desalination, 266 (2011) 46-50.

[124] Y.F. Gu, P. Hacarlioglu, S.T. Oyama, Hydrothermally stable silica-alumina composite membranes for hydrogen separation, J Membr Sci, 310 (2008) 28-37.

[125] J. Mrowiec-Bialon, A.B. Jarzebski, Fabrication and properties of silica monoliths with ultra large mesopores, Micropor Mesopor Mat, 109 (2008) 429-435.

[126] J. Cihlar, Hydrolysis and Polycondensation of Ethyl Silicates .2. Hydrolysis and Polycondensation of Ets40 (Ethyl Silicate-40), Colloid Surface A, 70 (1993) 253-268.

[127] D.P. Sabde, S.G. Hegde, M.K. Dongare, Synthesis of titanium silicalite-1 using ethyl silicate-40: a new silica source for zeolite synthesis, J Mater Chem, 10 (2000) 1365-1370.

[128] H.D. Cogan, C.A. Setterstrom, Ethyl Silicates, Ind Eng Chem, 39 (1947) 1364-1368.

[129] T.R. Gaydhankar, U.S. Taralkar, R.K. Jha, P.N. Joshi, R. Kumar, Textural/structural, stability and morphological properties of mesostructured silicas (MCM-41 and MCM-48) prepared using different silica sources, Catal Commun, 6 (2005) 361-366.

[130] T.R. Gaydhankar, V. Samuel, R.K. Jha, R. Kumar, P.N. Joshi, Room temperature synthesis of Si-MCM-41 using polymeric version of ethyl silicate as a source of silica, Mater Res Bull, 42 (2007) 1473-1484.

[131] J. Mrowiec-Bialon, W. Turek, A.B. Jarzebski, Preparation of highly active heteropolyacid-silica composite catalysts using the sol-gel method, React Kinet Catal L, 76 (2002) 213-219.

[132] J. Mrowiec-Bialon, A.B. Jarzebski, L. Pajak, Z. Olejniczak, M. Gibas, Preparation and surface properties of low-density gels synthesized using prepolymerized silica precursors, Langmuir, 20 (2004) 10389-10393.

[133] J.C. Diniz da Costa, G.Q. Lu, V. Rudolph, Molecular Sieve Silica (MSS) Membranes in: Encyclopedia of Nanomaterials and Nanotechnology, American Scientific Publishers, California, USA, 5 (2004) 723-741.

[134] A.F.M. Leenaars, A.J. Burggraaf, The Preparation and Characterization of Alumina Membranes with Ultrafine Pores .2. The Formation of Supported Membranes, J Colloid Interface Sci, 105 (1985) 27-40.

[135] B.C. Bonekamp, Preparation of asymmetric ceramic membrane supports by dip-coating in: Fundamentals of inorganic membrane science and technology, eds. A.J. Burggraaf and L. Cot. Elsevier, Amsterdam, the Netherlands, (1996) 141-226.

[136] L. Liu, D.K. Wang, D.L. Martens, S. Smart, J.C.D. da Costa, Interlayer-free microporous cobalt oxide silica membranes via silica seeding sol-gel technique, J Membr Sci, 492 (2015) 1-8.

[137] C.J. Brinker, G.C. Frye, A.J. Hurd, C.S. Ashley, Fundamentals of Sol-Gel Dip Coating, Thin Solid Films, 201 (1991) 97-108.

[138] M. Guglielmi, S. Zenezini, The Thickness of Sol-Gel Silica Coatings Obtained by Dipping, J Non-Cryst Solids, 121 (1990) 303-309.

[139] T. Miki, K. Nishizawa, K. Suzuki, K. Kato, Microstructure control of porous alumina film using aqueous sol containing poly(ethylene glycol), J Electroceram, 21 (2008) 524-527.

[140] I. Strawbridge, P.F. James, The Factors Affecting the Thickness of Sol-Gel Derived Silica Coatings Prepared by Dipping, J Non-Cryst Solids, 86 (1986) 381-393.

[141] D. Uhlmann, S. Smart, J.C.D. da Costa, High temperature steam investigation of cobalt oxide silica membranes for gas separation, Sep Purif Technol, 76 (2010) 171-178.

[142] M.C. Schillo, I.S. Park, W.V. Chiu, H. Verweij, Rapid thermal processing of inorganic membranes, J Membr Sci, 362 (2010) 127-133.

[143] E.J. Kappert, A. Nijmeijer, N.E. Benes, Expeditious calcination of inorganic membranes by an instant temperature increment, Micropor Mesopor Mat, 151 (2012) 211-215.

[144] D.K. Wang, J. Motuzas, J.C.D. da Costa, S. Smart, Rapid thermal processing of tubular cobalt oxide silica membranes, Int J Hydrogen Energ, 38 (2013) 7394-7399.

[145] D.K. Wang, J.C.D. da Costa, S. Smart, Development of rapid thermal processing of tubular cobalt oxide silica membranes for gas separations, J Membr Sci, 456 (2014) 192-201.

3 FUNDAMENTAL INVESTIGATION OF SOL-GEL PROCESS OF ETHYL SILICATE 40

Introduction

This chapter aims to investigate the ethyl silicate 40 (ES40) sol-gel process using water as hydrolyzing agent and ethanol as co-solvent. Both homogeneous and phase-separated sol-gel evolutions were followed by FTIR. The effect of reaction temperature and H_2O/Si ratios on the sol-gel processing and the physico-chemical properties of the produced silica xerogels were systematically studied.

Contribution

It is demonstrated for the first time the fundamental study of the ES40 sol-gel process in both miscible and immiscible regions in the ES40-EtOH-H_2O ternary phase diagram. It was found that hydrolysis and condensation reactions occurred from the interface of the phase-separated system. The degree of sol-gel evolution was evaluated by the relative peak area ratios of silanol to siloxane groups calculated from FTIR spectra, which showed that high temperature promoted ES40 sol-gel process and production of microporous structure whilst mesoporous silica xerogels were obtained when the reaction was carried out at 25 ℃ due to the lower dry stress and cage formation from the oligomer silica precursor ES40. High H_2O/Si ratios encouraged faster sol-gel process and larger porosity of the product, because H_2O is the hydrolyzing agent in the reactions and phase separation induced by high H_2O/Si ratio reduced the proximity of the reactive species, thus facilitating further reactions and formation of lager pores. This work was published in Scientific Report as:

S.N. Wang, D.K. Wang, S. Smart, J.C.D. da Costa, Ternary Phase-Separation Investigation of Sol-Gel Derived Silica from Ethyl Silicate 40, Sci. Rep., 5, 2015, 1-11.

Ternary Phase-Separation Investigation of Sol-Gel Derived Silica from Ethyl Silicate 40

Abstract

A ternary phase-separation investigation of the ethyl silicate 40 (ES40) sol-gel process was conducted using ethanol and water as the solvent and hydrolysing agent, respectively. This oligomeric silica precursor underwent various degrees of phase separation behaviour in solution during the sol-gel reactions as a function of temperature and H_2O/Si ratios. The solution composition within the immiscible region shows that the hydrolysis and condensation reactions of the ES40 phase-separated sol-gel decreased with decreasing reaction temperature. A mesoporous structure was obtained at low temperature due to weak drying forces from slow solvent evaporation on one hand and formation of unreacted ES40 cages in the other. Contrary to dense silica structures obtained from sol-gel reactions in the miscible region, higher microporosity was conferred through a phase-separated sol-gel system by using high H_2O/Si ratios. Silica structural microporosity was easily tuned by changing reactant ratios, thus allowing the most reactive species close proximity. This tailoring process facilitated further condensation reactions and crosslinking of silica chains, which coupled with stiffening of the network, made it more resistant to compression and densification. The larger pores obtained in phase-separated sol-gel system were attributed to the concentration of the reactive sites around the phase-separated interface, which enhanced the condensation and crosslinking. Combined with weaker drying stresses from slower solvent evaporation, this reduced network shrinkage and produced larger pores. Hence, texture properties of the xerogels prepared from phase-separated solutions can also be easily tuned by changing reactant ratios.

3.1 Introduction

Silica porous materials have attracted growing scientific interest due to their unique properties in terms of large surface area, thermal stability and chemical inertness and consequently have found diverse applications in absorption,[1] catalysis,[2] energy[3] and separation applications.[4] The

silica sol-gel method generally comprises of reacting a silica precursor in the presence of solvents and catalysts by the well-established hydrolysis and condensation reactions. Here, the reactant ratios, pH of the solution, reaction temperature, and nature of silica precursor all affect the reaction mechanisms and kinetics [5, 6] and the final xerogel structure. To effectively tailor the porosity of xerogels by the sol-gel method, it is necessary to understand how the reactions influence the porous structure formation, arising from the formation of silanol (Si-OH) groups via hydrolysis and siloxane (Si-O-Si) bridges via the condensation reaction.

The use of Fourier transform infrared spectroscopy (FTIR) is widely used for examining the evolution of the silica frameworks through their functional groups in a sol-gel reaction system,[7-10] and xerogel characterisation.[11-13] However, FTIR analysis of aqueous silica sol-gel is seldom reported. In a few examples, Tejedor-Tejedor et al. monitored the hydrolysis and condensation reactions of tetraethyl orthosilicate (TEOS) under rich water conditions and suggested that the hydrolysis is a first-order reaction.[14] In another work, Jiang et al. investigated the activation energy and Arrhenius factor of the hydrolysis of methyltriethoxysilane under different temperatures.[15] Further, Neville et al. followed the sol-gel process of methyltrimethoxysilane by measuring the peak intensity variation of silanol (Si-OH) groups generated from hydrolysis and siloxane bridges (Si-O-Si) from condensation and in so doing, introduced the silica particle growth mechanism.[16] These studies strongly suggest that FTIR is a strong characterisation tool for assessing the silica sol-gel process.

ES40 is a partially-condensed form of TEOS, with five silicon atoms per molecular on average, thus providing higher silica content but lower solubility in aqueous solutions. ES40 became more attractive in recent years due to higher silica productivity thus making this silica precursor economically desirable for a range of applications. Of particular attention, ES40 xerogels delivered superior thermal stability than analogous TEOS xerogels.[17] Recently, Wang et al. produced an ES40-derived silica/cobalt membrane by rapid thermal processing techniques which showed superior performance as membranes films that otherwise could not be achieved with TEOS.[18] ES40 has also been found to improve the hydrothermal stability of silicas when prepared at high water and low ethanol contents.[19] Considering these desirable aspects, it is important to study the ES40 sol-gel process in order to better tailor materials.

In principle, the preparation of homogeneous solutions is preferable when using the silica sol-gel method, particularly when it involves thin film coating and / or controlling the porous structure. However, in this work we show that, under our testing conditions, ES40 tends to form a heterogeneous two phase system induced by phase separation behaviour. Therefore, this work

investigates the sol-gel process leading to the formation of porous silica, in contrast to previous work with homogeneous ES40 sol-gel leading to extremely microporous or ultimately dense silica. The evolution of the phase-separated ES40 sol-gel method is studied as a function of reaction temperatures and molar ratios of water to ES40 (H_2O/ES40).

3.2 Experimental

ES40 was purchased from Colcoat Co., Japan. Ethanol (EtOH, AR grade) and all the chemicals were used as received. Initially, distilled reverse osmosis (RO) water was mixed with ethanol and 1 M nitric acid (HNO_3) to obtain solution with pH~1. Then ES40 was added to the mixture dropwise under stirring in an ice bath and the molar ratio of the reactants Si (ES40): H_2O: EtOH was kept at 4: 140: 15, hence for this sample, H_2O/Si is 35. After stirring for 10 mins, the solution was kept undisturbed in an open Schott bottle and dried in oven at varying temperatures of 25, 40 or 60 ℃ for 96 h. As soon as stirring ceased, the mixture developed into two phases. The evolution of the sample was investigated by characterising aliquots taken from each phase at varying drying times. A series of samples prepared from different molar ratios of H_2O to Si (35, 22, 11 and 3.5) were also studied.

Fourier transform infrared (FTIR) spectroscopy characterization was performed with a Shimadzu IRAffinity-1 with a Pike MIRacle diamond attenuated total reflectance (ATR) attachment. The analysis was performed over a wavenumber range of 4000–600 cm^{-1}. Background subtraction and peak deconvolution of the spectra were performed using the Fityk program. Samples were analyzed in both the sol-gel and xerogel states. The contribution of ethanol solvent in the sol-gel samples was removed from the FTIR spectra by normalizing against the pure ethanol spectrum using the characteristic peak ~870 cm^{-1} for the ethanol and then followed by background subtraction.[14] To cross-check this procedure, no absorption peaks between 3000 and 2800 cm^{-1} range attributable to the ethoxy groups of ethanol or TEOS precursor were observed after the background subtraction. This means that the contribution of ethoxy groups of the TEOS precursor between 1300 and 900 cm^{-1} vibrational range is also negligible and that the spectra contained only the silica species. After this step, peak fitting analysis between 1300 and 900 cm^{-1} spectral range was performed for all the spectra by using a local baseline and Gaussian peaks with the square of correlation coefficient values ≥0.95. The same number of peaks was used in all the spectral peak fitting. The half width at half maximum (HWHM) was fixed for each peak, while the peak position was allowed to change slightly to realize qualified fitting. The gravimetric analyses of the silica sol-gel solutions were

performed on a Shimadzu thermogravimetric analyzer TGA-50 using air flow rate of 5 mL min^{-1} at room temperature, 40 and 60 ℃ until mass loss was no longer detected. Nitrogen adsorption was conducted at -196 °C on a Micromeritics TriStar 3020 apparatus. Samples were degassed at 200 °C overnight before each measurement. The pore size distributions were determined from adsorption branch of the isotherms using the Density Functional Theory (DFT) model of cylindrical pores with oxide surfaces.

3.3 Results and discussion

Figure 3.1 shows the ternary phase diagram of an ES40–ethanol–water system. The red miscibility line which divides the diagram into miscible and immiscible regions was determined by visual inspection of the miscibility of mixtures. The black boundary line for TEOS is adapted from Brinker and Scherer without modification.[5] It is evident that ES40 exhibited a lower solubility than TEOS in water-ethanol mixtures as seen by the reduced miscible area in Figure 3.1. Such behaviour is manifested by its longer molecular chains of the precursor, as well as the ability to form larger silica particles during the hydrolysis and condensation sol-gel process.[18, 20] Due to these factors, the extent of phase separation of the growing silica species is heightened, and should be carefully monitored.
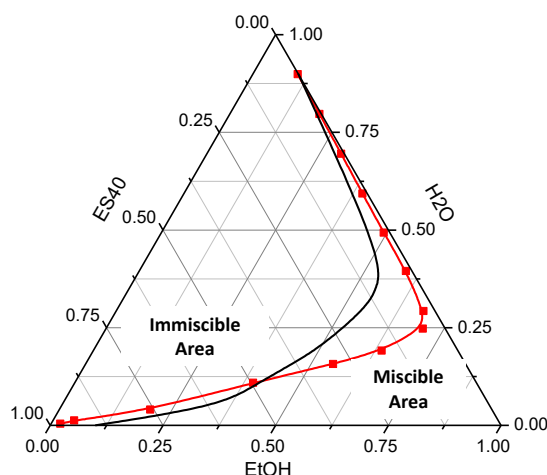
Figure 3.1 Ternary phase diagrams of ES40–ethanol–water (red line) and TEOS–ethanol–water system (black line) at 25 ℃.

The phase-separated sol-gel of ES40 in acidic ethanol-water solutions was characterised by ATR-FTIR. Phase separation was obvious from the beginning of the sol-gel process as shown by the inset photo in Figure 3.2A. The FTIR spectrum (at time = 0) of the cloudy phase on the bottom as indicated on Figure 3.2A is identical with that of pure ES40 (Figure 3.2B), while the clear solution on the top is a mixture of only water and ethanol species.
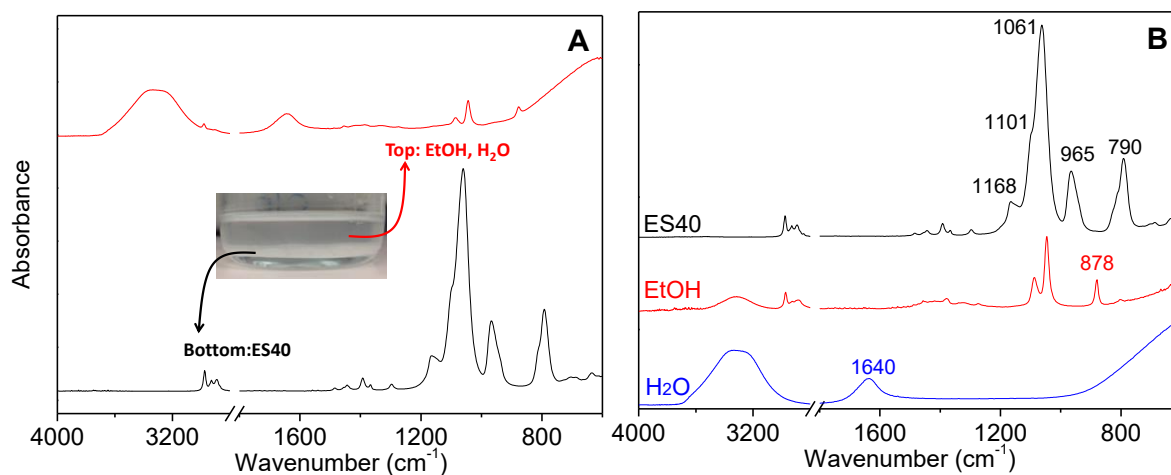
Figure 3.2 FTIR spectra of (A) sol-gel solutions before drying with photo (inset) and (B) pure ES40, ethanol and water.

Table 3.1 Band assignments of the FTIR vibrations of the reactants in Figure 3.2.[21-24]

Wavenumber (cm^{-1})	Vibration mode	Chemicals
~3320	ν(O-H)	water, ethanol, Si-OH
~3000-2800	ν(C-H)	ethanol, Si-OCH$_2$CH$_3$
~1640	δ(H-O-H)	water
~1168	ρ(CH$_3$)	Si-OCH$_2$CH$_3$
~1101, 1061	ν_{as} (C-O)	Si-OCH$_2$CH$_3$
~1086	ν(C-C)/(C-O)	ethanol
~1045	ρ(CH$_3$/CH$_2$)	ethanol
~965	ρ(CH$_3$)	Si-OCH$_2$CH$_3$
~878	ν(C-C)/(C-O)	ethanol
~790	ν(C-O)	Si-OCH$_2$CH$_3$

Table 3.1 summarizes the correlations between the frequencies and vibration modes based on the literature.[21-24] The broad peak observed at around 3320 cm^{-1} is attributed to the O-H stretching vibration of H$_2$O and EtOH. The appearance of this peak is affected by environment, including the neighbouring network and / or hydrogen bonds connected to O-H. The weak bands located in the

region of 3000-2800 cm^{-1} are assigned to C-H stretching vibrations of ethanol and Si-OCH$_2$CH$_3$. A H-O-H deformation band appears exclusively at 1640 cm^{-1} in the pure H$_2$O spectrum, which was used to monitor water in the samples. The peak at 878 cm^{-1} is the characteristic absorption of EtOH, which is assigned to C-C and C-O stretching vibrations. The C-O stretching of the silica precursor is associated with the absorption band at 790 cm^{-1}. Numerous absorption bands appear between 1200 cm^{-1} to 900 cm^{-1}. Besides the C-O/C-C stretching vibration (1086 cm^{-1}) and CH$_3$/CH$_2$ rocking (1045 cm^{-1}) of EtOH, CH$_3$ rocking (1168 and 965 cm^{-1}) and C-O asymmetric stretching (1101 and 1061 cm^{-1}) of silica precursor also exhibit within this range.

Figure 3.3 shows the FTIR spectra of the phase separated sol-gel system at different time intervals during the gelling stage of samples drying at 60 ℃. The appearance of H-O-H deformation band at 1640 cm^{-1} in the top phase (Figure 3.3A) and intermittently from 6 to 24 h in the bottom phase (Figure 3.3B) confirms the existence of water, which could be attributed to the co-solvent or a condensation by-product. After 24 h of gelling, the sol mixture was no longer liquid and only the bottom phase remained as a hard gel. This is consistent with the gradual decreasing C-H stretching vibrations of ethanol and water around 3000-2800 cm^{-1} due to the evaporation of solvents and the by-products of ethanol and water arising from hydrolysis and condensation reactions. This is supported by the characteristic absorption of EtOH at 878 cm^{-1}, as a single peak, which also decreased intensity, corresponding with ethanol evaporation. Therefore, it can be concluded that the presence of ethanol and water species were insignificant after the initial 24 h of gelation during drying.

Another important observation to be made from Figure 3.3 is that most of the absorption bands of silicon-containing sol-gel derived materials are located in the region of 1200 to 900 cm^{-1}. The frequency of CH$_3$ rocking in ES40 alkoxy groups (~965 cm^{-1}) shifted to lower wavenumber (~950 cm^{-1}) in Figure 3.3B and is attributed to the replacement of Si-OCH$_2$CH$_3$ by Si-OH. The intensity of silanol groups at ~950 cm^{-1} increases with reaction time. The shape of this band became wider and increasingly asymmetric, implying that this band should include two constituents as previously reported; one at ~960 cm^{-1} corresponding to silanol and the other one at ~930 cm^{-1} attributed to the deprotonated form (Si-O $^-$).[25] In contrast, the evolution of siloxane bands is less straight-forward in comparison to the silanol bands as it is overlapped by the vibration peaks attributing to ethanol between 1200 and 1000 cm^{-1} as shown in Figure 3.2B. However, it is noticeable that the intensity ratio of the 1085 cm^{-1} peak to the 1045 cm^{-1} peak is not equal to that in the pure ethanol. This ratio increases over time, which is exclusively associated to the more intense absorption of the siloxane groups due to the on-going condensation reactions. These observations agree well with previous reports on silica sol-gel process.[16, 26-28]
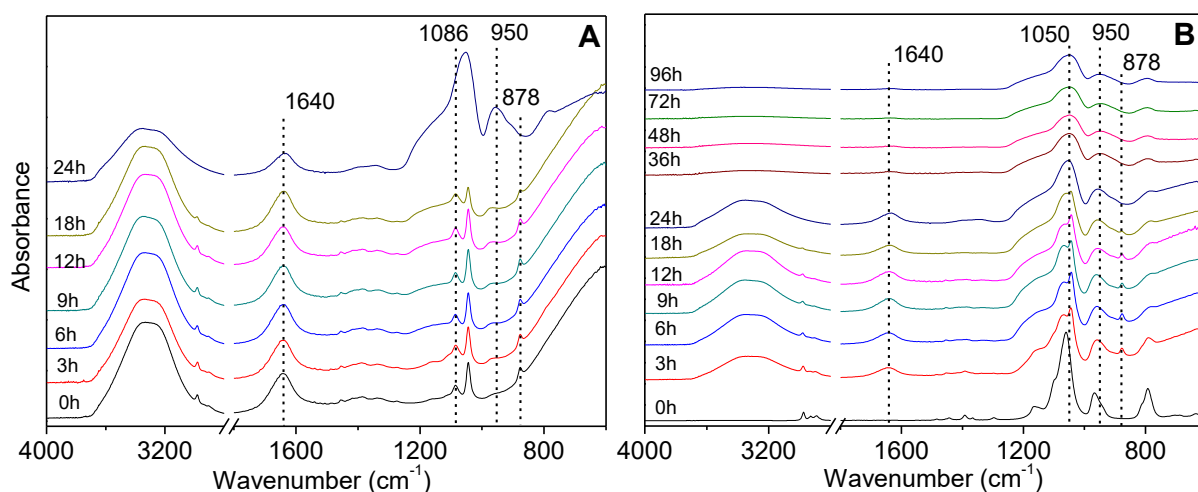
Figure 3.3 FTIR spectra of the (A) top phase and (B) bottom phase of ES40 sol-gel solutions at different drying times.

These results indicate that ES40 sol-gel reaction did occur in the heterogeneous phase-separated systems. It is hypothesized that hydrolysis took place at the interface of the two phases. As the silica polymerization progressed, the ethoxyl groups bonded to the silica atoms (Si-OEt) in the bottom phase turned into hydrophilic silanol groups (Si-OH), which subsequently produced the siloxane groups (Si-O-Si) as evidenced by the increasing intensity of the 950 cm^{-1} and 1065 cm^{-1} peaks. After further condensation and solvent evaporation (ethanol and water), the sol-gel solution became a single phase and eventually formed xerogels after drying.

Besides the investigation of sol-gel process at 60 ℃, different temperatures during the gelling stage were also investigated and analysed using the same FTIR methodology. The evolution of the silica structure at 25, 40 and 60 ℃ at 9 and 72 h of drying time in the bottom phase are shown Figure 3.4 (temporal evolution of full FTIR spectra for the 25 and 40 ℃ samples are supplied in ESI). As shown in Figure 3.4A, the spectrum only shows the pure ES40 absorption peaks at 25 ℃, indicating no detectable reaction has taken place after 9 h, while the extent of hydrolysis at 40 and 60 ℃ is much greater as manifested by the reduced C-O vibration at ~780 cm^{-1} and the C-H stretching vibrations of Si-OCH$_2$CH$_3$ at 2800 cm^{-1}, which almost vanishes after 9 h at 60 ℃. In addition, the degree of condensation is furthered at higher temperature conditions as demonstrated by the broadening of the absorption peak at ~ 1150 cm^{-1} (Si-O-Si). At 72 h, as seen in Figure 3.4B, the condensation of silica at different drying temperatures is also different. The absorbance intensity of uncondensed silica species, Si-OH and Si-O$^-$, at ~950 cm^{-1} is much weaker at 60 ℃ system compared to that in the 40 and 25 ℃ spectra. These results demonstrate that the sol-gel process in phase-separated system is significantly affected by reaction temperature in this study.
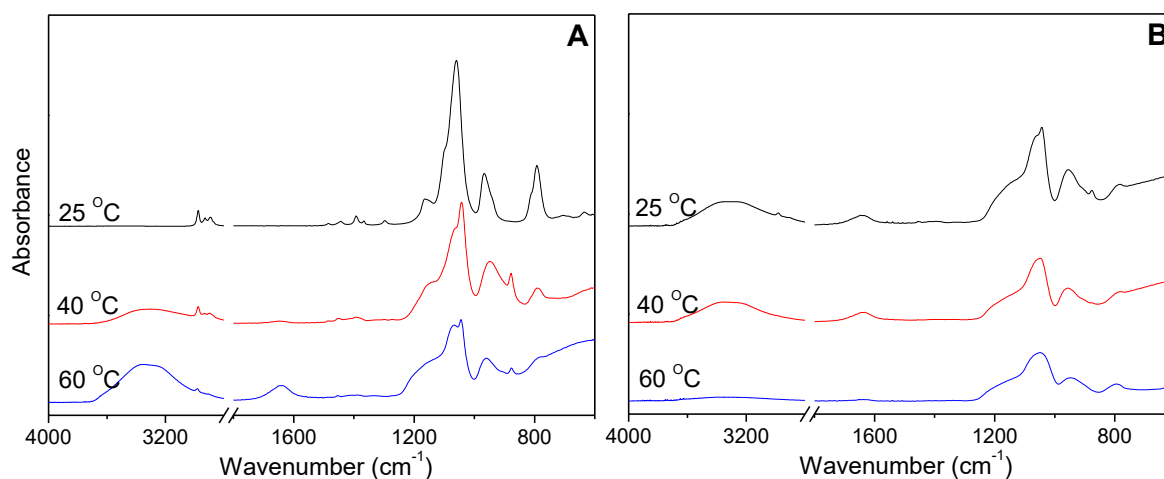
Figure 3.4 FTIR spectra of the bottom phase of ES40 sol-gel solutions after drying for (A) 9 h and (B) 72 h at 25, 40 and 60 ℃.
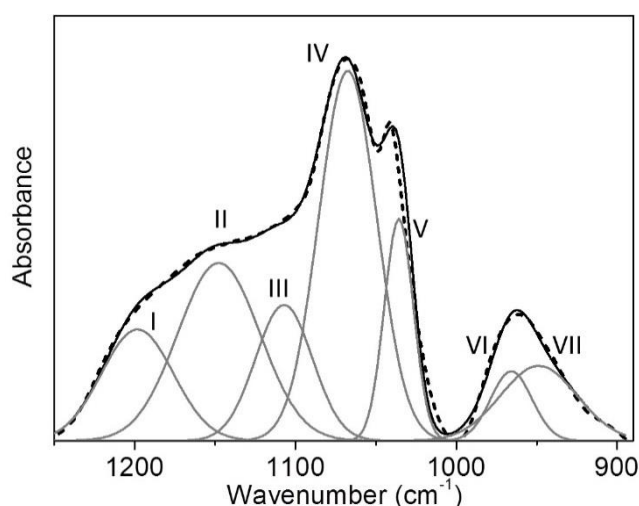
Figure 3.5 FTIR spectrum (dotted line) and peak deconvolution of the bottom phase for 9 h sample dried at 60 ℃ after EtOH spectral subtraction. The solid lines are summation (black) of the fitted peaks (grey) with an R^2 value ≥0.995.

Further analysis of the FTIR spectra provided meaningful information about the subtle differences in these phase-separated sol-gel systems by measuring the intensity of absorption corresponding to the various chemical species, i.e. Si-OH and Si-O-Si. In silica sol-gel process, the quantification of absorption peaks relating to silanol and siloxane species could provide some valuable insight into the extent of hydrolysis and condensation in the sol-gel process. However, due to the overlapping nature between the absorption peaks of ethanol and ES40 in the region of between 1200 and 1000 cm^{-1}, careful spectral subtraction was carried out to remove the contribution of the ethanol solvent in the initial sol-gel reaction (for times < 24 h) according to Tejedor-Tejedor et al.[14]. To perform a quantitative analysis, deconvolution of the peaks was used to identify various vibrations in the

45

overlapping regions. Figure 3.5 illustrates a representative example of peak deconvolution of a spectrum (60 ℃, 9 h) after ethanol spectral subtraction and the assignment of the fitted peaks is summarized in Table 3.2.

Table 3.2 Band assignments of the FTIR vibrations of the products in Figure 3.5 [29, 30]

Deconvoluted peaks	Wavenumber (cm^{-1})	Vibration mode	Chemicals
I	~1205	LO_3 mode of ν_{as}(Si-O-Si)	6-ring siloxane $(SiO)_6$
II	~1146	LO_4 mode of ν_{as}(Si-O-Si)	4-ring siloxane $(SiO)_4$
III	~1105	TO_4 mode of ν_{as}(Si-O-Si)	4-ring siloxane $(SiO)_4$
IV	~1065	TO_3 mode of ν_{as}(Si-O-Si)	6-ring siloxane $(SiO)_6$
V	~1035	ν_{as}(Si-O-Si)	chain silicate
VI	~962	ν(Si-OH)	silanol
VII	~934	ν(Si-O$^-$)	silica open rings

As shown in Figure 3.5, peaks VI and VII are corresponding to the products of the hydrolysis reaction for Si-OH and Si-O$^-$ bonds, respectively. While for the broad band in the region 1250 to 1000 cm^{-1}, five fitted peaks centred at ~1205, 1146, 1105, 1065 and 1035 cm^{-1} are related to product of condensation reaction Si-O-Si bond. According to the literature, the absorption at peak V (1035 cm^{-1}) is characteristic of chain and sheet silicates.[14] The peaks II (1146 cm^{-1}) and III (1105 cm^{-1}) have been assigned to the longitudinal optical (LO)-transverse optical (TO) splitting modes of 4-ring siloxane, while the other two absorption I (1205 cm^{-1}) and IV (1065 cm^{-1}) correspond to the LO-TO pair of a 6-ring network. These assignments are consistent with the report that the discrepancy of LO-TO splitting for 6-ring silica locates within the wavenumber boundary of 140 to 160 cm^{-1}.[29, 31] The proportion of LO mode is reported to be an indicator showing the extent of condensation. Primeau et al. demonstrated that the LO_3 vibration mode is not observable if the sol-gel process does not sufficiently evolve and the siloxane groups are not fully converted.[32] In our work, the LO_3 mode at ~1205 cm^{-1} is detectable after 6 h as shown in Figure 3.3B, indicating the high degree of siloxane condensation.

The ratio of the peak area originated from comparing the area of uncondensed silicon species (peaks VI and VII) to that from condensed silica (the dominant siloxane band IV). This can be used as an

indicator of the degree of hydrolysis and condensation reactions. Figure 3.6 shows the calculated peak area ratio as a function of reaction time at different temperatures. It can be observed from Figure 3.6 that the peak area ratio of Si-O(H)/Si-O-Si for all the samples increases and then decreases at different point in the gelling time. On a closer examination, the induction period of hydrolysis is significantly delayed with decreasing temperature from 6 to 25 h for the 40 and 25 ℃ samples, respectively. As such, the 25 and 40 ℃ samples had not completely reached equilibrium at the end of 96 h. This result was expected for two reasons. Firstly, sol-gel reactions are known to be promoted by temperature. Secondly, due to solvent evaporation, the sol-gel species are forced to come in close proximity which promotes chemical reactions.
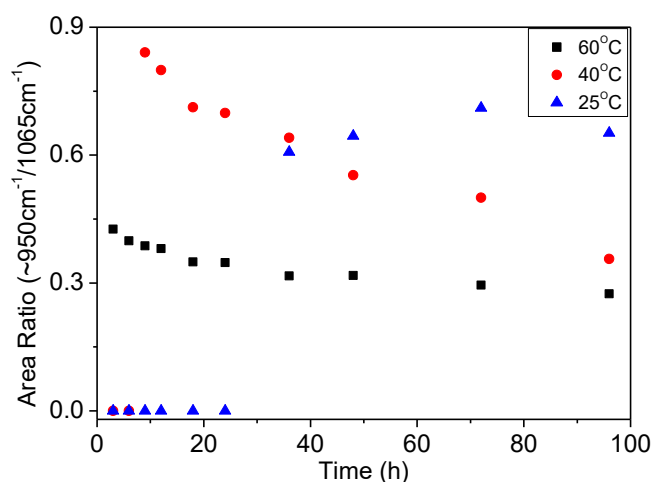
Figure 3.6 Comparative FTIR ratios of Si-OH to Si-O-Si as a function of time at different reaction temperatures (25, 40 and 60 ℃) (estimated standard error = ±4%).

More importantly, as shown in Figure 3.6, the point when the Si-OH/Si-O-Si ratio reaches a maximum were measured at 3, 9 and 72 h for 60, 40 and 25 ℃, respectively. In other words, this time indicates that hydrolysis is being overtaken by condensation reactions, and thus more siloxane species are being generated at the expense of the silanol species regardless of their molar absorptivity. This further indicates that the shift in the reaction equilibrium is favoured towards the condensation reactions. These results demonstrate that the sol-gel process in phase-separated system is suppressed by low temperature due to a slower hydrolysis reaction and subsequently inhibits the condensation reactions. This is not so dissimilar to those reported for homogeneous TEOS derived silica sol-gel systems.[15, 28, 33]

The structure properties of the resultant xerogels after calcination were studied by N_2 sorption. It can be observed from Figure 3.7A that xerogels dried at 40 and 60 ℃ show Type I isotherms, indicating that micropores are dominant in their texture. The xerogel dried at 60 ℃ had an

adsorption isotherm which achieved saturation at a higher relative pressure than the sample dried at 40 °C, in addition to a larger amount of N_2 volume adsorbed. For the xerogel dried at 25 °C, the N_2 adsorption and desorption isotherms exhibit a type IV hysteresis loop, characteristic of a mesoporous structure. In addition, the DFT pore size distribution (Figure 3.7B) of the 25 °C xerogel exhibited a much wider profile than the others, also implying a larger pore size. These results illustrate that when the drying temperature decreases from 60 to 40 °C, the effect on structure properties is not obvious and the product is still microporous. Whereas when the temperature is further decreased to 25 °C, a mesoporous material is obtained.
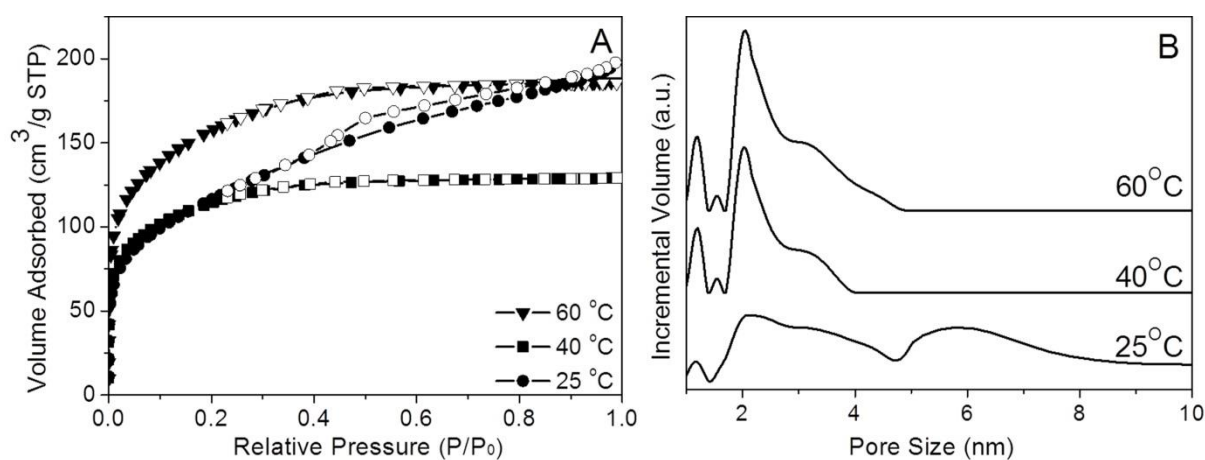
Figure 3.7(A) N_2 adsorption (solid symbols) and desorption (open symbols) isotherms and (B) DFT pore size distribution of silica xerogels dried at 25, 40 and 60 °C.

To shed further light on the structural formation of the xerogels as a function of the drying temperature, TGA was conducted by holding the sample at constant temperatures until completely dried. It can be observed from Figure 3.8A that, for the gels dried at 60 °C, a sharp weight loss appears after 2 h. This was much faster than for the sample dried at 25 °C, as shown in Figure 3.8B. The system keep losing weight due to evaporation of solvent and by-product of sol-gel reactions until equilibration is achieved after 4h at 60 °C or 20 h at 25 °C. The equilibration of the sol-gel process at 60 °C appeared at much earlier period than the 25 °C system, which is consistent with the FTIR results in Figure 3.6.
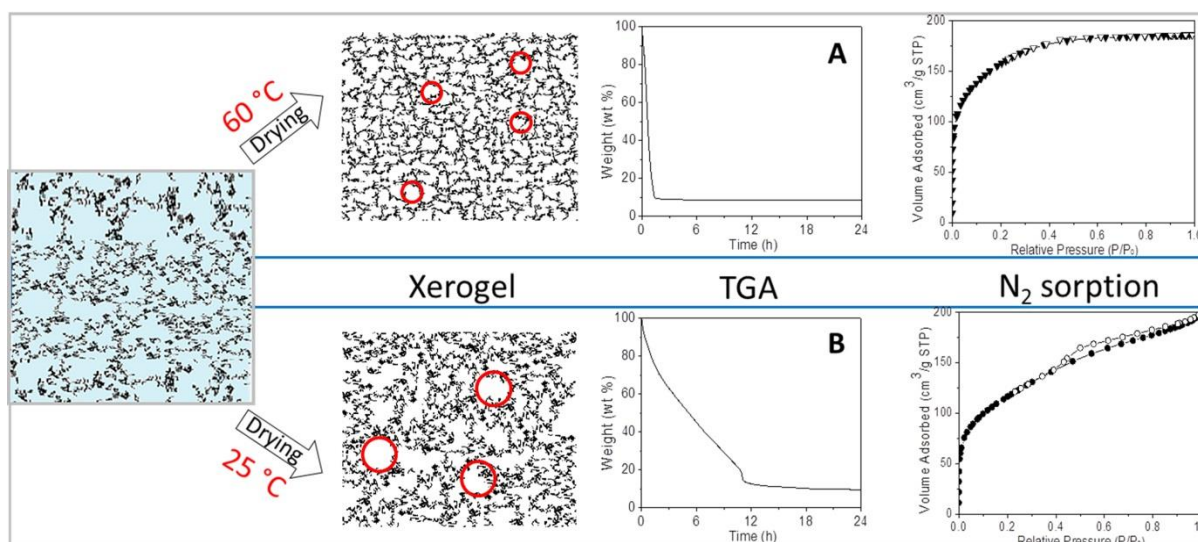
Figure 3.8 TGA curves of silica sol-gel solutions and schematic silica matrix obtained after dying at 25 and 60 ℃. Red circles are used to illustrate example pores.

Figure 3.8 also shows a schematic of the ES40 sol-gel process. The mesoporous structure obtained at 25 ℃ in principle could be attributed to the much slower solvent evaporation during drying as confirmed by the TGA curves. It has been reported that the degree of shrinkage of silica network during drying depends on the relative rate of solvent evaporation and stiffening of the network,[5] as it is the case for TEOS derived sol-gel. As solvent evaporates, surface tension and drying stress created in the gel results in the collapse of the network.[34] Concomitantly, the stiffness of network also enhanced due to increasing crosslinking of the silica chains by sol-gel reaction and decreasing porosity through shrinking. This in turn acts against network shrinkage. In the case of the ES40 derived sol-gel, it could be expected that the gel dried at 25 ℃ would have a denser structure due to the higher content of Si-OH groups as shown in Figure 3.6. These groups are generally deemed to collapse under capillary forces, whilst Si-O-Si bridges stiffen the silica structure and oppose densification. This is not the case for the ES40 derived sol-gel process, suggesting that a different mechanism is occurring.

ES40 is a partially condensed TEOS, so it is no longer a monomer leading to oligomers like TEOS. The mesoporosity of the gel dried at 25 ℃ suggests that the slow reaction process led to the formation of unreacted ES40 cages filled with solvent. These cages were large enough to have lower capillary pressures and reduced drying stress. These cages hindered the ES40 oligomers to get in closer contact to react, and favoured the formation of mesoporous structures. This can be clearly observed in Figure 3.7B, as the pore size distribution for the gel dried at 25 ℃ broadened from ~5 to 9 nm, which is not observed for the gels dried at 40 and 60 ℃. In the case of the latter, faster evaporation allowed for closer contact of the ES40 oligomers and fast reaction leading to the

formation of Si-O-Si bridges and structural interpenetration as evidenced by the microporous character of their adsorption isotherms. Hence, these results strongly suggest that solvent evaporation played an important role in the structural formation of ES40 derived sol-gel, coupled with the effect of reaction.
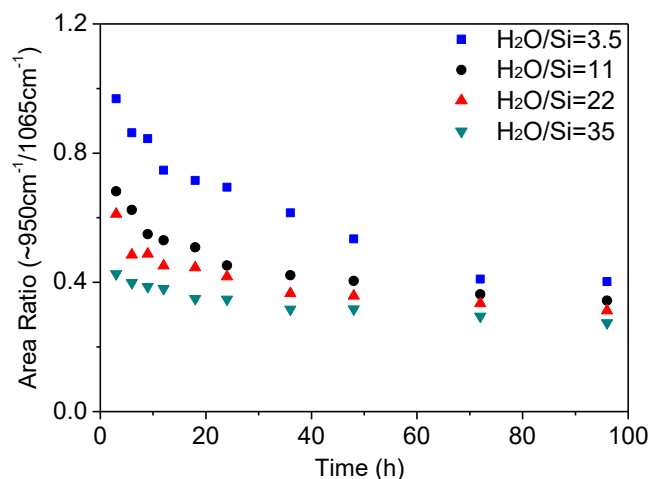
Figure 3.9 Comparative FTIR ratios of Si-O(H) to Si-O-Si as a function of time with different H_2O/Si ratios (3.5, 11, 22 and 35) (estimated standard error = ±4%).

The effect of H_2O/Si ratios on phase-separated sol-gel performance was also studied. Based on the previous FTIR results, for a molar ratio of H_2O/Si = 35, the sol-gel process was promoted by increasing the reaction temperature during the drying process at 60 ℃. Therefore, samples with reduced H_2O/Si ratio of 22, 11 and 3.5 were prepared at the same temperature for comparison. A homogeneous solution was obtained when H_2O/Si ratio decreased to 3.5, as per Figure 3.1. The Si-O(H)/Si-O-Si ratio in Figure 3.9 increased at the beginning of the reaction and decreased afterwards until equilibrium was reached. The Si-O(H)/Si-O-Si ratio during the whole drying process decreased with increasing H_2O/Si ratio. It is also noteworthy that the Si-O(H)/Si-O-Si ratio of the homogeneous solution (H_2O/Si=3.5) was significantly higher than the phase-separated systems. This can be attributed to the dilutive effect of the solvent on the homogeneous sol-gel reaction solution, which suppresses the condensation reaction. On the contrary, in phase-separated systems, the reactive species are highly concentrated around the reaction interface thus promoting further condensation. The time point when equilibrium was reached was also affected by the water content, which increased from 36 h to 72 h when H_2O/Si ratio decreased from 35 to 3.5. These results demonstrate that condensation is furthered by a high H_2O/Si ratio. This is expected as water is a hydrolysing agent commonly employed in the sol-gel process, which promotes the condensation reaction, and yields a lower Si-O(H)/Si-O-Si ratio and faster equilibrium.

The N_2 sorption results in Figure 3.10A shows that xerogel prepared from homogeneous sol-gel solution with low H_2O ratio of 3.5 was mainly dense with no N_2 adsorbed. The other isotherms are all Type I, indicating microporous networks. The volume adsorbed increases with increasing H_2O ratios, implying a larger total pore volume. This was confirmed through DFT pore size distributions (Figure 3.10B) which shows an increasing fraction of larger pores with increasing H_2O ratio. Similar to the homogeneous reaction system, such an effect can be explained by acceleration of hydrolysis resulting from a high H_2O ratio. This is also indicated by FTIR analysis in Figure 3.9. As more reactive sites appear, silica chains with higher degree crosslinking are produced. These are beneficial to the formation of larger silica particles and a more open silica network with a lower silanol to siloxane ratio.
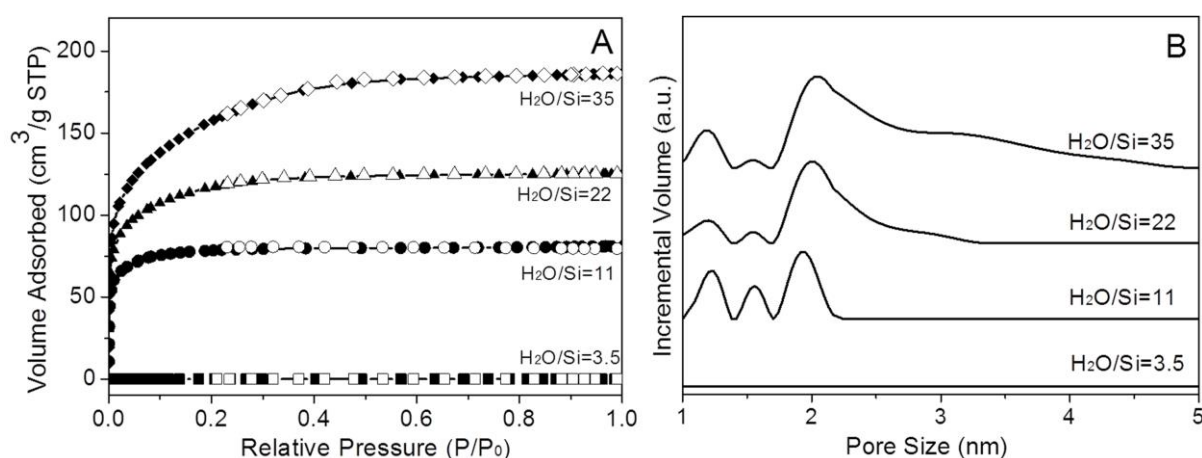
Figure 3.10 (A) N_2 adsorption (solid symbols) and desorption (open symbols) isotherms and (B) DFT pore size distribution of silica xerogels prepared with different H_2O/Si ratios (35, 22, 11 and 3.5).

The relationship between total pore volume of silica xerogels and comparative silanol to siloxane ratios is shown in Figure 3.11A. Based on these results, it can be deduced that high porosity can be obtained through phase-separated sol-gel systems with high H_2O to Si ratios. Further the textural properties of the xerogels prepared from phase-separated solution can also be easily tuned by changing reactant ratios. Figure 3.11B shows that the solvent evaporation in the homogenous solution is much faster than that in the phase-separated solution with high H_2O/Si ratio. Faster evaporation led to larger drying stresses which caused more network compression. As the homogeneous sample had a higher content of silanol groups, indicating a limited crosslinking of the silica chains, this weak structure was unable to oppose the drying stress. Hence the silica network collapsed, resulting in a dense or perhaps ultra-microporous structure. Contrary to this trend, the slower evaporation rate and higher siloxane content induced stiffening of the network and prevented shrinking of the phase-separated gels.

51
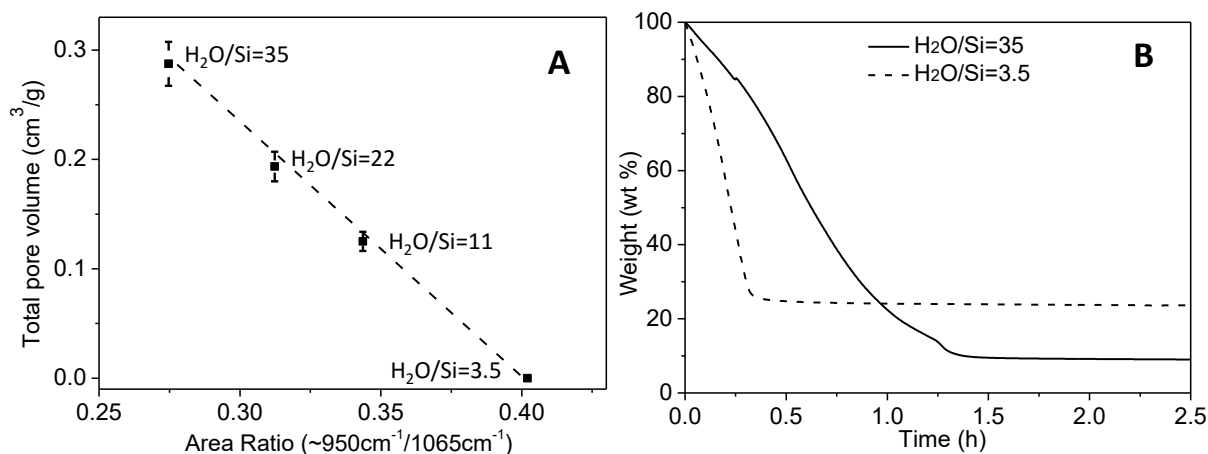
Figure 3.11(A) Total pore volume of silica xerogels as function of comparative FTIR area ratios of silanol to siloxane vibrational peaks (B) TGA curves of sol-gel solutions drying at 60 ℃.

3.4 Conclusions

The phase behaviour of ES40 in water-ethanol co-solvent was evaluated and the phase diagram of these three components was obtained, which shows smaller miscible region than that of TEOS. The evolution of the sol-gel process in phase-separated ES40 solutions demonstrated that the ES40 sol-gel reactions can occur, commencing at the interface of the two layers. This may be followed by migration of silanol groups generated from hydrolysis and condensation reactions. The FTIR area ratio of Si-O(H)/Si-O-Si increased at the beginning of the sol-gel process due to the hydrolysis reaction and then decreased over time due to condensation reactions. The phase-separated ES40 sol-gel process was affected by the reaction temperature and the initial H_2O/Si ratios. High temperatures favoured faster solvent evaporation thus bringing the reactive species in closer contact to facilitate their reaction. Microporous xerogels were produced at 60 and 40 ℃, while mesoporous structures were obtained when reaction temperature further decreased to 25 ℃. The formation of larger pores under low temperature was attributed to two factors. Firstly, slow solvent evaporation reduced the drying stress and consequently the silica network compression was weak. Secondly, the oligomer silica precursor ES40 can form cages, inducing lower capillary forces as well as larger pores.

The phase-separated sol-gel process of ES40 was furthered studied by increasing the H_2O/Si ratio as water is a hydrolyzing agent. N_2 sorption analysis of the resultant xerogels indicates that contrary to dense silica structures derived from homogeneous solutions, higher porosity was delivered through phase-separated sol-gel system by using high H_2O/Si ratios. The porous properties of the xerogels prepared from phase-separated solutions can also be easily tuned by changing reactant ratios. In

phase-separated sol-gel systems, most reactive species are concentrated around the interface, and this close proximity facilitated further condensation reactions and crosslinking of silica chains. In turn this induced stiffening of the network making it more resistant to compression and densification.

Acknowledgements

References

[1] E.L. Margelefsky, R.K. Zeidan, M.E. Davis, Cooperative catalysis by silica-supported organic functional groups, Chem Soc Rev, 37 (2008) 1118-1126.

[2] Y.H. Zhang, R. Ciriminna, G. Palmisano, Y.J. Xu, M. Pagliaro, Sol-gel entrapped visible light photocatalysts for selective conversions, Rsc Adv, 4 (2014) 18341-18346.

[3] Y.G. Jin, S.Z. Qiao, Z.P. Xu, Z.M. Yan, Y.N. Huang, J.C.D. da Costa, G.Q. Lu, Phosphonic acid functionalized silicas for intermediate temperature proton conduction, J Mater Chem, 19 (2009) 2363-2372.

[4] C. Yacou, S. Smart, J.C.D. da Costa, Long term performance cobalt oxide silica membrane module for high temperature H-2 separation, Energ Environ Sci, 5 (2012) 5820-5832.

[5] C.J. Brinker, G.W. Scherer, Sol-gel science: the physics and chemistry of sol-gel processing, Academic Press, Boston, 1990.

[6] J.E. Mark, The sol-gel route to inorganic-organic composites, Heterogen Chem Rev, 3 (1996) 307-326.

[7] J. Ambati, S.E. Rankin, Reaction-induced phase separation of bis(triethoxysilyl)ethane upon sot-gel polymerization in acidic conditions, J Colloid Interf Sci, 362 (2011) 345-353.

[8] G. Olguin, C. Yacou, S. Smart, J.C.D. da Costa, Influence of surfactant alkyl length in functionalizing sol-gel derived microporous cobalt oxide silica, Rsc Adv, 4 (2014) 40181-40187.

[9] K. Lee, J.L. Look, M.T. Harris, A.V. McCormick, Assessing extreme models of the Stober synthesis using transients under a range of initial composition, J Colloid Interf Sci, 194 (1997) 78-88.

[10] B. Riegel, S. Blittersdorf, W. Kiefer, S. Hofacker, M. Muller, G. Schottner, Kinetic investigations of hydrolysis and condensation of the glycidoxypropyltrimethoxysilane/aminopropyltriethoxy-silane system by means of FT-Raman spectroscopy I, J Non-Cryst Solids, 226 (1998) 76-84.

[11] C.P. Tripp, M.L. Hair, Reaction of Methylsilanols with Hydrated Silica Surfaces - the Hydrolysis of Trichloromethylsilanes, Dichloromethylsilanes, and Monochloromethylsilanes and the Effects of Curing, Langmuir, 11 (1995) 149-155.

[12] L. Liu, D.K. Wang, D.L. Martens, S. Smart, E. Strounina, J.C.D. da Costa, Physicochemical characterisation and hydrothermal stability investigation of cobalt-incorporated silica xerogels, Rsc Adv, 4 (2014) 18862-18870.

[13] Y. Masuda, S. Kugimiya, Y. Kawachi, K. Kato, Interparticle mesoporous silica as an effective support for enzyme immobilisation, Rsc Adv, 4 (2014) 3573-3580.

[14] M.I. Tejedor-Tejedor, L. Paredes, M.A. Anderson, Evaluation of ATR-FTIR spectroscopy as an "in situ" tool for following the hydrolysis and condensation of alkoxysilanes under rich H2O conditions, Chem Mater, 10 (1998) 3410-3421.

[15] H.M. Jiang, Z. Zheng, X.L. Wang, Kinetic study of methyltriethoxysilane (MTES) hydrolysis by FTIR spectroscopy under different temperatures and solvents, Vib Spectrosc, 46 (2008) 1-7.

[16] F. Neville, A. Seyfaee, Real-Time Monitoring of in Situ Polyethyleneimine-Silica Particle Formation, Langmuir, 29 (2013) 14681-14690.

[17] T.R. Gaydhankar, V. Samuel, R.K. Jha, R. Kumar, P.N. Joshi, Room temperature synthesis of Si-MCM-41 using polymeric version of ethyl silicate as a source of silica, Mater Res Bull, 42 (2007) 1473-1484.

[18] D.K. Wang, J.C.D. da Costa, S. Smart, Development of rapid thermal processing of tubular cobalt oxide silica membranes for gas separations, J Membr Sci, 456 (2014) 192-201.

[19] S. Wang, D.K. Wang, K.S. Jack, S. Smart, J.C. Diniz da Costa, Improved hydrothermal stability of silica materials prepared from ethyl silicate 40, Rsc Adv, 5 (2015) 6092-6099.

[20] C.R. Miller, D.K. Wang, S. Smart, J.C. Diniz da Costa, Reversible Redox Effect on Gas Permeation of Cobalt Doped Ethoxy Polysiloxane (ES40) Membranes, Sci Rep-Uk, 3 (2013) 1-6.

[21] A. Fidalgo, L.M. Ilharco, Correlation between physical properties and structure of silica xerogels, J Non-Cryst Solids, 347 (2004) 128-137.

[22] N.L. Allinger, M. Rahman, J.H. Lii, A molecular mechanics force field (MM3) for alcohols and ethers, J Am Chem Soc, 112 (1990) 8293-8307.

[23] M.G.M. van der Vis, R.J.M. Konings, A. Oskam, T.L. Snoeck, The vibrational spectra of gaseous and liquid tetraethoxysilane, J Mol Struct, 274 (1992) 47-57.

[24] M.A. Mondragón, V.M. Castaño, M. J. Garcia, S. C.A. Téllez, Vibrational analysis of Si(OC2H5)4 and spectroscopic studies on the formation of glasses via silica gels, Vib Spectrosc, 9 (1995) 293-304.

[25] A. Fidalgo, L.M. Ilharco, The defect structure of sol–gel-derived silica/polytetrahydrofuran hybrid films by FTIR, J Non-Cryst Solids, 283 (2001) 144-154.

[26] V.R. Koganti, S. Das, S.E. Rankin, In Situ FTIR Investigation of the Kinetics of Silica Polycondensation in Surfactant Templated, Mesostructured Thin Films, J Phys Chem C, 118 (2014) 19450-19461.

[27] D. Niznansky, J.L. Rehspringer, Infrared study of SiO2 sol to gel evolution and gel aging, J Non-Cryst Solids, 180 (1995) 191-196.

[28] S. Amoriello, A. Bianco, L. Eusebio, P. Gronchi, Evolution of two acid steps sol–gel phases by FTIR, J Sol-Gel Sci Technol, 58 (2011) 209-217.

[29] A. Fidalgo, L.M. Ilharco, Chemical tailoring of porous silica xerogels: Local structure by vibrational spectroscopy, Chem-Eur J, 10 (2004) 392-398.

[30] P. Innocenzi, Infrared spectroscopy of sol-gel derived silica-based films: A spectra-microstructure overview, J. Non-Cryst. Solids, 316 (2003) 309-319.

[31] M.F. Thorpe, S.W. de Leeuw, Coulomb effects in disordered solids, Phys Rev B, 33 (1986) 8490-8505.

[32] N. Primeau, C. Vautey, M. Langlet, The effect of thermal annealing on aerosol-gel deposited SiO2 films: a FTIR deconvolution study, Thin Solid Films, 310 (1997) 47-56.

[33] R. Dumas, I. Tejedor-Tejedor, M. Anderson, Dependence of SiO2> Gel Structure on Gelation Conditions and Sol Reaction Temperature as Followed by FTIR and Nitrogen Adsorption Measurements, J Porous Mater, 5 (1998) 95-101.

[34] R.K. Iler, The chemistry of silica : solubility, polymerization, colloid and surface properties, and biochemistry Wiley, New York, 1979.

4 IMPROVED HYDROSTABILITY OF SILICA MEMBRANE MATERIALS PREPARED FROM ETHYL SILICATE 40

Introduction

This chapter aims to improve the hydrostability of ES40-derived microporous silica membrane materials. The effects of water (hydrolyzing agent), acid (catalyst) and ethanol (solvent) ratios on the microstructure and hydrostability of the resultant silica products were systematically investigated by exposing the xerogels to water vapour and calculating the BET surface area variation during exposure.

Contribution

It was found that the degree of microporosity of the produced microporous molecular sieving silica xerogels can be finely controlled and highly microporous silica materials were favored by low water and acid ratios, or high ethanol ratio. The most hydrostable matrices were obtained by increasing the ratio of water to 140, acid to 0.4 and decreasing ethanol to 15. The improved hydrostability of the microporous silica material is attributed to the lower percentage of silanol groups on one hand and the formation of a more robust, open silica microstructure from larger silica particles on the other. This work was published in RSC Advances as:

S.N. Wang, D.K. Wang, K.S. Jack, S. Smart, J.C.D. da Costa, Improved hydrothermal stability of silica materials prepared from ethyl silicate 40, RSC Adv., 2015, 5, 6092.

Improved hydrothermal stability of molecular sieving silica materials prepared from ethyl silicate 40

*Reproduced in part with permission from Shengnan Wang, David K. Wang[a], Kevin S. Jack, Simon Smart and João C. Diniz da Costa, RSC Adv., 5, 2015, 6092.

Abstract

Microporous silica materials with improved hydrothermal stability were synthesized through a sol-gel process using ethyl silicate 40 as the starting silica precursor. The effects of reactants for water (hydrolysing agent), acid (catalyst) and ethanol (solvent) ratios on the microstructure of the silica matrices and their hydrothermal stability under harsh conditions (550 °C, 75 mol% vapour, 20 h) were systemically studied. All the calcined silica matrices were microporous and the degree of microporosity was found to increase with decreasing water and acid ratios, or increasing ethanol ratio. The most hydrothermally stable matrix was obtained by promoting the water and acid ratios whilst decreasing the ethanol ratio. A strong correlation was found between the FTIR area ratio of silanol/siloxane vibrational peaks and the initial micropore volume, and this relationship revealed that the greatest pore volume loss (> 70%) occurred in the xerogels possessing high silanol/siloxane ratio (> 0.16) and high initial micropore percentage (> 85%). SAXS data also revealed that the most robust, hydrothermally stable silica matrices are closely associated with the formation of a more open silica microstructure derived from thermal consolidation of larger silica particles.

4.1 Introduction

Silica porous materials have been widely applied in catalysis, adsorption, sensor, and molecular sieving membranes materials.[1-4] These materials are typically prepared via the conventional sol-gel methods, in which an alkoxysilane precursor undergoes hydrolysis and condensation reactions in the presence of a mineral acid or base catalyst to produce a silica matrix. Tetraethyl orthosilicate (TEOS) has been extensively investigated, due to the ease of processing and good control of physicochemical properties offered by this silica precursor. However, a major potential downside of this approach is that the structural integrity of microporous silica matrices is generally compromised under water vapour exposure.[5-9] The issue here is that the surface functional groups responsible for the formation of microporous silica networks (i.e. silanols groups (Si-OH)), are also responsible for the hydrothermal instability. They attract water molecules to adsorb to the surface which reacts (by hydrolysis) with the neighboring siloxane backbone. This process creates unconstrained mobile silanol species, which migrate within the silica matrix to minimize the surface energy of the pore

network by filling in the small pores.[10, 11] As a result of the restructuring and recondensation, the silica matrices densify which leads to a significant loss of selectivity and functionality.

To address this problem, several strategies have been reported to obtain hydrothermally stable silica materials namely: (i) post-synthesis hydrothermal treatment as a pre-emptive process aimed at reducing the concentration of available silanol species;[12] (ii) incorporation of another ceramic component for example using Ti, Al or Zr to form Si–O–M bonds (M; metal), which are less susceptible to hydrolysis;[13, 14] (iii) increasing surface hydrophobicity by embedding carbon groups using organosilica precursors,[15-18] which include terminal alkyl groups, such as $\equiv$Si–CH$_3$ or organic bridges, such as Si–CH$_2$–CH$_2$–Si in their structure, or by post-synthesized silylation; and iv) by doping with metal/carbon particles to limit silanol migration and reconstruction.[11, 19-21] It has also been reported that silica matrices modified by the incorporation of inorganic salts during the sol-gel synthesis process not only produce an improved hydrothermal stability but also a thicker pore walls leading to a better structural integrity.[22, 23] A considerable drawback of these strategies is the use of relatively expensive organosilica precursors, secondary component and/or additional post-treatment.

In this work, we propose another alternative strategy to produce a more stable silica structure by using ethyl silicate 40 (ES40) as the silica precursor of choice instead of TEOS. ES40 is a partially-condensed TEOS oligomer composed of 40% of the silica by mass. ES40 is also commercially available and is lower in cost compared to the TEOS precursor. Although ES40-dervied silica materials have not been fully explored, ES40 has generally been employed in the preparation of mesoporous materials.[24-27] For examples, mesoporous silica xerogels and aerogels using ES40 had shown to produce a low concentration of silanol groups[27] and ES40-derived MCM-41 exhibited a higher wall thickness than that of the TEOS counterpart, leading to a higher thermal stability.[24] Recently, Miller and co-workers pioneered the preparation of ultra-microporous ES40-derived materials combined with cobalt oxide.[28] Subsequently, Wang et al.[29] showed for the first time that ES40 could also be used for the preparation of microporous silica/cobalt oxide by rapid thermal treatment which could not be realized using the TEOS precursor. Hence, ES40 has demonstrated potential as a precursor in the synthesis of hydrostable microporous materials due to its improved structural stability.

Based on a limited number of studies into ES40-based materials, the sol-gel conditioning of ES40-derived microporous materials without any additives, specifically the effect of sol-gel ratios on the structural formation and hydrothermal stability, remains unexplored. Therefore, this work

investigates the hydrothermal effect of ES40 derived materials. Of particular importance, many industrial processes require microporous materials for processing gas streams containing water vapour. To this end, this work studies the effects of sol-gel synthesis conditions, including different ethanol, acid catalyst and water ratios, on the structural formation and chemical properties. The hydrothermal stability of the resultant ES40 xerogels is also investigated using a harsh hydrothermal treatment condition (550 °C, 75 mol% vapour, 20 h).

4.2 Experimental

4.2.1 Sol-gel Synthesis

Table 4.1 Molar ratios of the reactants used in the sol-gel process.

Sample Code[*]	Si	EtOH	H_2O	HNO_3
H_2O-44	4	15	**44**	0.4
H_2O-92			**92**	
H_2O-140			**140**	
HNO_3-0.05	4	15	44	**0.05**
HNO_3-0.1				**0.1**
HNO_3-0.2				**0.2**
HNO_3-0.4				**0.4**
HNO_3-0.8				**0.8**
EtOH-15	4	**15**	44	0.4
EtOH-50		**50**		
EtOH-100		**100**		

[*] Samples are named as N-y, where N is the name of the varying component (H_2O, HNO_3 or EtOH) and y is the molar ratio of N component.

The sol-gel procedure to produce microporous materials was adopted from Miller and co-workers.[28] Briefly 1 M nitric acid (HNO_3), distilled water and ethanol (EtOH, AR grade) were mixed briefly followed by dropwise addition of ES40 (Colcoat Co., Japan) into the solution under stirring in an ice bath. The mixture was stirred for 10 min and then the sols were dried in an oven at 60 °C for over 4 days. Subsequently, the dried gels were ground into powders and calcined in air at 630 °C for 2.5 h with a ramp up and down rate of 1 °C min^{-1} to obtain the resultant xerogel samples for material characterization and hydrothermal treatment. The final molar ratios ($ES40:EtOH:H_2O:HNO_3$) of the sol compositions are listed in Table 4.1. The molar ratio of H_2O was altered from 44 to 140, HNO_3 from 0.05 to 0.8 and EtOH from 15 to 100 respectively to study the effect of these three reactant components.

4.2.2 Hydrothermal test

Hydrothermal stability was evaluated by exposing the xerogels to harsh conditions of 75 mol% vapor at 550 °C for 20 h with a ramp up and down rate of 5 °C min^{-1}. As shown in Figure 4.1, the flow rate of carrier nitrogen gas was set to 40 ml min^{-1} by a flow meter and the rate of water was set to 5.4 g h^{-1} by liquid flow controller, both of which were mixed and heated to 200 °C in a vaporizer to produce 75 mol% vapour. The vapour continuously flowed through a quartz tube furnace controlled by a PID temperature controller. The xerogel samples were placed in the middle of the quartz tube.
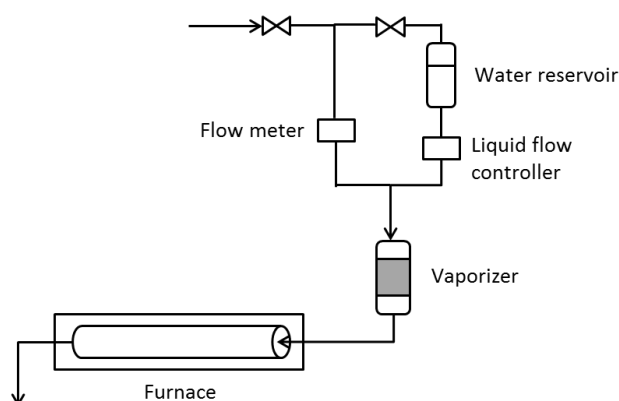
Figure 4.1 Schematic diagram for the hydrothermal treatment set up.[30]

4.2.3 Material Characterizations

Fourier transform infra-red (FTIR) characterization was performed by a Shimadzu IRAffinity-1 with a Pike MIRacle diamond attenuated total reflectance (ATR) attachment. The spectra were collected over a wavenumber range of 1400–600 cm^{-1}. Peak deconvolution of the silanol (960 cm^{-1}) and siloxane (1050 cm^{-1}) vibrations was performed using the Fityk program. Both peak positions and height were allowed to vary between samples to achieve the best possible fit. Half width half max parameter was fixed for each peak across all the samples. The intensity of siloxane peak was normalized to 100% for each spectrum. Cross-polarisation magic-angle-spinning (CP/MAS) solid-state ^{29}Si nuclear magnetic resonance spectroscopy (NMR) was performed on an Avance III spectrometer (Bruker) for silicon groups. Nitrogen adsorption was performed at -196 °C by a Micromeritics TriStar 3000. Prior to each measurement, samples were degassed at 200 °C overnight. The specific surface area was calculated from the adsorption isotherms by the Brunner-Emmett-Teller (BET) method. The pore size distributions were calculated by using Density Functional Theory (DFT) method applied to the whole adsorption branch of the isotherms using the

model of cylindrical pores in oxide surfaces. Small-angle X-ray scattering (SAXS) was measured on an Anton Paar SAXSess instrument which employs an anode source (Cu Kα radiation at 40 kV and 35 mA), a CCD detector and a line-focus (Kratky) geometry. Samples of fine powders were measured between thin polymer films at room temperature and the resultant data were reduced to remove the background scattering and detector dark current.

4.3 Results and discussion

4.3.1 Nitrogen Sorption

Three series of sol-gel ES40-derived silica xerogels were prepared by parametrically changing the feed ratios of H_2O, HNO_3 and EtOH as listed in Table 4.1, and their textural properties were studied by N_2 sorption. Figure 4.2 shows the nitrogen adsorption-desorption isotherms of the resultant xerogels. It can clearly be seen that all the isotherms are Type I without any hysteresis, which is characteristic of microporous materials. However, the isotherm profiles of the individual series of silica xerogels consistently changes with increasing or decreasing the sol-gel ratios. For example, the relative pressure at which adsorption saturation plateaus and the amount of volume adsorbed increases with increasing H_2O and HNO_3 ratios, indicating higher total pore volume and surface area.
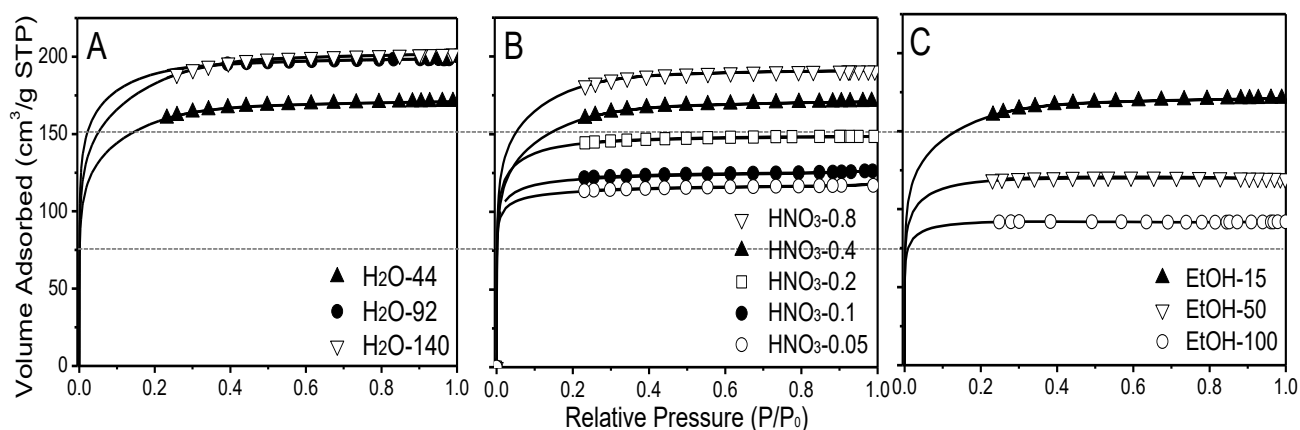
Figure 4.2 N_2 adsorption (solid line) and desorption (symbols) isotherms of silica xerogels prepared with different ratio of H_2O (A), HNO_3 (B) and EtOH (C) to Si, respectively.

In comparison increasing the EtOH ratio has the opposite effect. These trends are clearly reflected by the total pore volume as shown in Figure 4.3. The total pore volumes increase from 0.18 to 0.30 cm^3 g^{-1} for the HNO_3-0.05 and HNO_3-0.8 samples respectively. Similarly, the BET surface areas (see Supporting Information Figure S4.1) increase from 380 to 617 m^2 g^{-1} with increasing HNO_3 ratio. The same trend is also observed for the samples in the H_2O series, but conversely for the

EtOH sample series. Interestingly, the EtOH-100 xerogel samples exhibit the lowest total pore volume and BET surface area of all samples investigated. This is directly attributed to the dilutive effect of the EtOH solvent on the ES40 hydrolysis and condensation reactions which are expected to be slowed down in EtOH excess.[31] Based on these results, by changing the initial sol-gel reactant ratios, the final textural properties and xerogel pore volumes can be easily controlled with a high degree of reproducibility and fidelity.
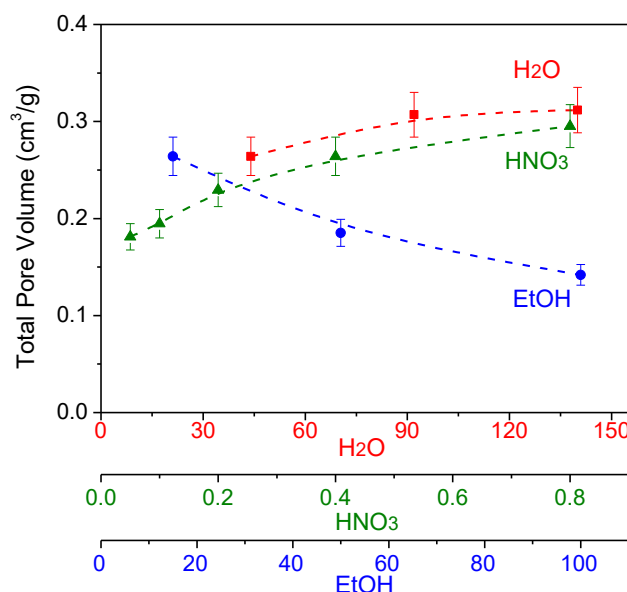
Figure 4.3 Total pore volume of silica xerogels prepared from different ratio of H_2O (red ■), HNO_3 (green ▲) and EtOH (blue ●) to Si, respectively.

To examine the hydrothermal stability of the as-synthesized ES40 silica microstructure, xerogel samples were heated to 550 °C for 20 h in the presence of 75 mol% steam vapour. The structural integrity of these samples was determined from the calculated loss of total pore volume before and after hydrothermal treatment. The results are summarized in Figure 4.4. It can clearly been seen that xerogel samples with less than 40% loss in total pore volume were prepared by a relatively high H_2O or HNO_3 ratios and low EtOH ratio. For example, the H_2O series produced a small amount of pore volume loss (15%–32%), particularly in the H_2O-92 and 140 samples. Similarly, when the HNO_3 ratio is greater than 0.2, the hydrothermal stability of the xerogels greatly improved. By contrast, increasing the EtOH ratio beyond 15, profoundly increases the pore volume loss such that the samples are observed to become almost non-porous. These trends exhibited by the three series of xerogels are also in good accord with the results of BET surface area loss after hydrothermal treatment (not shown), as pore volumes are linearly proportional to surface areas.
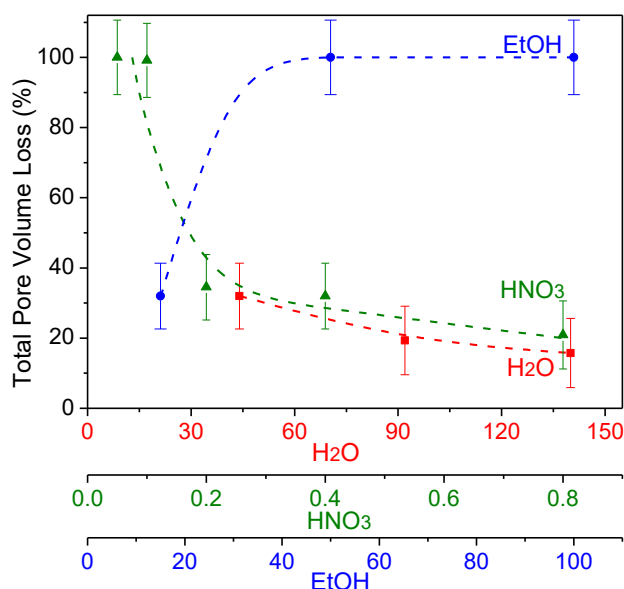
Figure 4.4 Total pore volume loss of silica xerogels prepared from different ratio of H_2O (red ■), HNO_3 (green ▲) and EtOH (blue ●) to Si, respectively.

Hydrothermal densification of the microporous silica is further qualitatively discussed by the change in pore size distribution as displayed in Figure 4.5, which shows the DFT pore size distribution before and after hydrothermal treatment. By comparing the incremental pore volume of the xerogels pre-and post-treatment, the distribution curves either significantly decreased in volume or shifted to high pore diameters after treatment. Where xerogel samples completely densified (e.g. HNO_3-0.05, -0.1, and EtOH-50, -100), the pore size distribution curve became a flat line, implying the closure of pores. In the other cases, the profiles of stable samples showed a shift towards a larger pore size distribution. On closer inspection, these samples seemed to have widened the mesopores (2–4 nm) at the expense of micropore closure (< 2 nm). This means that the hydrothermal treatment imposed on these series of xerogels caused a significant loss of the observed micropores and/or micropore narrowing which may be too small to be accessed by N_2.

It is worthy to mention that by increasing the H_2O and HNO_3 ratios, the distribution profiles of the samples without hydrothermal treatment show an increasing proportion of pore size towards a mesoporous domain which enlarges upon hydrothermal exposure (post treatment), which in turn resisted pore densification. Meanwhile, by increasing the EtOH ratio, the distribution and the trend are reversed. Similar observations were also reported for ordered mesoporous silica materials, of which the micropores were collapsed first followed by partial blocking of the mesopores via acid stability testing.[32] The behavior of hydrothermal densification of silica xerogels is consistent with the previous works on bulk porous silica[11, 33-35] in that the mobile silica generated by hydrothermal treatment prefer to migrate from the larger pores towards the smaller pores to

minimise the overall silica surface energy. Thus after recondensation reactions, the smaller pores are closed while larger pores are widened, leading to a loss in porosity in the microporous region.
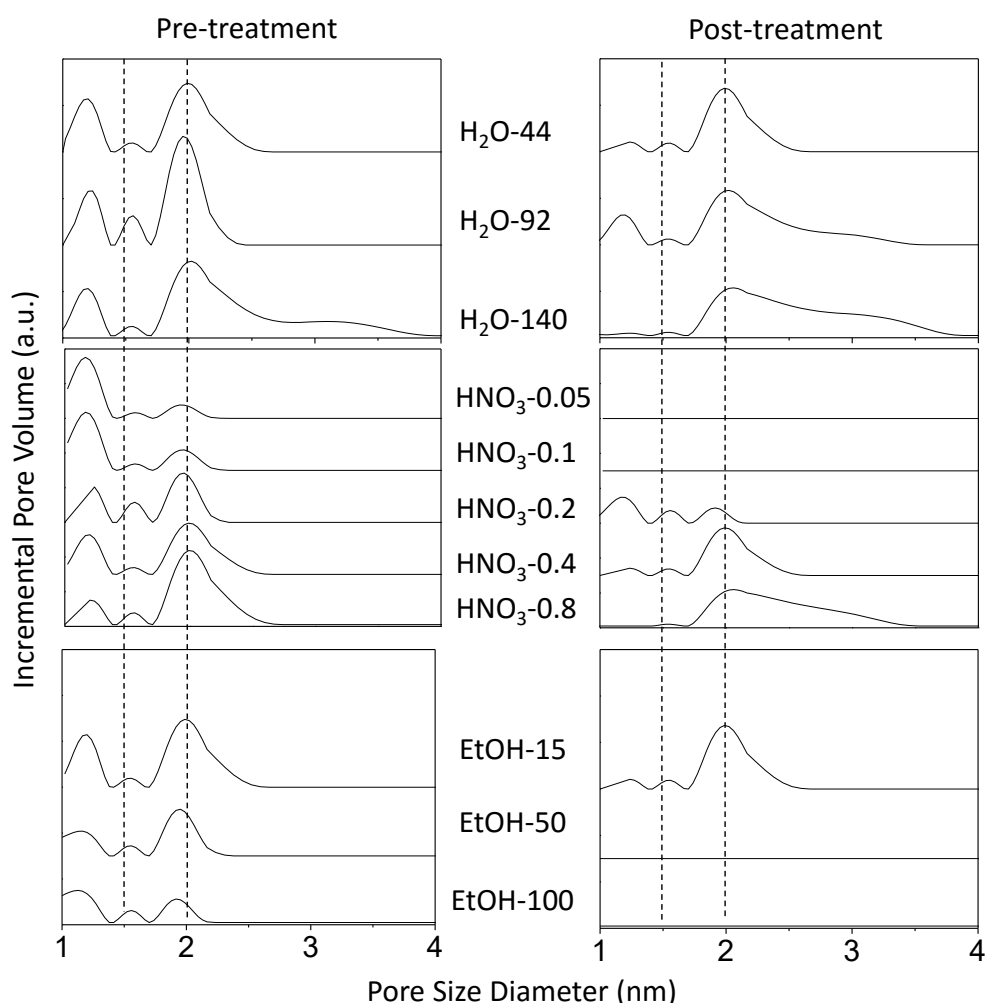
Figure 4.5 DFT pore size distribution of the xerogels before and after hydrothermal treatment. The broken lines are guidelines only for pore sizes of 1.5 and 2.0 nm.

Since the initial micropore content ($d_p < 2$ nm) of the pre-treated samples leading to the majority of pore closure is directly attributed to hydrothermally unstable matrices, this relationship is further examined. Figure 4.6 shows the micropore volume percentage of the pre-treated samples against the total pore volume loss. At a first glance, the samples with an initial micropore volume larger than 85% (highly microporous) became completely dense after hydrothermal test, while the other samples having lower micropore volume preserved their total pore volume to varying degrees. Therefore, it can be deduced that hydrothermal stability of these silica xerogels is closely correlated to the initial micropore volume which can be simply controlled by changing the feed reactant ratios during the sol-gel process.
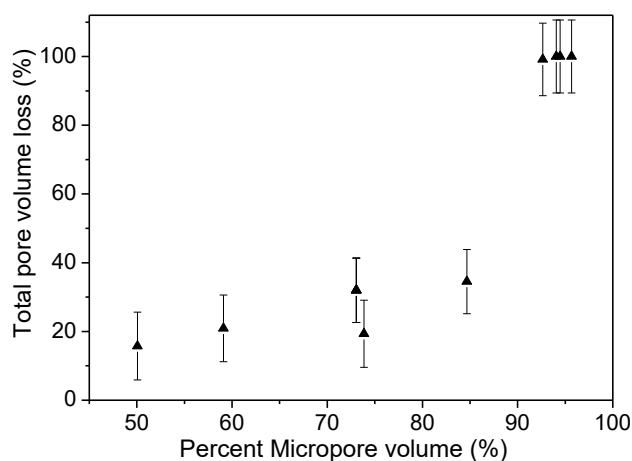
Figure 4.6 Total pore volume loss of the hydrothermally treated xerogels as function of percent micropore volume (%) of the as-synthesized silica xerogels before hydrothermal test.

4.3.2 FTIR and CP/MAS ^{29}Si NMR Spectroscopies

Another important aspect of thermal consolidation of microporous silica matrices is the chemical and molecular properties which can be probed by FTIR-ATR technique readily. Figure S4.2 shows the FTIR spectra of the three series of calcined xerogel samples in the range from 1400 to 600 cm^{-1}, where the peak at ~960 cm^{-1} is assigned to the vibration of the silanol bonds and the major peak at ~1050 cm^{-1} is assigned to the stretching vibrations of the siloxane bonds. The latter also shows various bands near 800, 1090 and 1160 cm^{-1} associated with various symmetric and anti-symmetric Si–O–Si vibrations which arise from highly condensed siloxane ring species.[29, 36, 37] In order to provide a semi-quantitative analysis of the chemical compositions, the peak at ~1050 cm^{-1} is normalized for all the spectra and these peaks were deconvoluted with a special attention given to the silanol band at 960 cm^{-1} and the siloxane band at 1050 cm^{-1} according to a previously reported methodology.[29, 30]
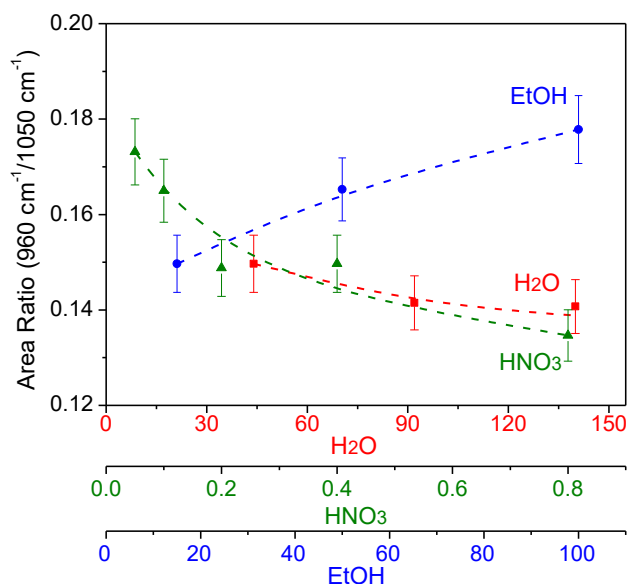
Figure 4.7 Comparative FTIR ratios of silanol to siloxane of silica xerogels prepared from different ratios of H$_2$O (red ■), HNO$_3$ (green ▲) and EtOH (blue ●) to Si, respectively.

Figure 4.7 shows the area ratio analysis of the bands 960 cm^{-1}/1050 cm^{-1} which allows a comparison of the degree of condensation between the different sample series; where a high ratio corresponds to a high silanol concentration and vice versa. There is a strong correlation between the area ratio and the reactant sol-gel ratios. It can be seen that the concentration of the silanols is significantly promoted by low HNO$_3$ ratio (< 0.2) or high EtOH ratio (> 15). As mentioned earlier, a high concentration of silanol species can lead to an unstable silica structure. This is evidenced by the similarity in results between Figure 4.7 and the hydrothermal densification as summarized in Figure 4.4.

Figure 4.8 shows the total pore volume loss of the xerogels as function of the same peak area ratios irrespective of the reactant ratios. One can clearly observe that the results can be separated into two groups. Silica matrices with a relatively higher silanol concentration (area ratio > 0.16) completely collapsed after the hydrothermal treatment. By contrast, the group with a lower total pore volume loss inherently possesses a lower silanol concentration. This further suggests that hydrothermal stability of the silica microstructure in this work is related to the presence of these silanol species with a ratio threshold of 0.16.
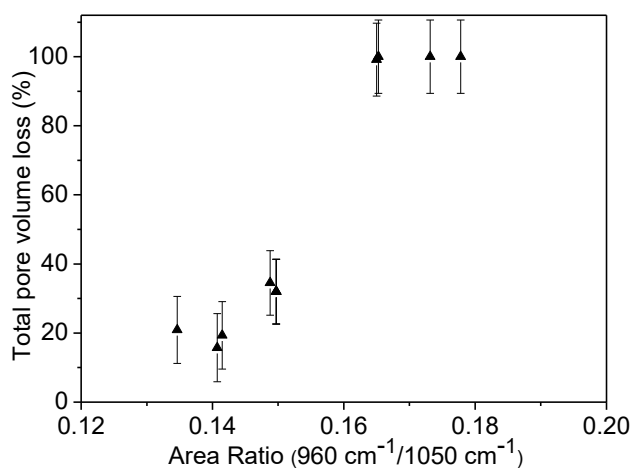
Figure 4.8 Total pore volume loss of silica xerogels as function of comparative FTIR area ratios of silanol to siloxane vibrational peaks.

Incidentally, these results also point towards a correlation between the FTIR peak area ratio and the micropore volume (Figure 4.6) whereby both trends of the pore volume loss demonstrate in the region of high silanol ratio (> 0.16) and high initial micropore percentage (> 85%). This indicates that the probability of hydrothermal densification of the silica matrices is greatly increased in a more microporous sample with higher silanol content. In a similar vein, Zhao and co-workers [9, 38, 39] have reported that the surface of micropores of silica matrix possess an abundance of silanol groups, which preferentially condense upon hydrothermal treatment over the mesopores. Therefore, based on these observations, hydrothermal stability of these series of microporous silica xerogels is intrinsically linked to the physical and chemical properties which can be easily controlled by changing the reactant ratios.

Furthermore, the evolution of the silica structure can be further confirmed by the structural transition of the silanol to siloxane groups based on the comparative CP/MAS ^{29}Si NMR quantification of the Q^n species populations before and after hydrothermal treatment. The results of the ^{29}Si NMR spectra of the H_2O-44 and H_2O-140 xerogels samples are shown in Figure S4.3 (supporting information). By peak deconvolution, the percent variation of the Q^n species of the pre- and post-treatment silica samples is shown in Figure 4.9. Both samples show an increase in Q^4 population after treatment, at the cost of Q^2 and Q^3, illustrating restructuring of silanols to siloxanes. However, the increase in the Q^4 species as a result of loss of Q^3 is larger for the H_2O-44 samples indicating further silanol condensation took place, which is in good agreement with the total pore volume loss of the H_2O-44 samples (32%) being twice as much as that of the H_2O-140 samples (15%). These findings are also consistent with the previous reports by Duke et al.[11] and Liu et al.,[30] who also observed that an increase of the Q^4 species after treatment is more pronounced in

the more unstable silica samples than the stable ones. Nevertheless, these reports only demonstrated that the modified silica matrices with carbon[11] and cobalt oxide[30] are stable, whereas that the pure silica matrices are completely dense after hydrothermal treatment.
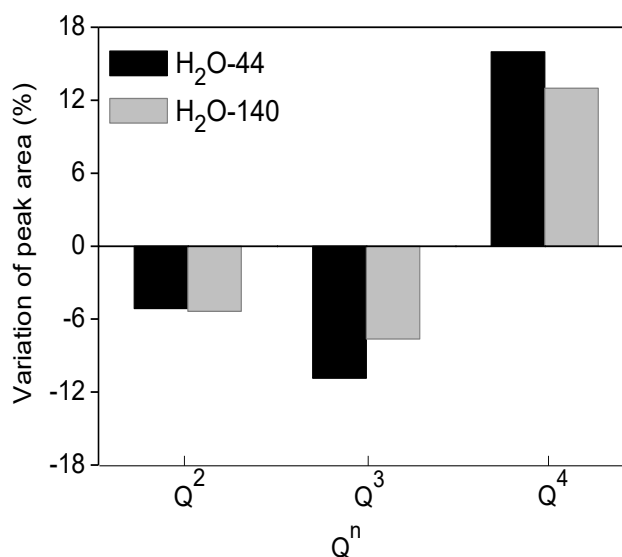
Figure 4.9 Percentage variation of the deconvoluted peak area of Q^n species between the as-synthesized and the treated xerogels (H_2O–44 and H_2O–140).

4.3.3 SAXS Measurements

The further shed more light into the microstructure of the calcined silica xerogels, these powders were further investigated by SAXS. Figure 4.10A and B show the forward scattering presented as ($I(q)\times q^3$) as a function of q (where q is the wave vector and $I(q)$ is the measured, line-focused, scattered intensity at q) for the HNO_3-0.05 and HNO_3-0.8 as-synthesized xerogel powder samples, respectively. These two samples in the HNO_3 series were selected as representative samples for each of the hydrothermally weak and stable silica matrices. In both of the SAXS profiles, the presence of a plateau can be seen at relatively higher q values, indicating the onset of the Porod scattering region in the SAXS profile of the powder. This Porod scattering indicates that the powder is comprised of well-defined smooth surfaces, i.e. the gels consist of a well-dispersed homogenous silica microstructure and is consistent with the SAXS typically reported for silica gels.[26, 27]
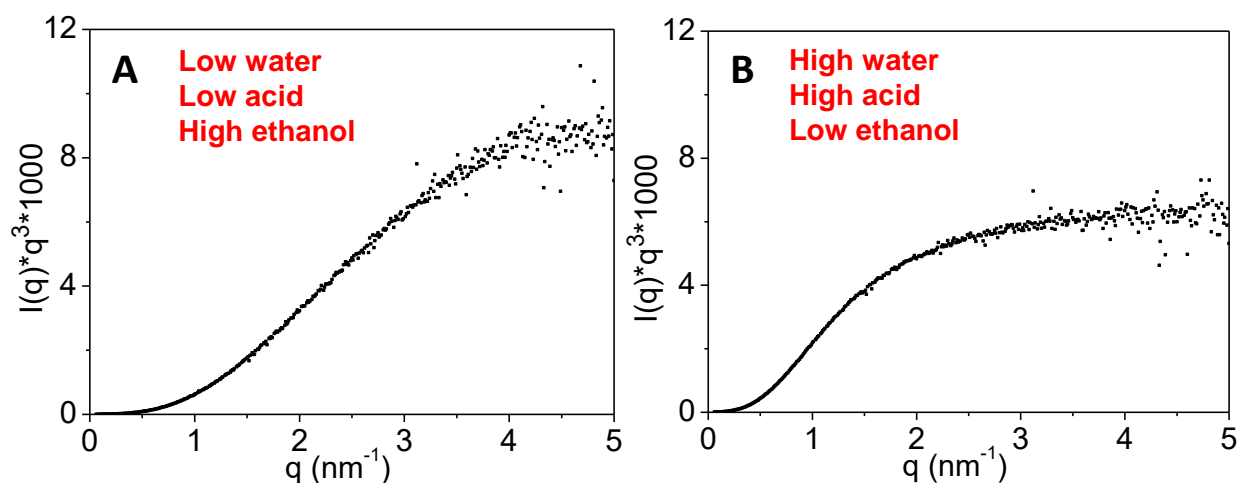
Figure 4.10 SAXS profiles of the as-synthesized HNO$_3$-0.05 (A) and HNO$_3$-0.8 (B) xerogel powder samples.

Moreover, it can be seen in Figure 4.10 that the value of q at the onset of the plateau (q$_c$) is greater for the HNO$_3$-0.05 sample (4.3 nm^{-1}) compared with the HNO$_3$-0.8 sample (2.3 nm^{-1}). Indeed the mean radius of the primary silica particles can be approximated from these onset values: r$_0$ ≈ π/q$_c$.[40] The silica particles (r$_0$) of the HNO$_3$-0.8 sample are, therefore, estimated to be twice as large as that of the HNO$_3$-0.05 xerogel sample. Thus, it is hypothesized that the thermal consolidation of silica particles in the HNO$_3$-0.8 xerogel sample creates a relatively larger average pore sizes and total pore volume as shown in the schematics of Figure 4.10. Such hypothesis is consistent with the larger total pore volume (Figure 4.3) and DFT pore size distributions (Figure 4.5) derived from N$_2$ sorption analysis.

Based on these results, the microstructure of the HNO$_3$-0.8 xerogel sample with a larger pore volume and pore size conferred a better structural integrity as evidenced by a total pore volume loss (<30 %) being significantly lower than that of the HNO$_3$-0.05 sample (>70%). Therefore, the improved hydrothermal stability of silica matrices obtained by the controlled sol gel conditions in this work (higher H$_2$O, HNO$_3$ ratios and lower EtOH ratio) is attributed to the formation of a more robust, open silica microstructure condensed by larger silica particles on one hand and a lower proportion of silanol groups in the matrix on the other.

4.3.4 Sol-Gel Process

By comparing the silica xerogels made from the different reactant ratios, it can be deduced that the use of higher H$_2$O, HNO$_3$ ratios and lower EtOH ratio during the sol-gel process can produce a

silica matrix with larger pore volume and better hydrothermal stability. It is clear that these properties are attributed to the formation and subsequent packing of larger silica particles. As water is the main reactant responsible for hydrolysis reaction in the sol gel process, a low H_2O ratio demotes the hydrolysis and condensation reactions. In this case, hydrolysis is more inclined to proceed via the most basic Q^1 species on the ES40 molecules due to a lower steric hindrance. As can be expected, the reactive hydrolyzed sites which allow the condensation to propagate (polymerization) are primarily located at the chain ends where reaction is spatially limited, hence forming smaller silica particles. This process is anticipated to form a better packing density of the final silica matrices with more silanol groups, which is reflected by a more microporous texture (Figure 4.2) with a significantly lower total pore volume (Figure 4.3).

On the other hand, high H_2O ratio can promote hydrolysis and thus produce more reactive sites from the Q^1 species as well as the more acidic Q^2 species on the pendant groups of the ES40 molecules. As a consequence, fast chain-to-chain random polymerization due to a higher statistical crosslinking is expected. Such a process also promotes a tendency to form clusters leading to a much larger silica particles and more open microstructure with relatively lower silanol groups. Similar trends have also been reported for sol-gel derived cobalt oxide silica systems by Wang et al. [29] by using the ES40 precursor. Therefore, during the hydrothermal treatment, the silica network is firmly supported by the more robust, larger silica particles which resisted densification.

Similarly, increasing the HNO_3 ratio also promotes the sol-gel process due to its catalytic effect. All of the initial sol systems in this work had a measured pH value of around 1 except for the HNO_3-0.05 sample, which was near 2. In the acidic conditions, when pH is significantly lower than the point of zero charge (~2) of silica polymeric particles,[31] the sol-gel reactions rapidly proceeds through the protonated alkoxide group ($SiORH^+$) during the hydrolysis and protonated silanol groups ($SiOH_2^+$) during the condensation reactions.[31] Protonation of these groups makes the silicon atom more electrophilic and thus more reactive towards water or silanol species. This would lead to a faster hydrolysis and condensation reactions causing larger silica particles to form in the system as evidenced by the SAXS results.

On the contrary, excess ethanol retards the hydrolysis process by favoring the reverse reaction since it is a by-product of the sol-gel process. Moreover, by increasing the ethanol concentration, the sol solution is significantly diluted resulting a diffusion-limited polymerization process with a longer gelation time.[31, 41] Essentially, the resultant xerogel is formed by smaller polymeric particles with higher silanol species present in the silica matrix, hence leading to a more microporous texture and a weaker microstructure.

4.4 Conclusion

Microporous molecular sieving silica xerogels with improved hydrothermal stability are prepared by using ES40 as silica precursor. The effects of synthesis conditions, including water (hydrolysing agent), acid (catalyst) and ethanol (solvent) ratios on the structure properties and hydrothermal stability of the resultant xerogels are systemically studied. All silica xerogels were found to possess a Type I microporous texture, but the degree of microporosity (pore volume, pore size, and pore size distribution) can be finely controlled by changing these ratios. Highly microporous silica matrices were promoted by low water and acid ratios, or high ethanol ratio in this work. By exposing xerogels to harsh conditions (550 °C, 75 mol% vapour, 20 h), the most hydrothermal stable matrix with a minimum total pore volume reduction of 15% was obtained by adjusting the ratio of water to 140, acid to 0.4 and ethanol to 15. A correlation between the FTIR area ratio of silanol/siloxane vibrational peaks and the micropore volume revealed that the greatest pore volume loss (> 70%) occurred in the region of high area ratio (> 0.16) and high initial micropore percentage (> 85%). SAXS data also revealed that the improved hydrothermal stability of the microporous silica material is attributed to the formation of a more robust, open silica microstructure condensed by larger silica particles on one hand and a lower proportion of silanol groups in the matrix on the other. This work paves ways for a simple sol-gel synthesis of structurally stable microporous silica matrices with predictable physicochemical properties that are desired for a variety of technological applications, such as catalysis, adsorption, sensor, and molecular sieving membranes materials.

References

[1] C. Yacou, S. Smart, J.C. Diniz da Costa, Long term performance cobalt oxide silica membrane module for high temperature H_2 separation, Energ. Environ. Sci., 5 (2012) 5820-5832.

[2] E.L. Margelefsky, R.K. Zeidan, M.E. Davis, Cooperative catalysis by silica-supported organic functional groups, Chem. Soc. Rev., 37 (2008) 1118-1126.

[3] S.K. Parida, S. Dash, S. Patel, B.K. Mishra, Adsorption of organic molecules on silica surface, Adv. Colloid Interface Sci., 121 (2006) 77-110.

[4] W. Yang, P.J. Lopez, G. Rosengarten, Diatoms: Self assembled silica nanostructures, and templates for bio/chemical sensors and biomimetic membranes, Analyst, 136 (2011) 42-53.

[5] K. Cassiers, T. Linssen, M. Mathieu, M. Benjelloun, K. Schrijnemakers, P. Van Der Voort, P. Cool, E.F. Vansant, A Detailed Study of Thermal, Hydrothermal, and Mechanical Stabilities of a Wide Range of Surfactant Assembled Mesoporous Silicas, Chem. Mater., 14 (2002) 2317-2324.

[6] G.R. Gallaher, P.K.T. Liu, Characterization of Ceramic Membranes .1. Thermal and Hydrothermal Stabilities of Commercial 40 Angstrom Membranes, J Membr Sci, 92 (1994) 29-44.

[7] G.R. Gavalas, C.E. Megiris, S.W. Nam, Deposition of H-2-Permselective SiO_2-Films, Chem Eng Sci, 44 (1989) 1829-1835.

[8] H. Imai, H. Morimoto, A. Tominaga, H. Hirashima, Structural changes in sol-gel derived SiO2 and TiO3 films by exposure to water vapor, J Sol-Gel Sci Techn, 10 (1997) 45-54.

[9] F. Zhang, Y. Yan, H. Yang, Y. Meng, C. Yu, B. Tu, D. Zhao, Understanding effect of wall structure on the hydrothermal stability of mesostructured silica SBA-15, J Phys Chem B, 109 (2005) 8723-8732.

[10] R.K. Iler, The chemistry of silica : solubility, polymerization, colloid and surface properties, and biochemistry Wiley, New York, 1979.

[11] M.C. Duke, J.C. Diniz da Costa, D.D. Do, P.G. Gray, G.Q. Lu, Hydrothermally robust molecular sieve silica for wet gas separation, Adv Funct Mater, 16 (2006) 1215-1220.

[12] L. Chen, T. Horiuchi, T. Mori, K. Maeda, Postsynthesis Hydrothermal Restructuring of M41S Mesoporous Molecular Sieves in Water, J. Phys. Chem. B, 103 (1999) 1216-1222.

[13] G.P. Fotou, Y.S. Lin, S.E. Pratsinis, Hydrothermal Stability of Pure and Modified Microporous Silica Membranes, J Mater Sci, 30 (1995) 2803-2808.

[14] S. Araki, Y. Kiyohara, S. Imasaka, S. Tanaka, Y. Miyake, Preparation and pervaporation properties of silica-zirconia membranes, Desalination, 266 (2011) 46-50.

[15] M. Selvi, M.R. Vengatesan, S. Devaraju, M. Kumar, M. Alagar, In situ sol-gel synthesis of silica reinforced polybenzoxazine hybrid materials with low surface free energy, RSC Adv., 4 (2014) 8446-8452.

[16] R.M. de Vos, W.F. Maier, H. Verweij, Hydrophobic silica membranes for gas separation, J Membr Sci, 158 (1999) 277-288.

[17] D.-H. Park, N. Nishiyama, Y. Egashira, K. Ueyama, Enhancement of Hydrothermal Stability and Hydrophobicity of a Silica MCM-48 Membrane by Silylation, Ind. Eng. Chem. Res., 40 (2001) 6105-6110.

[18] Q. Wei, Y.-L. Wang, Z.-R. Nie, C.-X. Yu, Q.-Y. Li, J.-X. Zou, C.-J. Li, Facile synthesis of hydrophobic microporous silica membranes and their resistance to humid atmosphere, Microporous Mesoporous Mater., 111 (2008) 97-103.

[19] N. Coustel, F. Di Renzo, F. Fajula, Improved stability of MCM-41 through textural control, J. Chem. Soc., Chem. Commun., (1994) 967-968.

[20] D. Zhao, J. Feng, Q. Huo, N. Melosh, G.H. Fredrickson, B.F. Chmelka, G.D. Stucky, Triblock Copolymer Syntheses of Mesoporous Silica with Periodic 50 to 300 Angstrom Pores, Science, 279 (1998) 548-552.

[21] G. Olguin, C. Yacou, S. Smart, J.C. Diniz da Costa, Influence of surfactant alkyl length in functionalizing sol-gel derived microporous cobalt oxide silica, RSC Adv., 4 (2014) 40181-40187.

[22] J.M. Kim, S. Jun, R. Ryoo, Improvement of hydrothermal stability of mesoporous silica using salts: reinvestigation for time-dependent effects, J. Phys. Chem. B, 103 (1999) 6200-6205.

[23] J. Yu, J.-L. Shi, H.-R. Chen, J.-N. Yan, D.-S. Yan, Effect of inorganic salt addition during synthesis on pore structure and hydrothermal stability of mesoporous silica, Microporous Mesoporous Mater., 46 (2001) 153-162.

[24] T.R. Gaydhankar, V. Samuel, R.K. Jha, R. Kumar, P.N. Joshi, Room temperature synthesis of Si-MCM-41 using polymeric version of ethyl silicate as a source of silica, Mater Res Bull, 42 (2007) 1473-1484.

[25] T.R. Gaydhankar, U.S. Taralkar, R.K. Jha, P.N. Joshi, R. Kumar, Textural/structural, stability and morphological properties of mesostructured silicas (MCM-41 and MCM-48) prepared using different silica sources, Catal Commun, 6 (2005) 361-366.

[26] J. Mrowiec-Bialon, A.B. Jarzebski, Fabrication and properties of silica monoliths with ultra large mesopores, Microporous Mesoporous Mater, 109 (2008) 429-435.

[27] J. Mrowiec-Bialon, A.B. Jarzebski, L. Pajak, Z. Olejniczak, M. Gibas, Preparation and surface properties of low-density gels synthesized using prepolymerized silica precursors, Langmuir, 20 (2004) 10389-10393.

[28] C.R. Miller, D.K. Wang, S. Smart, J.C. Diniz da Costa, Reversible Redox Effect on Gas Permeation of Cobalt Doped Ethoxy Polysiloxane (ES40) Membranes, Sci Rep-Uk, 3 (2013) 1-6.

[29] D.K. Wang, J.C. Diniz da Costa, S. Smart, Development of rapid thermal processing of tubular cobalt oxide silica membranes for gas separations, J Membr Sci, 456 (2014) 192-201.

[30] L. Liu, D.K. Wang, D.L. Martens, S. Smart, E. Strounina, J.C. Diniz da Costa, Physicochemical characterisation and hydrothermal stability investigation of cobalt-incorporated silica xerogels, RSC Adv., 4 (2014) 18862-18870.

[31] C.J. Brinker, G.W. Scherer, Sol-gel science: the physics and chemistry of sol-gel processing, Academic Press, Boston, 1990.

[32] S. El Mourabit, M. Guillot, G. Toquer, J. Cambedouzou, F. Goettmann, A. Grandjean, Stability of mesoporous silica under acidic conditions, RSC Adv., 2 (2012) 10916-10924.

[33] R.O. Fournier, J.J. Rowe, The solubility of amorphous silica in water at high temperatures and high pressures, Am. Mineral., 62 (1977) 1052-1056.

[34] R. Leboda, E. Mendyk, A. Gierak, V.A. Tertykh, Hydrothermal modification of silica gels (xerogels) 1. Effect of treatment temperature on their porous structure, Colloids Surf., A, 105 (1995) 181-189.

[35] R. Leboda, E. Mendyk, A. Gierak, V.A. Tertykh, Hydrothermal modification of silica gels (xerogels) 2. Effect of the duration of treatment on their porous structure, Colloids Surf., A, 105 (1995) 191-197.

[36] I. Halasz, M. Agarwal, R. Li, N. Miller, Characterisation of Porous Solids VIII: Structural Distinction of Silica Gels Using FTIR and Raman Spectroscopy, in: S. Kaskel, P. Llewellyn, F. Rodriguez-Reinoso, N.A. Seaton (Eds.) 8th International Symposium on the Characterisation of Porous Solids, Royal Society Of Chemistry, Great Britain, 2009.

[37] P. Innocenzi, Infrared spectroscopy of sol-gel derived silica-based films: A spectra-microstructure overview, J. Non-Cryst. Solids, 316 (2003) 309-319.

[38] Q. Li, Z.X. Wu, D. Feng, B. Tu, D.Y. Zhao, Hydrothermal Stability of Mesostructured Cellular Silica Foams, J Phys Chem C, 114 (2010) 5012-5019.

[39] Q. Li, Z.X. Wu, D. Feng, B. Tu, D.Y. Zhao, Hydrothermal Stability of Mesostructured Cellular Silica Foams, J. Phys. Chem. C, 114 (2010) 5012-5019.

[40] A.B. Jarzçbski, J. Lorenc, L. Pająk, Surface fractal characteristics of silica aerogels, Langmuir, 13 (1997) 1280-1285.

[41] D.W. Schaefer, Fractal models and the structure of materials, MRS Bull, 13 (1988) 22-27.

Supplementary Information
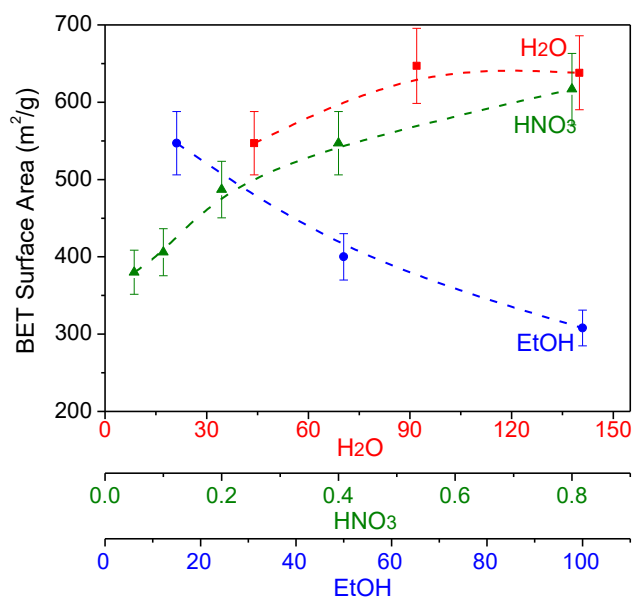
Figure S 4.1 BET surface area of silica xerogels prepared from different ratio of H_2O (red), HNO_3 (green) and EtOH (blue) to Si, respectively.
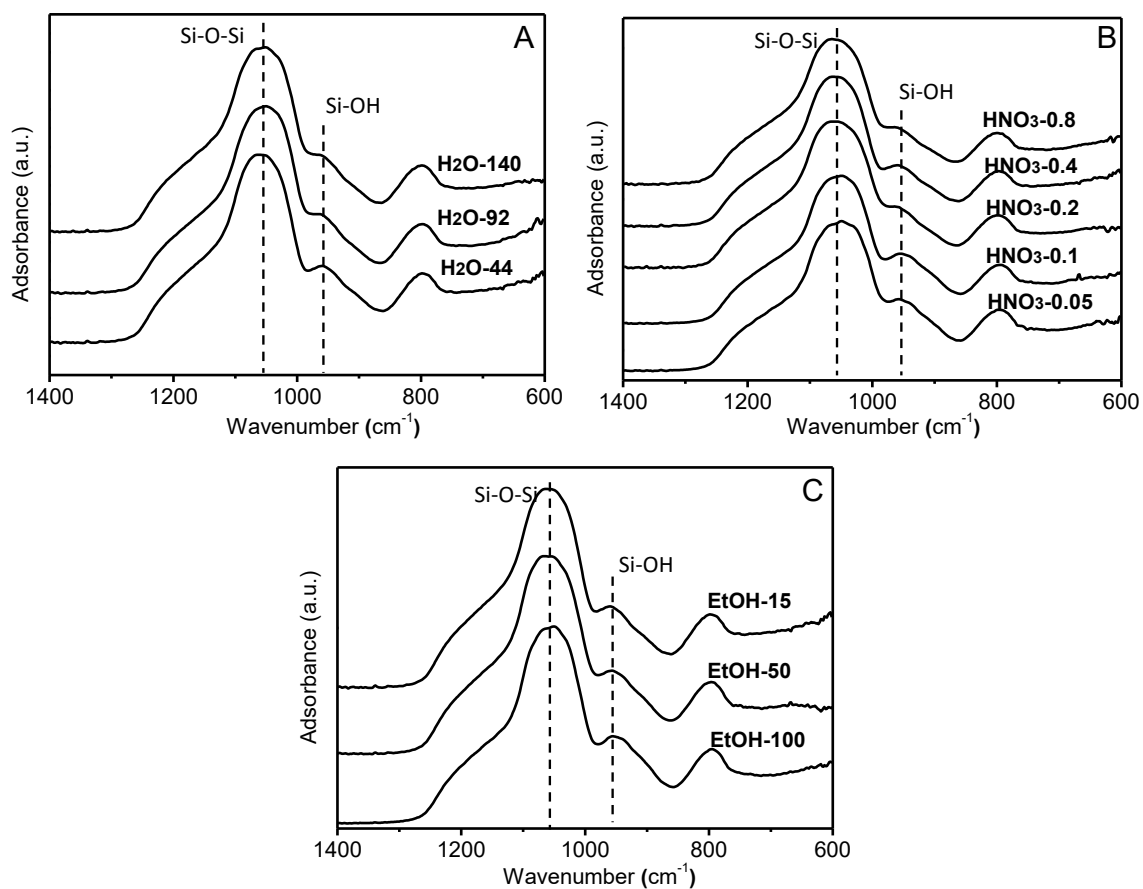
Figure S 4.2 FTIR spectra of the silica xerogels prepared from different ratio of H_2O (A), HNO_3 (B) and EtOH (C) to ES40, respectively.
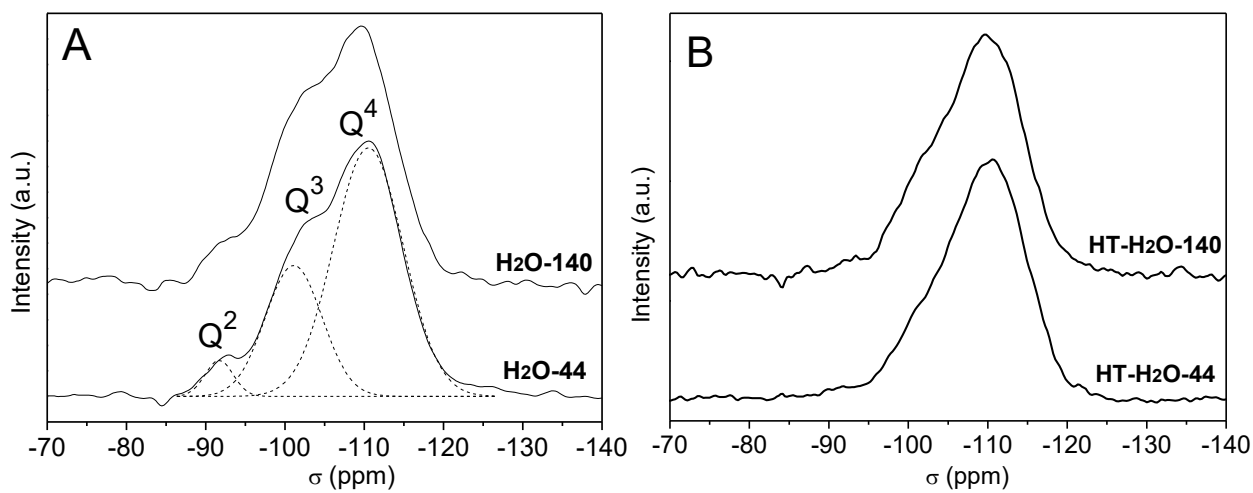
Figure S 4.3 –^{29}**Si NMR Spectra of H$_2$O–44 and H$_2$O–140 silica xerogels before (A) and after (B) hydrothermal test.**

5 PREPARATION OF INTERLAYER-FREE ETHYL SILICATE 40 DERIVED MEMBRANES BY RAPID THERMAL PROCESSING FOR DESALINATION

Introduction

This chapter aims to demonstrate the preparation of interlayer-free silica membranes using the optimized conditions obtained from previous chapter by the rapid thermal processing method (RTP). The comparison of RTP and conventional thermal processing (CTP) prepared membranes, in terms of silanol proportion, surface area and pore size distribution, was conducted. The desalination performance of the interlayer-free membranes was evaluated under various temperatures and salt concentrations.

Contribution

It is demonstrated for the first time the preparation of interlayer-free silica membranes by the RTP method. The membrane fabrication time was reduced to only 1% of that for conventionally prepared silica membranes due to the lack of interlayers and the novel rapid thermal treatment. The RTP silica xerogels offered stronger matrices than their CTP analogues and defect free membranes were produced by adjusting the pH of the sol-gel solution to 4 and/or 6. The best membrane performed high water flux of 17.8 kg m^{-2} h^{-1} at 60 ℃ and high salt rejection (>99%) for desalination of 3.5 wt% seawater. This work was submitted to Journal of Membrane Science as:

> S.N. Wang, D.K. Wang, J. Motuzas, S. Smart, J.C.D. da Costa, Rapid thermal treatment of interlayer-free ethyl silicate 40 derived membranes for desalination, Journal of Membrane Science, submitted.

Rapid Thermal Treatment of Interlayer-free Ethyl Silicate 40 Derived Membranes for Desalination

Abstract

This work demonstrates for the first time the preparation of interlayer-free silica membranes by the Rapid Thermal Processing (RTP) method using ES40 as a silica precursor. RTP resulted in water being retained inside the xerogel pores at higher temperatures, thus favouring the condensation reactions and formation of siloxane bridges. As a result, RTP ES40 xerogel matrices were stronger, leading to higher pore volumes and surface areas as compared to the analogous Convetional Thermal Processing (CTP) ES40 xerogels. Nevertheless, RTP ES40 xerogels were characterised by a tri-modal pore size distribution mainly in the microporous domain with a minor mesoporous region. The preparation feasibility of membranes was dependent on the pH of the sol-gel, as pH 4 and 6 sols penetrated into the α-alumina substrate and adhered well to form a top layer. The best interlayer-free RTP silica membrane was prepared with a pH 4 sol reaching high water fluxes of 17.8 kg m^{-2} h^{-1} at 60 ℃ and high salt rejection (>99%) for desalination of 3.5 wt% seawater. The EtOH:Si ratio to which the sols are diluted for dip coating played an important role on the long term hydrostability of the membrane, as pH 4 membranes prepared with EtOH:Si ratio of 255:4 were stable for 120 h, whilst changing this ratio to 200:4 increased the stability to 300 h. This improvement was attributed to thicker films derived from more viscous sols.

5.1 Introduction

Fresh water scarcity has become one of the most pressing global problems in recent decades due to the impacts of a growing population, increased industrial activity and altered rainfall patterns from rapid climate change [1]. Desalination of the vast seawater reserves is one of the potential solutions to tackle this challenge. Commercially this is accomplished either through traditional thermal techniques such as multi-stage flash and multi-effect distillation [2-4], or through reverse osmosis (RO) where static pressure is used to force fresh water through a semi-permeable membrane against the osmotic gradient [5]. Currently reverse osmosis (RO) membrane process is the gold standard of seawater desalination, though intensive pre-treatment is often needed to limit fouling [6]. Other techniques, such as electrodialysis [7, 8], capacitive deionisation [9], forward osmosis [10, 11], pervaporation [12], and membrane distillation [13] have enjoyed only modest commercial deployment but substantial research interest [14]. Membrane distillation (MD) and pervaporation

(PV) are thermal membrane based desalination techniques where water is evaporated across a membrane, driven by a difference in vapour pressure. The membrane can either be non-selective as for MD or selective for water as in PV. Both have attracted significant research attention in recent decades due to their simple, compact design, which utilises low temperatures (from solar or waste heat) [15].

Typically, hydrophobic polymer membranes with a pore radius between 50-500 nm have been used for MD processes [16, 17] and have seen the wide industry commercialisation. PV has used either dense polymeric membranes [18] or, less commonly, inorganic membranes such as microporous hybrid silica [19-21] and zeolites [22-24], or slightly mesoporous silica [25, 26] and titania [27, 28]. In order to avoid pore wetting, the water fluxes of inorganic membranes are generally sacrificed relative to desalination using MD. However, despite their market dominance, polymeric membrane still suffer from several issues such as swelling, scaling and poor thermal and chemical resistance, all of which negatively affect the membrane lifetime and performance capabilities [29]. Inorganic membranes, in particular silica membranes, have emerged in the membrane distillation literature for desalination applications. These membranes are prepared from a silica sol-gel method, which is ease of fabrication and effective to tailor the pore size in the microporous (d_p<2nm) and mesoporous ($2 \leq d_p \leq 50$nm) regimes [30]. In general, the silica membrane fabrication comprises three main procedures, (i) the synthesis of silica sol, (ii) dip or spin coating the substrate with the silica sol, and (iii) further thermal treatment including drying and calcination.

The traditional method of preparing silica membranes is by coating a thin silica film on the porous ceramic substrates containing a high quality smooth interlayer. The interlayers help reduce the surface roughness, reduce membrane defects and prevent the silica sol from penetrating too deeply into the substrate during coating [31]. Though deemed necessary, the coating of interlayers onto the support adds additional time and cost to the membrane fabrication process. Recently, Elma et al. [32] reported for the first time the production of interlayer-free silica membranes by carbonising tri-block copolymers in the silica membranes. In a similar recent development on interlayer-free membranes, Liu et al. [33] modified the silica sol-gel synthesis by adding larger silica colloids or 'seeds' to a sol-gel solution which prevented the infiltration of the sol-gel into porous substrates. These membranes were prepared via a conventional thermal processing (CTP), where the calcination process generally follows a very slow ramping and cooling rates (≤ 1 ºC min^{-1}) [34-36] to avoid thermal stress which leads to membrane defects and rendering the membranes ineffective for separation processes.

Another recent advancement was the first demonstration of the use rapid thermal processing (RTP) for membrane tubes by Wang and co-workers [37, 38]. Although RTP has been previously demonstrated for small surface area alumina [39] and silica [40] membranes, the scale up of the RTP method to membrane tubes opened a window of opportunities to greatly reduce the production cost of silica membranes. For instance, CTP silica membranes require multiple coating of silica thin-films to reduce the number of membrane defects [41]. Coupled with CTP's very slow ramping and cooling rates, CTP membranes required at least one week of production time, whilst RTP membranes can be synthesized in less than one day. The advancement of RTP scale up to tube membranes was mainly possible by replacing the conventional silica precursor tetraethyl orthosilicate (TEOS) with an industrial precursor ethyl silicate 40 (ES40). Essentially, ES40 is a partially polymerized TEOS with one to nine silica atoms per oligomer. Further, ES40 proved to be more amenable to rapid thermal processing owing to its improved material stability during thermal consolidation. On account of these desirable features, the ES40 derived membranes by the RTP [37, 38] and CTP [42] methods in literature is still limited, and these have all been prepared on interlayered porous ceramic substrates.

In this work, we report for the first time the preparation of interlayer-free silica membranes using the RTP method and ES40 as silica precursor. This work shows that the conditioning of the ES40 sol-gel is paramount to synthesise interlayer-free membranes by the RTP method directly on α-Al_2O_3 porous substrates. In particular, the effects of the sol-gel pH and thermal treatment (CTP and RTP) on the physico-chemical properties of the silica materials were systematically investigated by nitrogen adsorption, thermal gramimetric analysis and Fourier transform infrared. The membranes were tested using a PV desalination set up for water flux and salt rejection. Desalination testing conditions include varying the feed salt concentrations from pure water (NaCl 0 wt%) to brackish (0.3 wt%) and seawater (3.5 wt%). PV desalination experiments were also carried out at several solution temperatures (25, 40 and 60 °C) to study water mass transfer and the effect of temperature on the stability of the membranes.

5.2 Experimental

5.2.1 Sol-gel synthesis and characterisation

Sol-gels were prepared using ES40 (Wacker Chemicals Australia Pty Ltd), distilled water, ethanol (EtOH, AR grade) and 1 M nitric acid (HNO_3, AR grade, RCI Labscan) by dropwise adding ES40 into the mixed $EtOH/H_2O/HNO_3$ solution under stirring at room temperature for 1 h. The initial

molar ratio of Si (ES40): H_2O: HNO_3 was 4: 44: 0.4. Then ammonia solution (NH_3, 25%, Merck) diluted in EtOH was added to adjust the pH of the solution to 1, 2, 4 and 6, which make up a total EtOH molar ratio of 150. The samples were named by their pH x, where x was the pH value of the sol solution. After stirring for another 2 h at room temperature, the mixture was dried in oven at 60 ℃ for over 4 days to form xerogels. Then, the xerogels were calcined in air by the RTP method where the samples were placed directly into a furnace preheated at 630 ℃ for 1 h. For comparison, conventional thermal processing (CTP) was also carried out for preparing xerogels using a ramp and cool down rate of 1 ℃ min^{-1} from room temperature to 630 ℃ in air with a holding time of 1 h.

The xerogels was characterised by Fourier transform infrared (FTIR) spectroscopy performed by a Shimadzu IRAffinity-1 with a Pike MIRacle diamond attenuated total reflectance (ATR) attachment over a wavenumber range of 4000–600 cm^{-1}. Baseline setting and peak deconvolution of the spectra were performed using the Fityk program based on Gaussian peaks. The intensity of siloxane peak at ~1050 cm^{-1} was normalized to 100% for each spectrum. Nitrogen adsorption was conducted at 77 K using a Micromeritics TriStar 3020 instrument. Samples were degassed at 200 ℃ overnight before each measurement. The specific surface areas were calculated using the Brunner-Emmett-Teller (BET) method. The pore size distributions were determined from the adsorption branch of the isotherms using Density Functional Theory (DFT) assuming cylindrical pores with an oxide surface. A Thermo-gravimetric differential scanning colorimetric analysis TGA-DSC1 (Mettler Toledo) was used for the TGA analysis of xerogel samples. The testing conditions for all measurements were set at air flow rate of 60 ml min^{-1} and dwell time of 60 min at 630 ℃. The ramping rates were 100 ℃ min^{-1} for RTP and 1 ℃ min^{-1} for CTP.

5.2.2 Membrane preparation and testing

Dip-coating was conducted on macroporous α-Al_2O_3 substrate (Ceramic Oxide Fabricators, Australia) which were pre-calcined at 1000 ℃ for 8 h with a ramp rate of 5 ℃ min^{-1} to enhance mechanical strength and remove organic impurities. The substrate was dip-coated in the prepared sols with a dwell time of 1 min and dipping and withdrawal speed of 10 and 5 cm min^{-1}, respectively. The membrane was then dried at 60 ℃ for 30 min followed by calcination at 630 ℃ for 1 h using the RTP method as described in [37]. Once cooled, the dip coating and calcination process was repeated again (i.e. 2 membrane layers in total) to reduce the risk of membrane defects. Morphological features of the membranes were examined using a Jeol JSM-7001F SEM with a hot (Schottky) electron gun at accelerated voltage of 10kV.

Desalination performance was measured using a pervaporation custom rig as schematically shown in Figure 5.1. The outer shell of the membranes was contacted by the feed solution in a large beaker (1 L) whilst the inner shell (i.e. permeate line) was kept under constant vacuum (< 1 Pa). In order to avoid salt built up on the membrane surface, which may cause concentration polarization, the feed salt solution was under vigorous stirring at 1000 rpm, resulting in a turbulent flow regime around the membrane tube. The feed saline solution was prepared from sodium chloride (Sigma-Aldrich) at salt concentration ranging from 0 to 3.5 wt%. The beaker containing the feed salt solution was placed on a hot plate and the testing temperatures were controlled via a thermocouple. The water vapour in the permeate line was collected in a liquid nitrogen cooled condenser to ensure to capture all the vapour water diffused through the membrane. The water flux (F) was calculated from the equation $F=m/A\,t$, where m is the mass of permeate, A is active area of the testing membrane and t is the collection time. The salt rejection (R) was calculated from $R=(C_f\text{-}C_p)/C_f \times 100\%$, where C_f and C_p are the salt concentration of the feed side and permeate side, respectively, which were determined by the conductivities measured by a labCHEM CP conductivity meter using a standard curve.
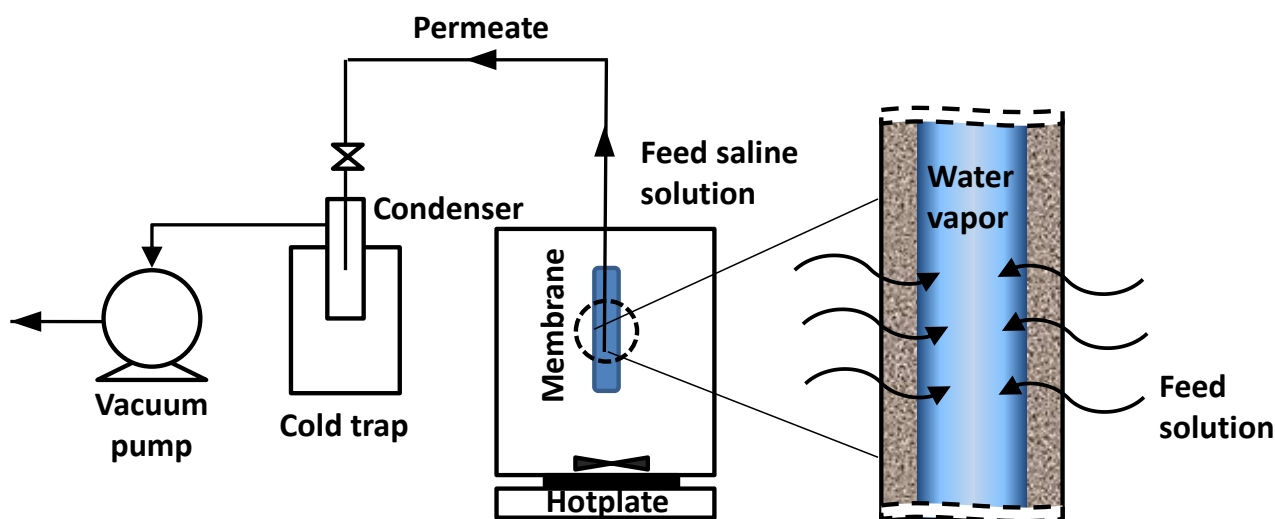
Figure 5.1 Schematic of the pervaporation set up for desalination.

5.3 Results and discussion

5.3.1 Material characterisation
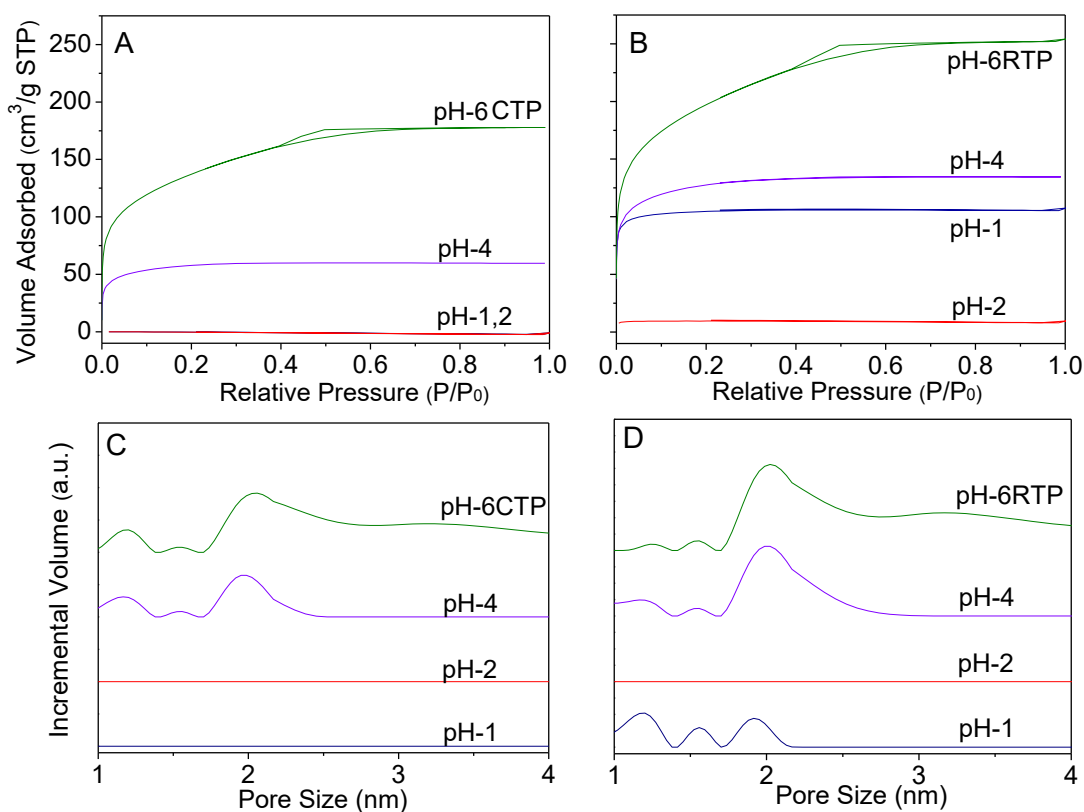
Figure 5.2 Nitrogen adsorption (A and B) and DFT pore size distribution (C and D) for the CTP and RTP xerogels.

Initially the xerogels were analysed by taking into consideration of gelling methods via CTP (slow calcination rate) and RTP (extremely fast calcination rate). This approach provides a comparison between the two calcination methods, coupled with the fact that there is a vast literature body on CTP, but non-existent for porous ES40 derived silicas by RTP. Nitrogen adsorption isotherms in Figures 5.2A and 5.2B show some notable trends. Figure 5.2A shows that (i) pH 6 xerogels became mesoporous structures, with a hysteresis at 0.4 <p/p_o<0.65, (ii) pH 4 xerogels gave type I isothermes, a characteristic of microporous materials, and (iii) pH 2 gave dense structures (almost no nitrogen adsorption) for both CTP and RTP xerogels. The different trends are related to pH 1 xerogels, where the CTP samples were dense whilst the RTP samples were microporous. Further, the RTP method delivered xerogels with higher total pore volumes for all pH samples, irrespective if the structures were mesoporous, microporous or dense. The DFT pore size distribution based on the nitrogen adsorption curves are shown in Figures 5.2C and 5.2D. Apart from the dense samples, the general trend is that all samples resulted in a ternary pore size distribution, thus demonstrating the amorphous nature of porous silica derived from sol-gel process. The ternary pore size distribution are also in line with the work of Duke and co-workers [43] who reported this type of distribution for silica materials derived from tetraethyl orthosilicate (TEOS) by using positron annihilation spectroscopy. For pH 4 and 6 samples, the overall trend is that RTP method led to a

slightly broader pore size distribution than the CTP method, however the overall distribution profile are quite similar.

Figure 5.3 shows the BET surface areas as a function of the xerogel pH values for CTP and RTP at 630 ℃. Apart from the variation at pH 1 samples (also observed in Figures 5.2A and 5.2B), there is a consistent trend that increasing the pH from 2 to 6 leads to an increase in surface area. The surface areas of RTP samples are generally higher than those of the equivalent CTP silica xerogels. For examples, at 630 ℃, the surface area of pH 4 and 6(RTP) xerogels were measured at 439 and 700 $m^2 g^{-1}$, which are 120% (pH4) and 43% (pH6) higher than the CTP method. In order to understand the effect of temperature on structural formation, xerogels were also prepared by RTP at 400 ℃, except for pH 2 which were not considered due to their dense structural formation. It is also noteworthy that increasing the RTP temperature from 400 to 630 ℃ consistently reduced the surface area of the xerogels for the pH 1, 4 and 6. This suggest that the densification of the gels is enhanced by thermal effect which causes an increase in the volumetric strain of the network as a result of further evaporation of the remaining solvent from the ES40 gels [44].
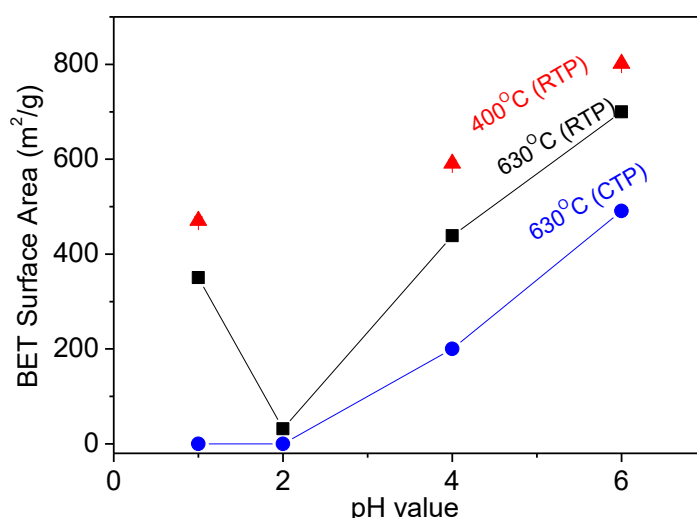
Figure 5.3 BET surface areas of CPT and RTP samples as a function of pH.

The lack of porosity in the RTP pH 2 samples is interesting, though it is consistent with the CTP pH 2 samples. It would be generally expected the production of porous materials at these acidic conditions for silica materials, although there is a single example of dense ES40 derived silica xerogels conventionally dried in an oven [45]. It should be mentioned that in that study, a different sol-gel preparation method with a H_2O:Si ratio of 14:4 was employed, which was much lower than 44:4 used in this work. It is hypothesized that due to the iso-electric point of silica surfaces is at approximately pH ~2 [30], the formation of charged silica species is at a minimum. This means that

the silicon atoms are neither electrophilic nor nucleophilic by nature, and thus are not reactive towards other water or silanol species in the sol-gel system. In other words, at the point of zero charge (pH ~2), there is no promotion of hydrolysis and condensation reactions, which would probably lead to smaller oligomeric species. On account of this process, the silica network is anticipated to pack more densely during thermal consolidation as evidenced by Figures 5.2 and 5.3.
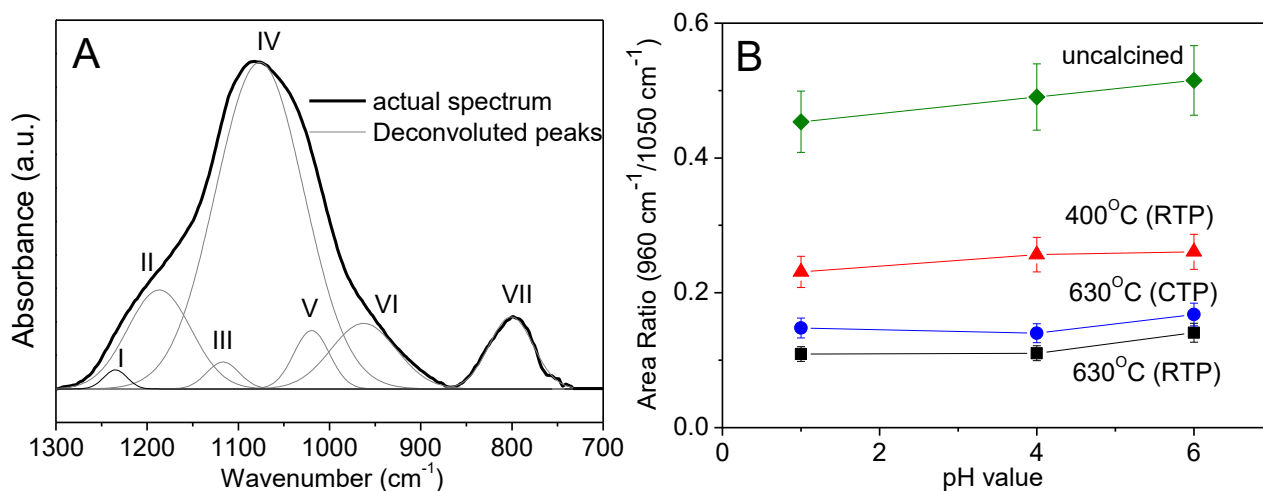
Figure 5.4 Representative FTIR spectrum with deconvoluted peaks (B) and comparative FTIR ratios of silanol to siloxane of CTP and RTP silica xerogels.

The functional groups of the microporous silica matrices were investigated by FTIR-ATR analyses. Figure 5.4A displays a representative FTIR spectrum in the range of $1400 - 600$ cm^{-1} for the silica derived xerogels. In order to further analyze the subtle differences in the chemical compositions of these xerogels in each series, deconvolution of the overlapping peaks was performed using the Fityk program. The deconvoluted peaks at ~1235 (peak I) and 1065 cm^{-1} (peak IV) are assigned to the longitudinal optical (LO)-transverse optical (TO) splitting mode of anti-symmetric stretching vibration of 6-ring siloxane, while the absorption vibrations at ~1200 (peak II) and 1150 cm^{-1} (peak III) correspond to the LO-TO mode of 4-ring siloxane, the fitted peak at ~1020 cm^{-1} (peak V) is attributed to the chain and sheet silicates , and the peak at ~800 cm^{-1} (peak VII) is assigned to the stretching mode of symmetric siloxane [46, 47]. Semi-quantitative analysis was conducted using the relative vibrational absorption of the uncondensed silanol (peak VI; 960 cm^{-1}) to the condensed siloxane (major peak IV; 1050 cm^{-1}) groups, of which the peak are ratio is used as an indicator of the degree of condensation. As depicted in Figure 5.4B, the Si–OH/Si–O–Si area ratio varied slightly with increasing pH, though the difference is not very evident and sits within the range of error. However, it is noteworthy that the RTP method delivered a higher concentration of siloxane species as compared to the silanol groups indicating that condensation reaction is favoured. On the

other hand, the CTP method produced a slightly higher concentration of silanol species leading to a less condensed network. The decrease of silanol groups with increasing RTP temperature (uncalcined, 400 and 630 °C) demonstrates the silica structures undergo an ongoing process of condensation and partial densification (Figure 5.3) during the thermal treatment. The FTIR results (Figure 5.4B) clearly indicate that the RTP method led to more siloxane bridges as compared to the CTP method.

To further understand the thermal effect during calcination, TGA results in Figure 5.5 show the mass loss of ES40 as-prepared gels exposed of very fast ramping rates as RTP and slow ramping rate as CTP to simulate the respective thermal processes. It is noteworthy that the mass loss profiles differ significantly between CTP and RTP irrespective of the xerogel's pH. A consistent trend in all the CTP samples is clearly observed at the onset of mass loss up to 100 °C, which is mainly attributed to physisorbed water trapped in the porous structure of the silica films [48]. In fact, the mass loss calculated at 100 °C is constant for samples in both the CTP and RTP methods as a function of pH (Figure 5.5D). The difference here is that the overall mass loss for RTP samples is only ~2.3 wt%, which is very marginal as compared that of ~17 wt% for the CTP samples at 100 °C. There is also a mass loss lag of 50-75 °C up to ~260-275 °C for the RTP method. This lag is most likely associated with heat transfer into the xerogel as the RTP ramping rate of 100 °C min^{-1} is 100 times higher than that of CTP method.

Nevertheless, it is also noteworthy the differences in mass loss pathways as a result of different pH condition. The pH 1 RTP xerogel final mass loss was significantly lower than the CTP xerogels, contrary to that of the pH 6 xerogel samples. It is interesting to note that the mass loss of the RTP xerogels has a pronounced sharp drop near 275 °C, which is much accentuated in the pH 6 samples. This result shows that a large amount of volatile species are released at this temperature point, despite that all of the samples were prepared using the same amount of the solvents in the initial sol preparation. Similarly, the CTP samples show the same pattern of profile but at a lower temperature of approximately 200 °C.

In principle, it could be assumed that the RTP method would cause a very fast solvent evaporate rates, due to the rapid exposure of very high temperatures at the onset of calcination, and should induce high capillary stresses which in turn would significantly densify the amorphous silica structure. However, this is not supported by the initial mass loss pattern of the RTP samples prior to 200 °C due to the mass loss lagging behaviour. Furthermore, the mass loss of the pH 6 RTP samples is significantly larger than that of the CTP samples as shown by a 50% final mass post 300 °C

inferring structural densification. Yet it is the most porous sample with the highest pore volume and surface area (Figure 5.3). Therefore, these results indicate that the matrix for this sample undergoes a significant degree of both chemical and physical restructuring. This is consistent with the FTIR results (Figure 5.4B), which clearly supports that the RTP method led to an increased formation of siloxane bridges, which oppose capillary densification, as compared to the CTP method.
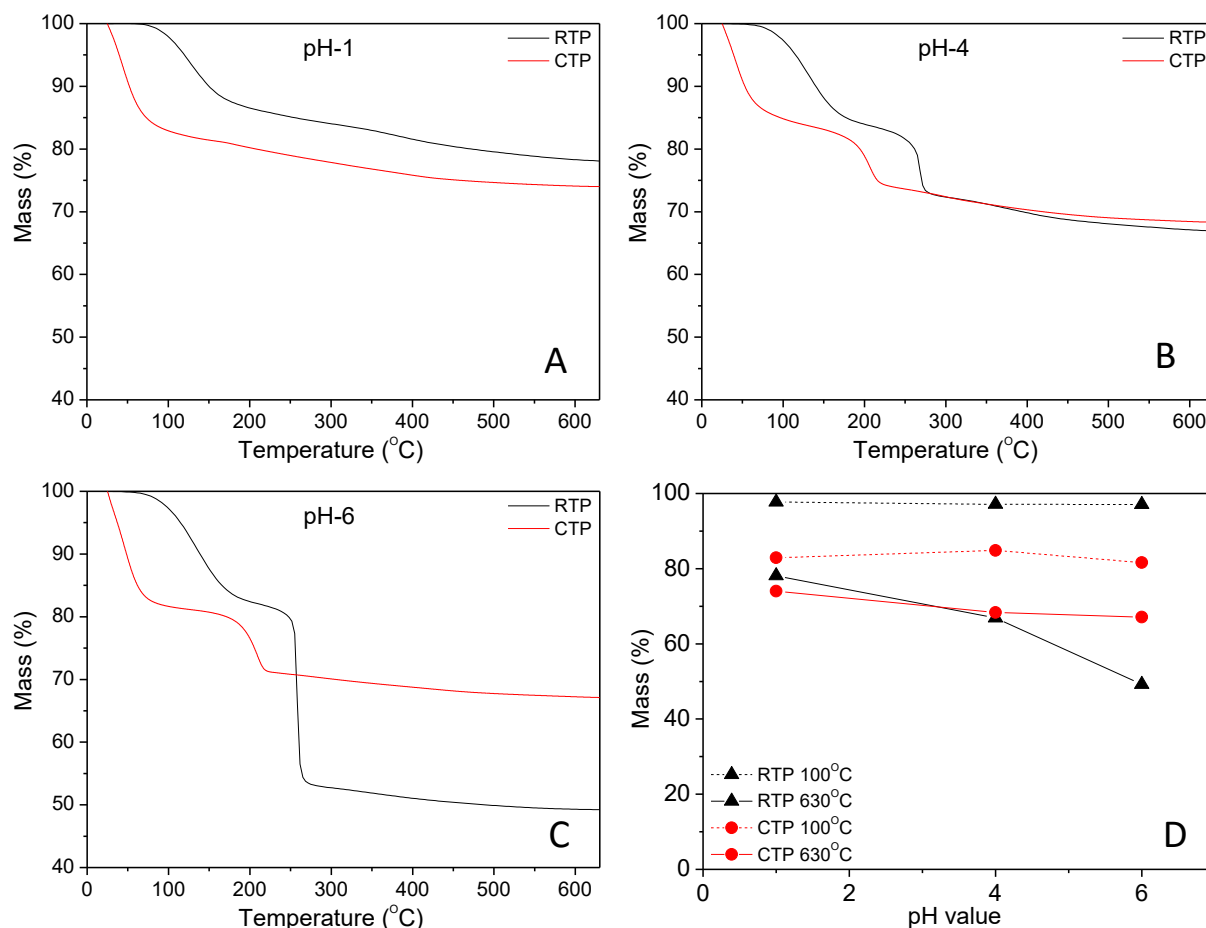
Figure 5.5 (A, B and C) Mass loss profiles as a function of xerogel pH, and (D) mass loss profile of RTP (100 °C min⁻¹) and CTP (1 °C min⁻¹) xerogel samples with respective to temperature.

5.3.2. Membrane performance

Interlayer-free membranes containing two silica layers only were prepared by the RTP method. The pH 6 sols were relatively viscous and had to be diluted with EtOH just before dip coating. This was necessary as the original sol viscosity was too high and produced membrane layers that were too thick and subsequently cracked under RTP method. The best final molar ratio of EtOH:Si is 255:4 after dilution with EtOH. Membranes prepared with pH 1 and pH 2 failed as part of the thin films

flaked off from the α-Al$_2$O$_3$ porous substrates. These membranes were also tested for desalination though significant pore wetting occurred at the onset of the experimental work, thus confirming that the pH 1 and pH 2 membranes had inherent major defects. Therefore, pH 4 and pH 6 membranes with a EtOH:Si dilution of 255:4 were successfully prepared and tested for desalination.
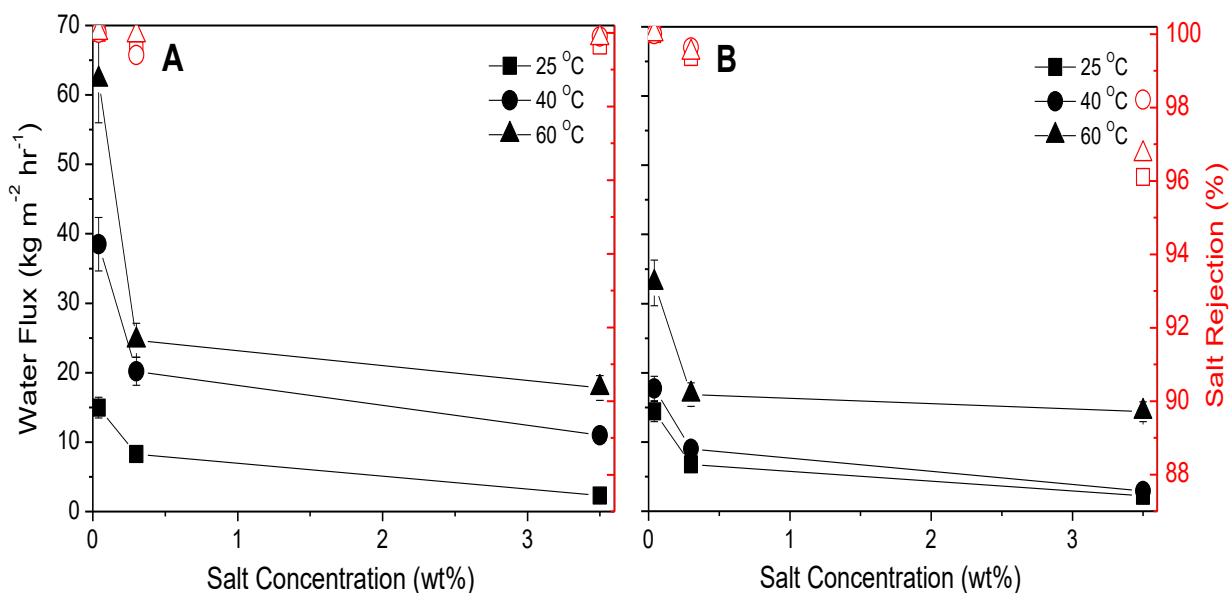
Figure 5.6 Water flux ($\pm$10) and salt rejection ($\pm$1) for membranes (A) pH 4 and (B) pH 6 as a function of salt concentration and feed temperature.

Figures 5.6A and 5.6B show the desalination performance of the pH4 and pH6 membranes for pure water, brackish water (NaCl 0.3 wt%) and sea water (NaCl 3.5 wt%) concentrations. Several points of interest should be noted for the results in these figures. Firstly, the salt rejection is over 99% for pH 4 membrane irrespective of salt concentration or temperature. The same cannot be said about pH 6 membrane as salt rejection decreased to 96%, though this performance is still considered very good. Secondly, the water flux increases as a function of temperature. This is associated with the evaporation process during PV desalination which is driven by the pressure difference across the membrane between the feed side and permeate side. Hence, the increase in temperature raises the vapour pressure in the feed side, thus producing larger vapour pressure gradient and higher water flux. There is a large drop in water flux as the salt concentration was raised from 0 to 0.3 wt%, followed by a minor reduction for seawater (3.5 wt%) concentration. This effect has been previously reported for silica membranes [49] and associated with concentration and/or temperature polarisation effect. This work, in addition to previous similar works on silica membranes, was carried out under similar testing conditions of Reynolds number of 90,000. In principle, concentration polarization should not be a concern at high Reynolds number [50], where the

concentration of the salt on the external membrane surface should have been disturbed and thoroughly mixed with water by the turbulent regime. Therefore, the reduction of water fluxes observed in this work, as previously associated with concentration polarization, is probably attributed to the ability of hydrophilic silica surfaces to adsorb hydrated ions. This was demonstrated by de Lint and co-workers [51] for the retention of of Na^+ and Cl^- ions on silica membranes coated on γ-alumina substrates. Therefore, hydrated ions are likely to block the pore entrance of the microporous silica, and hinder the diffusion of water through the membrane.
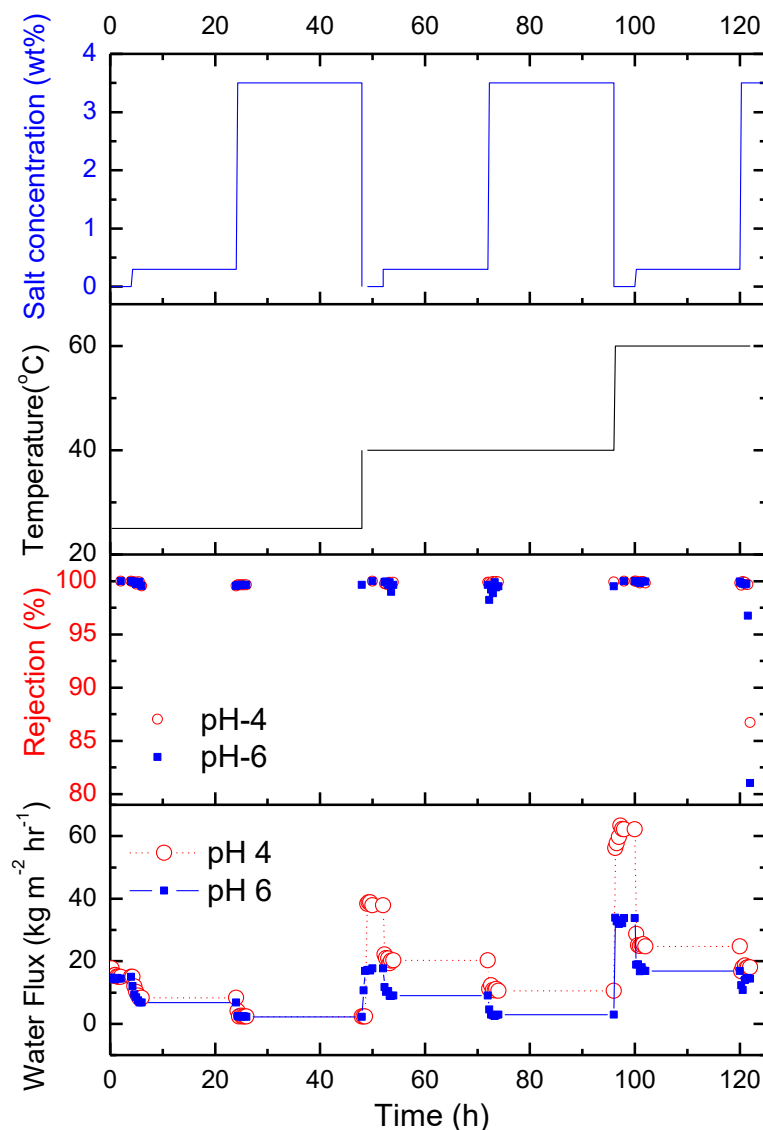
Figure 5.7 –120 h performance of pH 4 and pH 6membranes in terms of water flux (± 10%) and salt rejection (±1%).

Figure 5.7 show extended desalination operation of the pH4 and pH 6 membranes under various conditions of salt concentration and temperature. Both membranes delivered constant performance for each set of testing conditions until 120 h. Interestingly, the salt rejection was very high at 99%

up to 120 h, when salt rejection started to decrease. In principle, salt does not evaporate under the given conditions in this work. The reason for salt being measured from the permeate water collected in the cold trap is associated with hydrated ions being entrained into the water vapour molecules. In turn, this is given an indication that the ES40 derived matrix has been altered due to the interactions between the hydrophilic silica and water. The classical sol-gel science reported by Iler [52] describes that silanol groups form less rigid structure within the silica matrix which are less stable and interact with water molecules. Likewise silica rehydration occurs, where siloxane bridges break down forming silanol groups [53]. Many of these silanol groups become unconstrained and mobile when exposed to water, thus broadening the pore sizes of silica structures [54]. Therefore, the reduction in salt rejection after 120 h operation, coupled with the silanol groups (see Figure 5.4), confirms that water has irretrievably affected the silica matrix.
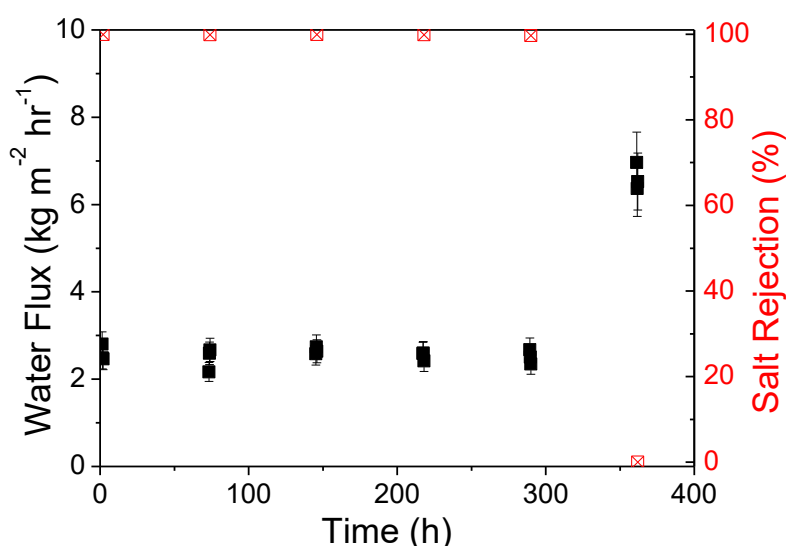
Figure 5.8 Water flux and salt rejection at NaCl 3.5 wt% at room temperature for membranes (A) as a function of the EtOH:Si dilution ratio, and (B) EtOH:Si of 200:4 for 350 h operation.

The interlayer-free RTP membranes prepared with pH 4 gave the best sol-gel condition and the effect of EtOH:Si in the preparation of membranes was further investigated. The membranes prepared with EtOH:Si of 200:4 and 150:4 delivered water fluxes of 1.80 and 1.45 kg m^{-2} h^{-1}, respectively, slightly lower than 2.32 kg m^{-2} h^{-1} for the 255:4 membrane (Figure 5.7). In Figure 5.8, the membrane prepared with EtOH:Si of 200:4 was further tested for 350 h operation at a single testing condition of NaCl 3.5 wt% at room temperature. This time the membrane was stable up to 300 hours delivering constant water fluxes of ~2.5 kg m^{-2} h^{-1} and ~99% salt rejection. At 350 h the membrane failed due to pore wetting. The improved long term operation of the 200:4 membranes

was attributed to its sol-gel being slightly more viscous than the 255:4 sol, so possibly forming a slightly thicker silica film. Another possibility is the effect of temperature which may have accelerated the degradation of membranes prepared with the EtOH:Si dilution ratio of 255:4, when it was tested at 60 ℃ for 120 h. Similar temperature degradation effect was also observed for alumina-silicate zeolites for desalting water [55].
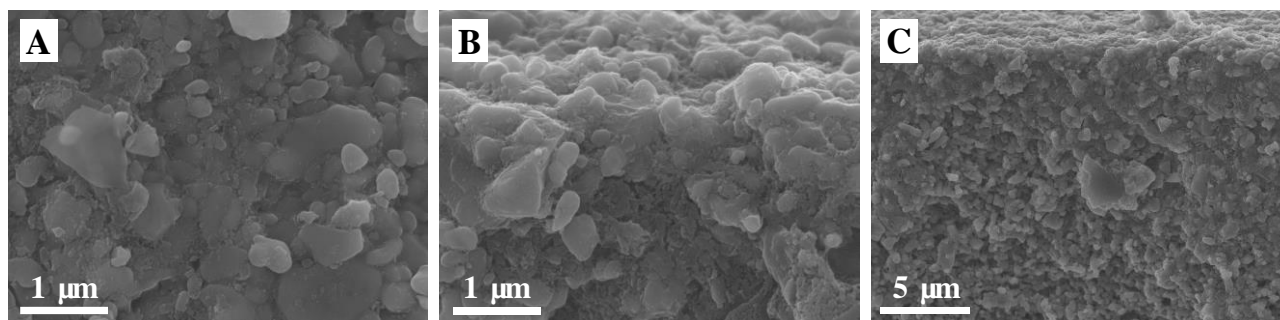
Figure 5.9 SEM images of (A) top surface, (B) and (C) cross sections also showing the top surface of the RTP interlayer free silica membranes.

Representative SEM images of the cross section of the RTP interlayer-free silica membrane are displayed in Figure 5.9. The porous α-Al$_2$O$_3$ porous substrates (Figure 5.9A) shows smooth surface particles ran 0.15 to 1.00 μm. The RTP interlayer-free membrane in Figure 5.9B shows that a top-film had not been formed. Indeed, the particles on the top surface of the substrate are clear demonstrating a rough surface. However, the cross-section displays a deep impregnation of the sol-gel, which filled the inter-particle spaces, though there are a few regions which show medium (0.03 to 0.11 μm) and large (0.20 μm) size pores. Due to the high salt rejections (up to 99%), these pores are not deemed to be connected, otherwise poor salt rejections could be induced. As such, the membrane structure was mainly controlled by small constrictions which hindered the passage of hydrated ions by pore size exclusion. It is interesting to observe how deep the sol-gel penetrated into the porous substrates. This is more evident in Figure 5.9C which shows a silica impregnation thickness of ~3.3 to ~5 μm. The impregnated silica structures into the α-Al$_2$O$_3$ porous substrate is a departure from the conventional methods of silica membranes by either CTP or RTP with substrates containing interlayers, where previous works resulted in the formation of thin-films with thicknesses of < 0.5 μm [56-58]. Apart from dispensing with costs associated with interlayer preparation, the RTP interlayer-free method in this work produced membranes in less than 3 hours with only 2 dipping-calcination cycles. This is a significant advantage over the CTP silica membranes, which typically require up to 10-14 days of fabrication. Furthermore, this work paves the way for the preparation of interlayer-free RTP membranes, where further silica structure

stability can be conferred by incorporating polymer additives or hydrophobic organic component as stabilizers for desalination applications.

The deep impregnation is caused the initial high capillary forces upon contact of a liquid (sol) with and a dry porous surface (substrate). As the solid substrate contains large pores, similar to capillaries, the liquid is immediately drawn into the substrate induced by the wetting force. This is the forces of attraction between liquid and solid and is the pressure difference across the liquid-gas interface as described by the well-known Laplace equation, $P_L = 2\gamma \cos\theta/r$, where γ is surface tension of the liquid, θ the contact angle, and r the pore radius [59]. As time progresses, the wetting force is reduced as free energy of liquid-solid interface takes over, at which point an equilibrium is reached. Therefore, further liquid inhibition is not realised [60].
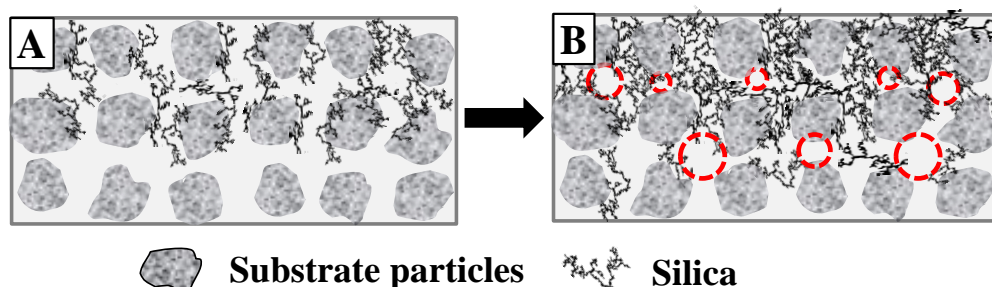
Figure 5.10 Conceptual schematic of the interlayer-free RTP membrane (A) first and (B) second dip coating steps.

Upon the first RTP calcination, the integrity of the membrane to reject salt was not achieved, thus confirming an inhomogeoues pore size distribution containing several large pores leading to pore wetting. Superior pore size control and pore wetting avoidance was achieved upon the second dip-coating RTP calcination, as confirmed by the high salt rejection in Figure 5.6. The structural evolutions of the membranes upon each RTP calcination step are schematically represented in Figure 5.10. The first dip-coating step led to the deep impregnation of the ES40 sol-gel as observed in Figure 5.9C. This led to the formation of a very porous silica structure. The second dip-coating step led to the formation of a top thick ES40 silica film. This is therefore the silica layer with the molecular dimensions to reject hydrated ion salts by size hindrance. The interlayer-free approach using ES40-derived silica membranes is presented for the first time in this work. ES40 played an important role as the oligomeric chains of silica species are prone to undergo cluster-cluster growth and confer higher degree of condensation [61]. In turn, the RTP method increased the degree of condensation over the CTP method, as evidenced by the relative increased formation of silanane bridges (Si–O–Si) over uncondensed silanol (Si–OH) groups. As a result, ES40 sol-gel synthesis in

this work, coupled with the RTP method, led to the formation of larger silica species in the sols and stronger polymeric network, which were able to resist drying stresses during rapid thermal consolidation within the α-Al$_2$O$_3$ porous substrate.

5.4 Conclusions

This work demonstrates for the first time the preparation of interlayer-free silica membranes by the RTP method. Besides the cost and time associated with interlayer preparation, the RTP interlayer-free method in this work produced membranes in less than 3 hours with only 2 dipping-calcination cycles. This achievement was realised by a systematic study of the sol-gel synthesis and using ES40 as a silica precursor. RTP ES40 xerogels formed structures with high surface area and siloxane bridges as compared to the analogous CTP ES40 xerogels. RTP resulted in water being retained inside the xerogel pores at higher temperatures, thus favouring the condensation reactions and formation of siloxane bridges. The pH of the sol-gel played an important role in the preparation of interlayer-free membranes, as pH 4 and 6 sols formed membranes with capabilities to avoid pore wetting and given high salt rejection. The best interlayer-free RTP silica membrane was prepared with a pH4 sol obtained, which reached high water fluxes of 17.8 kg m^{-2} h^{-1} at 60 ℃ and high salt reject (>99%) for desalination of 3.5 wt% sea water. The dilution of the sol with ethanol also played an important role, as pH4 membranes prepared with EtOH:Si ratio of 255:4 were stable for 120 h, whilst change this ratio to 200:4 increase the stability to 300 h. This improvement was attributed to thicker films derived from more viscous sols. Furthermore, this work paves the way for the preparation of interlayer-free RTP membranes, where further silica structure stability can be conferred by incorporating polymer additives or hydrophobic organic component as stabilizers for desalination applications.

References

[1]   S.J. Murray, P.N. Foster, I.C. Prentice, Future global water resources with respect to climate change and water withdrawals as estimated by a dynamic global vegetation model, J. Hydrology 448-449 (2012) 14-29.

[2]   A. M. Helal, A. Al-Jafri, A. Al-Yafeai, Enhancement of existing MSF plant productivity through design modification and change of operating conditions, Desalination 307 (2012) 76-86.

[3]   T.H. Dandah, A. Mitsos, Structural optimization of seawater desalination: I. A flexible superstructure and novel MED-MSF configurations, Desalination 344 (2014) 252-265

[4]   M.M. Alhazmy, Economic and thermal feasibility of multi stage flash desalination plant with brine-feed mixing and cooling , Energy 76 (2014) 1029-1035.

[5]   A. Rodriguez-Calvo, G.A. Silva-Castro, F. Osorio, J. González-López, C. Concepción Calvo, Reverse osmosis seawater desalination: current status of membrane systems, Desalination Water Treatm. 56 (2015) 849-861.

[6]   N. Misdan, A.F. Ismail, N. Hilal, Recent advances in the development of (bio)fouling resistant thin film composite membranes for desalination, Desalination 380 (2016) 105-111.

[7]   O.S. Burheim, F. Seland, J. G. Pharoah, S. Kjelstrup, Improved electrode systems for reverse electro-dialysis and electro-dialysis , Desalination 285 (2012) 147-152.

[8]   Y. Tanaka, Ion-exchange membrane electrodialysis program and its application to multi-stage continuous saline water desalination, Desalination 301 (2012) 10-25.

[9]   R.L. Zornitta, J.J. Lado, M.A. Anderson, L.A.M. Ruotolo, Effect of electrode properties and operational parameters on capacitive deionization using low-cost commercial carbons, Sep. Pur. Technol. 158 (2016) 39-52.

[10]   T.-W. Kim, Y. Kim, C. Yun, H. Jang, W. Kim, S. Park, Systematic approach for draw solute selection and optimal system design for forward osmosis desalination, Desalination 284 (2012) 253-260.

[11]   M. Qasim, N.A. Darwish, S. Sarp, N. Hilal, Water desalination by forward (direct) osmosis phenomenon: A comprehensive review, Desalination 374 (2015) 47-69.

[12]   W. An, X. Zhou, X. Liu, P.W. Chai, T. Kuznicki, S.M. Kuznicki, Natural zeolite clinoptilolite-phosphate composite Membranes for water desalination by pervaporation, J. Membr. Sci. 470 (2014) 431-438

[13]   E. Guillen-Burrieza, G. Zaragoza, S. Miralles-Cuevas, J. Blanco, Experimental evaluation of two pilot-scale membrane distillation modules used for solar desalination, J. Membr. Sci. 409 (2012) 264-275

[14]   A.D. Khawaji, I.K. Kutubkhanah, J.-M. Wie, Advances in seawater desalination technologies, Desalination 221 (2008) 47-69.

[15]   A. Subramani, J.G. Jacangelo, Treatment technologies for reverse osmosis concentrate volume minimization: A review, Sep. Purif. Technol. 122 (2014) 472-489.

[16]   M. Khayet, Membranes and theoretical modeling of membrane distillation: A review, Adv. Coll. Interface Sci. 164 (2011) 56-88.

[17]   Alkhudhiri, N. Darwish, N. Hilal, Membrane distillation: A comprehensive review, Desalination 287 (2012) 2-18.

[18]   P. Shao, R.Y.M. Huang, Polymeric membrane pervaporation, J. Membr. Sci. 287 (2007) 162-179.

[19]   M.C. Duke, S. Mee, J.C. Diniz da Costa, Performance of porous inorganic membranes in non-osmotic desalination, Water Res. 41 (2007) 3998-4004.

[20]   T. Tsuru, R. Igi, M. Kanezashi, T. Yoshioka, S. Fujisaki, Y. Iwamoto, Permeation properties of hydrogen and water vapor through porous silica membranes at high temperatures, AIChE J. 57 (2011) 618-629.

[21]   C.X.C. Lin, L.P. Ding, S. Smart, J.C. Diniz da Costa, Cobalt oxide silica membranes for desalination, J. Coll. Interface Sci. 368 (2012) 70-76

[22]   M.C. Duke, J. O'Brien-Abraham, N. Milne, B. Zhu, J.Y.S. Lin, J.C. Diniz da Costa, Seawater desalination performance of MFI type membranes made by secondary growth, Sep. Purif. Technol. 68 (2009) 343-350.

[23]   B. Zhu, L. Zou, C.M. Doherty, A.J. Hill, Y.S. Lin, X. Hu, H. Wang, M. Duke, Investigation of the effects of ion and water interaction on structure and chemistry of silicalite MFI type zeolite for its potential use as a seawater desalination membrane, J. Mater. Chem. 20 (2010) 4675-4683.

[24]   C.H. Cho, K.Y. Oh, S.K. Kim, J.G. Yeo, P. Sharma, Pervaporative seawater desalination using NaA zeolite membrane: Mechanisms of high water flux and high salt rejection, J. Membr. Sci. 371 (2011) 226-238.

[25]   Y.T. Chua, C.X.C. Lin, F. Kleitz, X.S. Zhao, S. Smart, Nanoporous organosilica membrane for water desalination, Chem. Comm. 49 (2013) 4534-4536.

[26]   Y.T. Chua, C.X.C. Lin, F. Kleitz, S. Smart, Synthesis of mesoporous carbon–silica nanocomposite water-treatment membranes using a triconstituent co-assembly method, J. Mater. Chem. A 3 (2015) 10480–10491.

[27]   T. Tsuru, K. Ogawa, M. Kanezashi, T. Yoshioka, Permeation Characteristics of Electrolytes and Neutral Solutes through Titania Nanofiltration Membranes at High Temperatures, Langmuir 26 (2010) 10897-10905.

[28]   C. Yacou, S. Smart, J. C. Diniz da Costa, Mesoporous TiO2 based membranes for water desalination and brine processing, Sep. Purif. Technol. 147 (2015) 166-171.

[29]   L.F. Greenlee, D.F. Lawler, B.D. Freeman, B. Marrot, P. Moulin, Reverse osmosis desalination: Water sources, technology, and today's challenges, Water Res. 43 (2009) 2317-2348.

[30]   C.J. Brinker, G.W. Scherer, Sol-gel science: the physics and chemistry of sol-gel processing, Academic Press, Boston, 1990.

[31]   C.J. Brinker, G.C. Frye, A.J. Hurd, C.S. Ashley, Fundamentals of sol-gel dip coating, Thin Solid Films 201 (1991) 97-108.

[32]   M. Elma, D.K. Wang, C. Yacou, J.C. Diniz da Costa, Inter layer-free P123 carbonised template silica membranes for desalination with reduced salt concentration polarisation tages, J. Membr. Sci. 475 (2015) 376-383.

[33]   L. Liu, D.K. Wang, D.L. Martens, S. Smart, J.C. Diniz da Costa, Interlayer-free microporous cobalt oxide silica membranes via silica seeding sol–gel technique, J. Membr. Sci. 492 (2015) 1-8

[34]   B. N. Nair, T. Yamaguchi, T. Okubo, H. Suematsu, K. Kaizer, S. I. Nakao, Sol-gel synthesis of molecular sieving silica membranes, J. Membr. Sci. 135 (1997) 237-243.

[35]   M. Duke, J. C. Diniz da Costa, G. Q. Lu, P. Grey, M. Petch, Carbonised Template Molecular Sieve Silica Membranes In Fuel Processing Systems: permeation, hydrostability and regeneration, J. Membr. Sci. 241 (2004) 325-333.

[36]   R. Igi, T. Yoshioka, Y.H. Ikuhara, Y. Iwamoto, T. Tsuru, Characterization of Co Doped Silica for Improved Hydrothermal Stability and Application to Hydrogen Separation Membranes at High Temperatures, J. Am. Ceramic Soc. 91 (2008) 2975-2981

[37]   D. K. Wang, J. C. Diniz da Costa, Simon Smart, Development of Rapid Thermal Processing of Tubular Cobalt Oxide Silica Membranes for Gas Separations, J. Membr. Sci. 456 (2014) 192–201.

[38]   D. K. Wang, J. Motuzas, J. C. Diniz da Costa, S. Smart, Rapid Thermal Processing of Tubular Cobalt Oxide / Silica Membranes, I. J. Hydrogen Energy 38 (2013) 7394-7399.

[39]   M. C. Schillo, I. S. Park, W. V. Chiu, H. Verweij, Rapid thermal processing of inorganic membranes, J. Membr. Sci. 362 (2010) 127-133.

[40]   E. J. Kappert, A. Nijmeijer A, N. E. Benes, Expeditious calcination of inorganic membranes by an instant temperature increment, Microporous Mesoporous Mater. 151 (2012) 211-215.

[41]   R.M. de Vos, H. Verweij, Improved performance of silica membranes for gas separation, J. Membr. Sci. 143 (1998) 37-51.

[42]   C. R. Miller, D. K. Wang, S. Smart, J. C. Diniz da Costa, Reversible Redox Effect on Gas Permeation of Cobalt Doped Ethoxy Polysiloxane (ES40) Membranes, Scientific Reports 3 (2013) 1648.

[43]   M. C. Duke, S. J. Pas , A. J. Hill, Y. S. Lin, J. C. Diniz da Costa, Exposing the Molecular Sieving Architecture of Amorphous Silica Using Positron Annihilation Spectroscopy, Adv. Funct. Mater. 18 (2008) 3818–3826.

[44]   G.W. Scherer, Sintering of Sol-Gel Films, J. Sol-Gel Sci. Technol. 8 (1997) 353-363.

[45]   S. Wang, D. K. Wang, S. Smart, J. C. Diniz da Costa, Ternary Phase-separation Investigation of Sol-Gel Derived from Ethyl Silicate 40. Scientific Reports 5 (2015) 14560.

[46]   A. Bertolluzza, C. Gagnano, M. A. Morelli, V. Gottardi, M. Guglielmi, Raman and Infrared spectra of silica gel evolving toward glass, J. Non-Cryst. Solids 48 (1982) 117-128.

[47]   A. Duran, C. Serna, V. Fornes, J. M. Fernandez Navarro, Structural considerations about SiO2 glasses prepared by sol-gel, J. Non-Cryst. Solids 82 (1986) 69-77.

[48]   J.M. Kim, S.M. Chang, S.M. Kong, K.-S. Kim, J. Kim, W.-S. Kim, Control of hydroxyl group content in silica particle synthesized by the sol-precipitation process, Ceram. Int. 35 (2009) 1015-1019.

[49]   M. Elma, D. K. Wang, C. Yacou, J. Motuzas, J. C. Diniz da Costa, High performance interlayer-free mesoporous cobalt oxide silica membranes for desalination applications, Desalination 365 (2015) 308–315.

[50]   Y.T. Chua, G. Ji, G. Birkett, C.X.C. Lin, F. Kleitz, S. Smart, Nanoporous organosilica membrane for water desalination: theoretical study on the water transport, J. Membr. Sci. 482 (2015) 56-66.

[51]   W.B.S. de Lint, T. Zivkovic, N.E. Benes, H.J.M. Bouwmeester, D.H.A. Blank, Electrolyte retention of supported bi-layered nanofiltration membranes, J. Membr. Sci. 277 (2006) 18–27.

[52]   R. K. Iler, The Chemistry of Silica: Solubility, Polymerization, Colloid and Surface Properties, and Biochemistry, Wiley, New York 1979, pp. 622

[53]   A. E. Burneau, J.-P. Gallas, in The Surface Properties of Silicas (Ed: A. E. Legrand),Wiley, Chichester, UK 1998, pp. 147–234.

[54]   M.C. Duke, J.C. Diniz da Costa, D.D. Do, P.G. Gray, G.Q. Lu, Hydrothermally robust molecular sieve silica for wet gas separation, Adv. Funct. Mater. 16 (2006) 1215-1220

[55]   M. Drobek, C. Yacou, J. Motuzas, A. Julbe, L. Ding, J. C. Diniz da Costa, Long Term Pervaporation Desalination of Tubular MFI Zeolite Membranes, J. Membr. Sci. 415–416 (2012) 816–823.

[56]   D. L. Meixner, P. N. Dyer, Characterisation of the transport properties of microporous inorganic membranes , J. Membr. Sci. 140 (1998) 81-95.

[57]   N. K. Raman, C. J. Brinker, Organic template approach to molecular sieving silica membranes, J. Membr. Sci. 105 (1995) 273-279.

[58]   K. Kusakabe, S. Sakamoto, T. Saie, S. Morooka, Pore structure of silica membranes formed by a sol-gel technique using tetraethoxysilane and alkyltriethoxysilanes, Sep. Purif. Technol. 16 (1999) 139-146.

[59]   P. Joos, P. Van Remoortere, M. Bracke, The kinetics of wetting in a capillary, J. Coll. Interface Sci. 136 (1990) 189-197.

[60]   K.G. Kornev, A.V. Neimark, Spontaneous penetration of liquids into capillaries and porous membranes revisited, J. Coll. Interface Sci. 235 (2001) 101-113.

[61]   S. Wang, D.K. Wang, K.S. Jack, S. Smart, J.C. Diniz da Costa, Improved hydrothermal stability of molecular sieving silica materials prepared from ethyl silicate 40, RSC Adv. 5 (2015) 6092–6099

6 INVESTIGATION ON THE EFFECT OF REACTANT RATIO (H2O:Si) ON MEMBRANE PERFORMANCE FOR DESALINATION

Introduction

The aim of this Chapter is to further develop the novel membrane preparation method as described in the last chapter by systematically investigating the effect of H_2O:Si ratio on membrane properties and consequent desalination performance, whilst using an acid catalyzed refluxed sol-gel synthesis.

Contribution

This chapter shows that by adjusting the H_2O:Si ratio in the sol-gel reactions, high quality interlayer-free silica membranes can be successfully prepared by RTP method through acid (pH=1) catalyzed sol-gel process. The membrane synthesis procedure was simplified by escaping the step of changing the sol pH to basic region (pH ~ 4 or 6) as required in Chapter 5. The best membrane performed high water flux up to 7 kg m^{-2} h^{-1} and high salt rejection (>99%) for desalination of 3.5 wt% seawater at 60 ℃. In addition, these membranes exhibited extraordinary hydrostability, as evidenced by the steady water flux and maintained salt rejection for desalinating seawater at room temperature for up to 818 h, prolonged by at least 500 h as compared to the best pH 4 membranes in Chapter 5. These works can be utilized as fundamental research for future membrane desalination development by further tailoring the pore size and/or surface chemistry through doping organic templates or metal oxides for instance.

Investigation on the Effect of Reactant Ratio (H₂O:Si) on Membrane Performance for Desalination

Abstract

This Chapter focuses on the further development of the interlayer-free ES40 membranes prepared by the rapid thermal processing (RTP) method. It is the aim of this Chapter to provide further insights of the novel membrane preparation method by systematically investigating the effect of H_2O:Si ratio, whilst using an acid catalyzed refluxed sol-gel synthesis. This chapter shows that by controlling the sol-gel method, particularly water as hydrolyzing agent, it is also possible to prepare interlayer-free ES40 membranes by the RTP method at pH = 1 to achieve the desired microporous structure with narrow pore size distribution. This chapter also shows that the hydrostability of the membranes derived from acid catalysed silica sols (pH=1) is greatly improved by more than ~500 h compared to that from membranes prepared using pH > 2 sols in Chapter 5 due to the formation of thicker silica films. The effect of H_2O/Si ratio on the hydrostability of the membranes is also studied, but the difference is attributed to the substrate quality.

6.1 Introduction

The previous Chapter 5 was devoted to show proof of concept that it is possible to prepare silica membranes directly on substrates by the RTP method. Therefore, Chapter 5 shows the first demonstration of this novel membrane preparation method, which was achievable by using ES40 being a much stronger silica precursor against thermal stresses during fast heating rates. Chapter 5 focused on adapting the ES40 sol-gel to the required conditions, a knowledge that was subsequently used to prepare membranes to separate water from sodium chloride ions whilst delivering high salt rejections in desalination. This was achieved by varying the pH of the sol-gel, where the best membranes were prepared with pH > 2, a value above the silica iso-electric point (IEP) [1]. A major achievement in Chapter 5 was the production of silica membranes in 3 hours, less than 1% of the time required for the fabrication of silica membranes by conventional thermal processes. A second achievement was showing silica membranes were hydrostable up to 300 h in desalination, well beyond of the state of art for pure silica membranes [2]. Although these results are encouraging, further research is warranted to understand the ES40 sol-gel method and further improve the long term performance of the synthesised membranes.

Numerous works in sol-gel science have documented that the H_2O:Si ratio plays a fundamental role in the formation of silanol and siloxane groups through hydrolysis and water condensation reactions, which are described in the Chapter 2 [1, 3]. Controlling the H_2O:Si ratio has been extensively studied to tailor silica membrane microstructure derived from TEOS for gas separation [4-9] and desalination [10-15]. As a general rule, the H_2O:Si ratio is typically limited to below 6:1 to delay the onset of the silica condensation reactions during the hydrolysis stage. This would lead to the formation of a high concentration of silanol groups, with a tendency to form ultra-microporous structures (d_p < 5Å) which is a necessity for molecular size exclusion. These are known to form molecular sieve structures, allowing the diffusion of water (which has a kinetic diameter of 2.6Å) in the case of desalination, and hindering the passage of the larger hydrated salt ions such as $Cl^-·H_2O$ (6.64 Å) and $Na^+·H_2O$ (7.16 Å) [16, 17]. However, as mentioned in the previous chapters, silanol groups are hydrophilic [18], and as such microporous silica membranes are known to become hydrothermally unstable [19-21] due to rehydration and recondensation of the siloxane bonds. Therefore, by systematically increasing the H_2O:Si ratio, one would expect to promote condensation reactions during the sol-gel process to form more siloxane bridges. This was indeed observed in Chapter 3. Furthermore, Chapter 4 showed that ES40-derived silica samples in the water series under acid-catalyzed conditions have all retained approximately 75% of their pore volume after the hydrothermal treatment due to a stronger microstructure leading to an improved hydrostability of the matrices. Based on these observations, interlayer-free RTP membranes prepared under this sol-gel regime may offer a better operational stability for desalination.

Therefore, this chapter investigates the preparation of microporous interlayer-free RTP silica membranes in the acid catalysis regime (below the IEP of silica species) as a function of H_2O:Si ratio. This was only possible by reducing the ethanol to silica ratio used in the sol-gel synthesis in Chapter 5. In order to provide further insights into the preparation of silica membranes by the novel interlayer-free RTP approach, the effects of H_2O:Si sol-gel ratio and thermal processing (CTP for comparison) on the physico-chemical properties of the silica microstructure were studied. Furthermore, the synthesised membranes were systematically tested for their performance in terms of water permeate flux and salt rejection for a range of operating conditions including desalinating pure water, feed salt concentration of 0.3 wt% and 3.5 wt% at various temperatures at 25, 40 and 60 °C, in addition to long term desalination operation.

6.2 Experimental

6.2.1. Membrane materials synthesis and characterisation

The membrane materials were produced by the sol-gel processing of ES40 (Wacker Chemicals Australia Pty Ltd). Firstly, distilled water, ethanol (EtOH, AR grade) and 1 M nitric acid (HNO_3) were mixed in a conical flask and the solution was maintained at pH 1. Then ES40 was added dropwise to the solution under stirring at room temperature. For the H_2O series (H_2O–x), the initial molar ratio of Si (ES40): EtOH: H_2O: HNO_3 was 4: 15: x: 0.4, where x (H_2O) equals to 20, 44 or 92. After stirring for 10 min at room temperature, the sol-gel mixture was heated up to 60 ℃ under reflux in water bath for 3 h to obtain a homogeneous solution. Subsequently, the mixture was dried in oven at 60 ℃ for over 2 days and then calcined in air at 630 ℃ for 1 h using the rapid thermal processing (RTP) adopted from Wang and co-workers as described in Chapters 5 [22].

The xerogels was characterised by Fourier transform infrared (FTIR) spectroscopy performed by a Shimadzu IRAffinity-1 with a Pike MIRacle diamond attenuated total reflectance (ATR) attachment over a wavenumber range of 4000–600 cm^{-1}. Baseline setting and peak deconvolution of the spectra were performed using the Fityk program based on Gaussian peaks. The intensity of siloxane peak at ~1050 cm^{-1} was normalized to 100% for each spectrum. Nitrogen adsorption was conducted at -196 °C using a Micromeritics TriStar 3020 instrument. Samples were degassed at 200 °C overnight before each measurement. The specific surface areas were calculated using the Brunner-Emmett-Teller (BET) method. The pore size distributions were determined from adsorption branch of the isotherms using the Density Functional Theory (DFT) method on cylindrical pores with oxide surfaces model. Cross-polarisation magic-angle-spinning (CP/MAS) solid-state ^{29}Si nuclear magnetic resonance spectroscopy (NMR) was performed on an Avance III spectrometer (Bruker) for silicon groups. A thermo-gravimetric differential scanning colorimetric analysis TGA-DSC1 (Mettler Toledo) was used for the TGA analysis of xerogel samples. The testing conditions for all measurements were set at air flow rate of 60 ml min^{-1} and dwell time of 60 min at 630 ℃. The ramping rates were 100 ℃ min^{-1} for RTP and 1 ℃ min^{-1} for CTP.

6.2.2. Membrane preparation and desalination performance measurement

The synthesized sol solutions were diluted by EtOH to a final EtOH:Si of 150:4 to reduce the sol viscosity immediately prior to dip-coating. Dip-coating was conducted directly on macroporous α-alumina substrate (Ceramic Oxide Fabricates, Australia) which was pre-calcined at 1000 ℃ for 8 h with a ramp rate of 5 ℃ min^{-1} to enhance mechanical strength and remove organic impurity. The substrate was dip-coated by the prepared sols with a dwell time of 1 min and dipping and withdrawal rates of 10 and 5 cm min^{-1}, respectively. The membranes were dried at 60 ℃ for 30 min

followed by calcination at 630 ℃ for 1 h using the RTP method, following the same procedure as for the xerogel preparation. The dip-coating, drying and calcination process were repeated twice to prevent the existence of membrane defects. Morphological features of the membranes were examined using a Jeol JSM-7001F SEM with a hot (Schottky) electron gun at an acceleration voltage of 10kV.

Desalination performance measurements were conducted using a classic pervaporation rig as described by Chapter 5. The set-up included a feed solution, membrane for testing, condenser and vacuum pump. Saline solutions (NaCl, Sigma-Aldrich) with salt concentrations ranging from 0 to 3.5 wt% were prepared as the feed solutions and the temperature was set at 25, 40 or 60 ℃. The feed solution was kept under constant turbulent stirring to minimize concentration polarization on the feed side. Vacuum was applied on the permeate side and water vapor was collected by the condenser immersed in liquid nitrogen. The mass of permeate (m) was measured and water flux (F) was calculated from the equation $F=m/A\,t$, where A is active area of the testing membrane and t is the collecting time. The salt rejection (R) was calculated from $R=(C_f-C_p)/C_f \times 100\%$, where C_f and C_p are the salt concentration of the feed side and permeate side, respectively, which were determined by the conductivities measured by a labCHEM CP conductivity meter.

6.3. Results and discussion

6.3.1. Membrane material properties

Figure 6.1 shows the nitrogen sorption isotherms and DFT pore size distribution of the xerogels prepared from different H_2O ratios calcined using both CTP and RTP methods. As can be seen from Figures 6.1A and 6.1B, all the isotherms exhibit Type I profiles, indicating micropores are dominant in the silica microstructure. However, the relative pressure where adsorption reaches saturation and total volume absorbed increases with increasing H_2O ratio, implying the existence of larger pores and total pore volume. These trends can also be clearly observed through the pore size distributions in Figures. 6.1C and 6.1D, which is derived from the adsorption isotherm branches in Figure 6.1A and 6.1B. Similar trends are observed to those in Chapter 5 for pH 4 and 6 ES40 xerogels, where the RTP method provided higher total pore volumes than the CTP method. Furthermore, the samples were mainly microporous, based on a tri-modal pore size distribution. However, a major difference in the results of this Chapter compared to those of the pH 1 and pH 2 samples in Chapter 5 is related to their isotherms which showed dense materials for the CTP method in Chapter 5. This can be explained by the effect of refluxing during the preparation of the sols in this work. It is well-

known that increasing reaction temperature promotes chemical reactions from the kinetics and thermodynamics perspectives. More specifically, the rationale of reflux is two-fold. Firstly, the sol-gel reactions are favoured in the forward directions due to the progressive removal of the ethanol from constant evaporation/recondensation of the ethanol and a small amount of water in the system. Secondly, increasing reaction temperature increases the entropy of the system thereby overcoming the diffusion-limited barrier and improves phase homogeneity of the system, which is in good accord with the findings in Chapter 3. As such, hydrolysis and condensation reactions in this sol-gel process are expected to be accelerated [1, 23]. Hence, the larger extent of the sol-gel reactions in this work is clearly evidenced by the final textural properties of the silica xerogels.
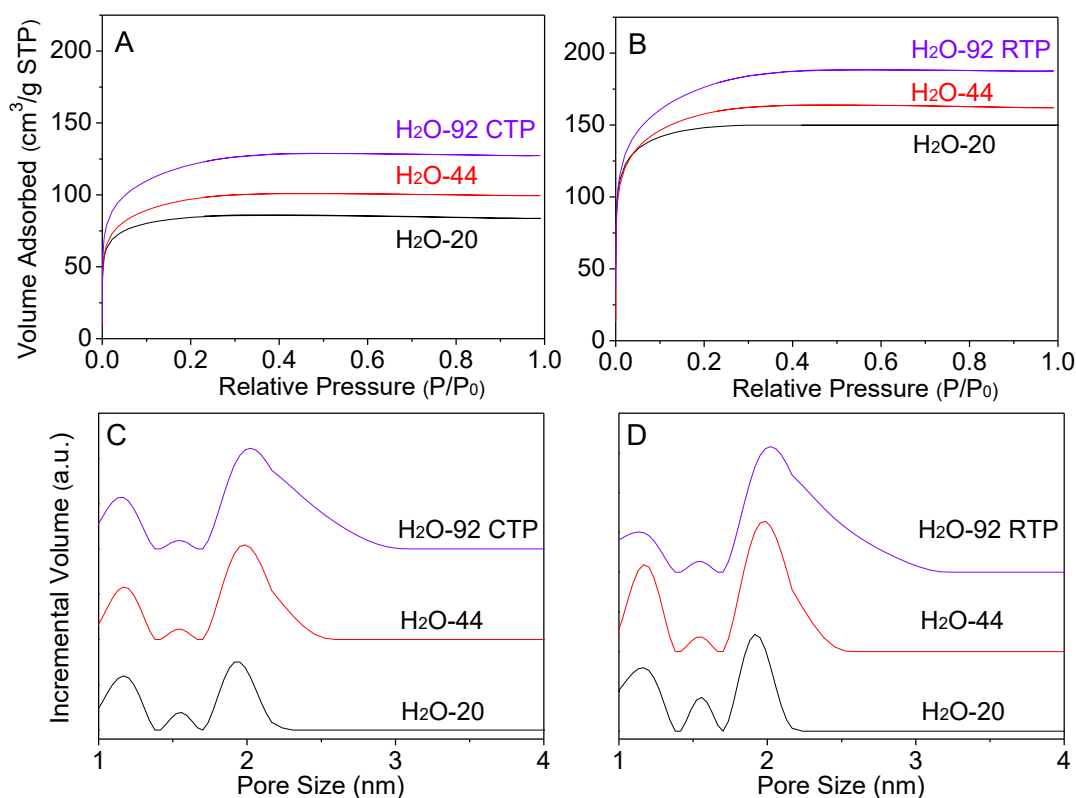
Figure 6.1 N_2 adsorption–desorption isotherms of xerogels prepared by the (A) CTP and (B) RTP methods, and DFT pore size distribution of silica xerogels prepared by the (C) CTP and (D) RTP methods as a function of different H_2O:Si ratios.

Figure 6.2 shows that the surface area increases as a function of the H_2O:Si ratio, irrespective of the method used (CTP or RTP) and temperature (400 and 630 °C). Further, surface areas were higher for the samples prepared by RTP method, and increasing the RTP temperature led to a slight densification of the silica matrix as surface area was reduced. These trends are also observed in Chapter 5. In comparison, the surface areas of the RTP samples are approximately 60% (506 to 616 m^2 g^{-1}) higher than those microporous samples in Chapter 5 for pH 1 (351 m^2 g^{-1}) and pH 4 (362 m^2

g^{-1}), though lower than the slightly mesoporous silica samples for pH 6 (700 m^2 g^{-1}). The structural features of the ES40 xerogels prepared in this Chapter suggest that the sol-gel reaction gave slightly different amorphous silica structures as compared to Chapter 5.
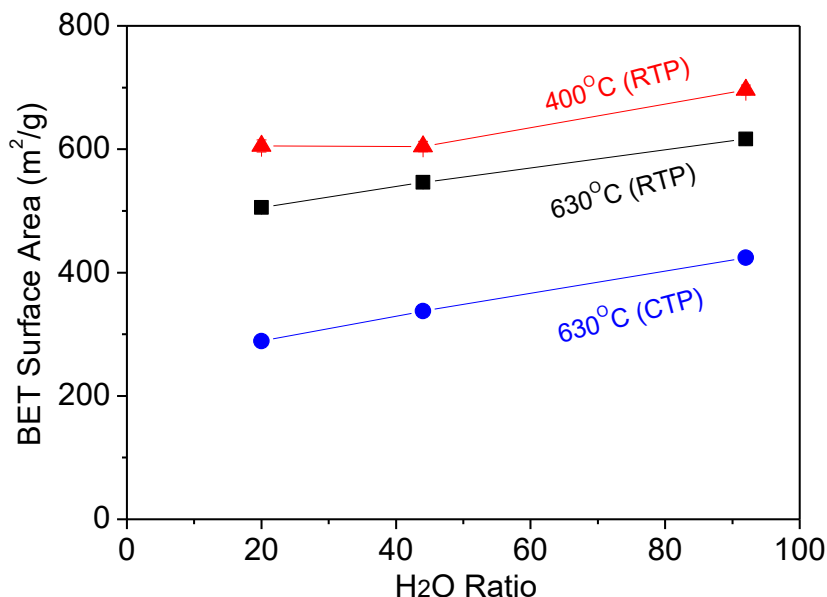

Figure 6.2 N$_2$ adsorption–desorption isotherms (A) and DFT pore size distribution (B) of silica xerogels prepared from different H$_2$O ratio.

In order to further understand the effect of the H$_2$O:Si ratio, the FTIR spectrum represented in Figure 6.3A was deconvoluted using the Fityk program. For the sake of clarity, the deconvoluted peaks as determined in Chapter 5 are repeated in this chapter again. The deconvoluted peaks at ~1235 (peak I) and 1065 cm^{-1} (peak IV) are assigned to the longitudinal optical (LO)-transverse optical (TO) splitting mode of anti-symmetric stretching vibration of 6-ring siloxane, while the absorption at ~1200 (peak II) and 1150 cm^{-1} (peak III) correspond to the LO-TO mode of 4-ring siloxane [24, 25], and the fitted peak at ~1020 cm^{-1} is attributed to the chain and sheet silicates [26]. Semi-quantitative analysis was conducted using the relative absorption of the uncondensed silanol (peak VI) to the condensed siloxane (the dominant peak IV) bonds, which is again used as indicator of the degree of condensation. The comparative FTIR area ratios in Figure 6.3B show that the change of the Si–OH/Si–O–Si ratios is insignificant under the same given calcination condition, irrespective of the water ratio. This result is interesting because in principle water is a hydrolysing agent. As a following reaction of hydrolysis, condensation reactions are expected to increase because of the shift in the reaction equilibrium to form the siloxane groups. However, due to the reaction temperature is raised during the sol-gel process, a possible explanation could be that the rates of formation of the silanol and the siloxane groups are both promoted by the input of thermal

energy and they remain relatively close throughout the process. Hence, the effect of increasing water ratio is only seen marginally as the effect of reaction temperature is most likely to dominate in the system.
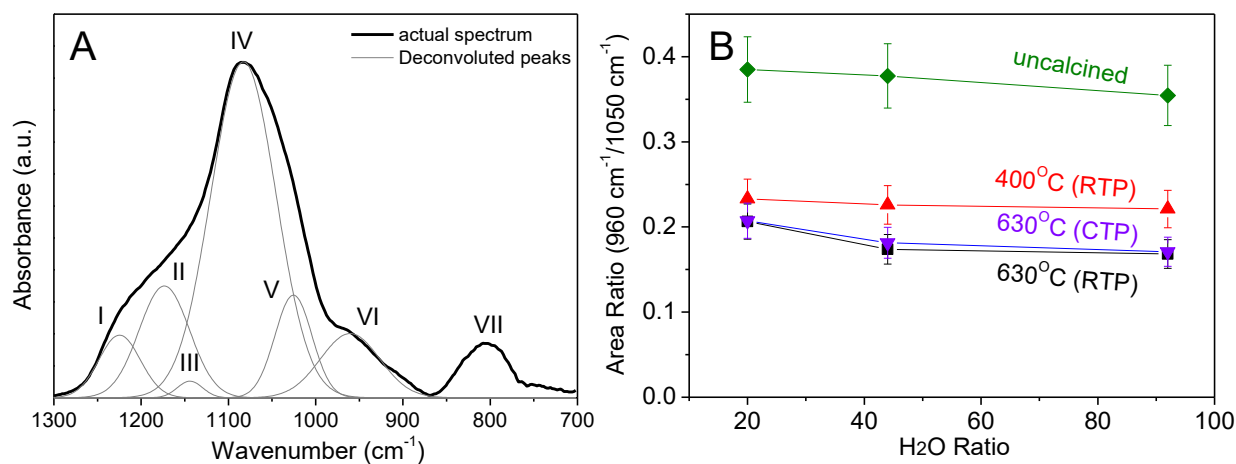
Figure 6.3 FTIR spectrum and peak convolution of H_2O–20 (A) and comparative FTIR ratios of silanol to siloxane (B) of silica xerogels.
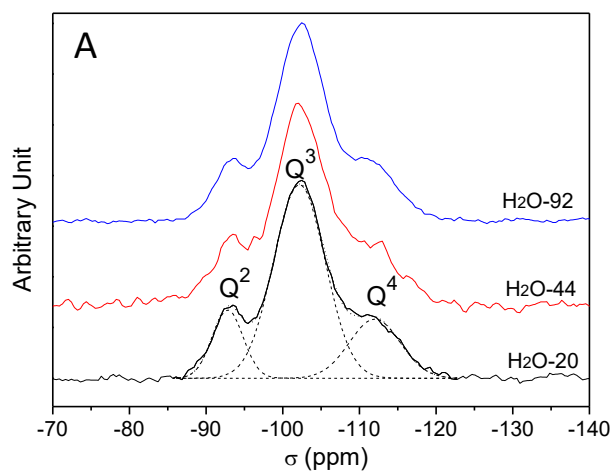
Figure 6.4 – ^{29}Si NMR spectra of silica xerogels prepared by RTP for the different H_2O:Si ratios.

To further evaluate the chemical structure and concentration of silica species in the xerogels, CP/MAS solid-state ^{29}Si NMR measurement was conducted and the spectra are given in Figure 6.4. The spectra were deconvoluted as shown by the dash line in Figure 6.4 and the percentage of Q^2, Q^3 and Q^4 and the ratios of Q^2/Q^4 and Q^3/Q^4 are calculated from the deconvoluted peaks and listed in Table 6.1 where Q^n represents $(SiO)_nSi(OH)_{4-n}$. It can be seen that the Q^2 species (i.e. silicon containing two equivalent silanol and siloxane bonds) have comparable resonance peak intensities

106

in all the samples, although a slight decrease in the ratio of Q^2/Q^4 can be seen with respect to increasing the water ratio. The decrease in Q^2 percentage from 14 in H_2O–20 to 12 in H_2O–92 samples is accompanied by the increase of Q^3 species from 66 to 69, respectively, whilst the proportion of Q^4 is almost equivalent. These results indicate that increase of water ratio in sol-gel solutions appears to promote the transformation of Q^2 to Q^3 sites. Since the Q^4 distribution remains almost unchanged, likewise are the ratios of silanol/siloxane (($Q^2 + Q^3$) / Q^4), which is in good accordance with the FTIR results in Figure 6.3B.

Table 6.1 Q^n percentage distributions of the xerogels calculated from ^{29}Si NMR measurement.

Sample Code	Q^2	Q^3	Q^4	Q^3/Q^4	Q^2/Q^4	($Q^2 + Q^3$) / Q^4
H_2O–20	14	66	20	3.3	0.70	4.0
H_2O–44	13	67	20	3.4	0.65	4.0
H_2O–92	12	69	19	3.6	0.63	4.3

The TGA results in Figure 6.5 show similar trends obtained in Chapter 5 for the mass loss of ES40 as-prepared gels exposed to very fast ramping rates as RTP and slow ramping rate as CTP. A consistent trend in all the CTP samples is clearly observed at the onset of mass loss up to 100 ℃, which is mainly attributed to physisorbed water trapped in the porous structure of the silica films [27]. Likewise to the results in Chapter 5, the mass loss calculated at 100 ℃ is constant for samples in both the CTP and RTP methods as a function of pH (Figure 6.5D). The difference here is that the overall mass loss for RTP samples is only ~3.9 wt%, which is very marginal as compared that of ~21 wt% for the CTP samples at 100 ℃. There is also a mass loss lag of 50-100 ℃ up to 200 ℃, which is at lower temperatures than in Chapter 5 (~260-275 ℃) for the RTP method. This lag is most likely associated with heat transfer into the xerogel, similar to Chapter 5, as the RTP ramping rate of 100 ℃ min^{-1} is 100 times faster than that of CTP method.

Furthermore, the mass loss of the RTP and CTP samples for the H_2O–44 and H_2O–92 tends to converge at high temperatures. This suggested that these samples condensation reactions pathway may be similar (e.g. also supported by the FTIR results), with the exception that the RTP method leads to the onset of evaporation of the physisorbed water from the silica matrices at higher temperatures than the CTP method. However, the H_2O–20 samples prepared with the lower water ratio did not achieve the same mass loss conversion, unlike the other H_2O–44 and H_2O–92 samples prepared with high water content. This is similar in the TGA results of the pH 1 samples in Chapter 5.
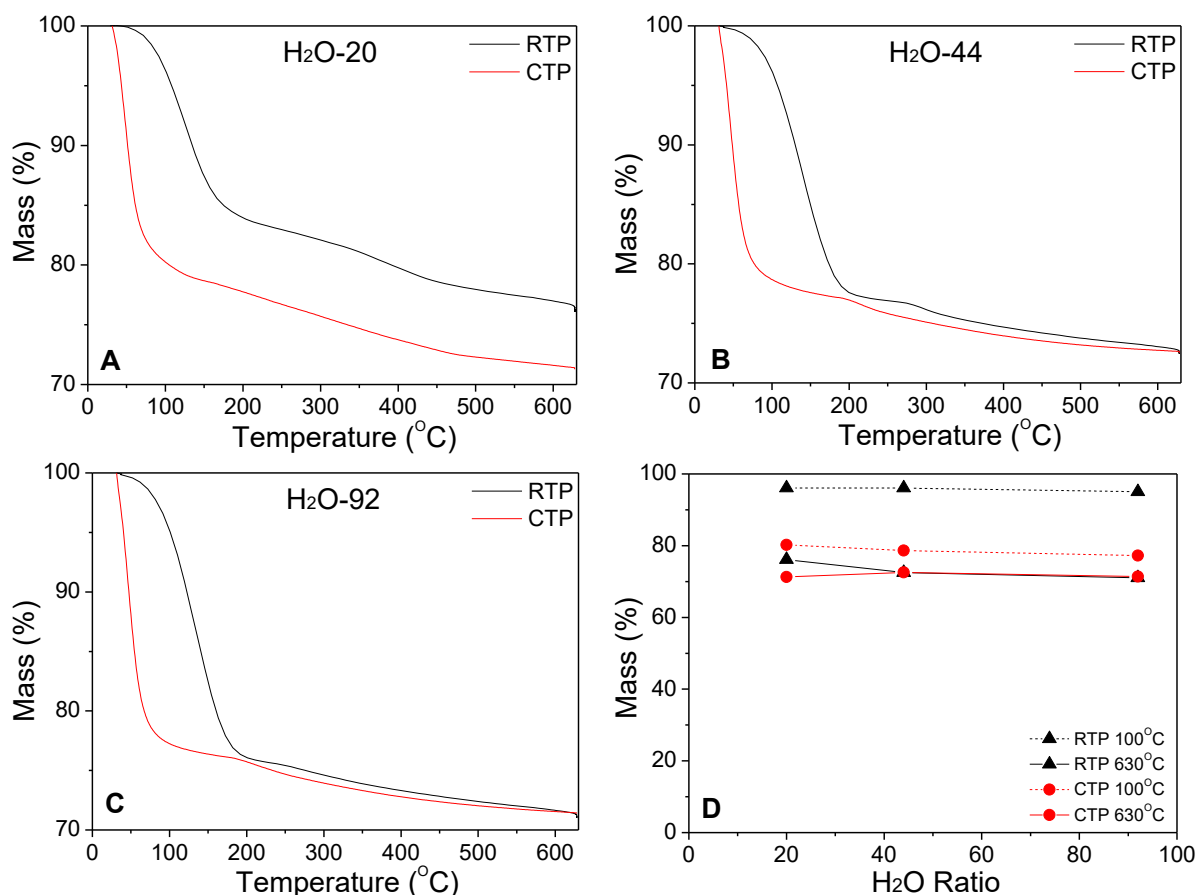
Figure 6.5 (A, B and C) Mass loss profiles as a function of different H$_2$O:Si ratios, and (D) weight change of RTP (100 ℃ min^{-1}) and CTP (1 ℃ min^{-1}) xerogel samples with respective to water ratio and temperature.

6.3.2. Membrane performance

The interlayer-free RTP membranes supported on alumina substrates in this work were prepared by two cycles of dip-coating, drying and RTP calcination. Figure 6.6 shows the desalination performances of the membranes in terms of water permeate fluxes and salt rejections via vacuum pervaporation. There are several points that are noteworthy in the membrane performance. Firstly, the salt rejections of the membranes under all the tested conditions are over 99% for all the membranes at various salt concentrations, indicating interlayer-free technique can deliver high quality silica membranes using the pH 1 ES40 sols after reflux. These results are superior to those obtained in Chapter 5 where salt rejections varied between 95 and 99%. Secondly, the water fluxes of membranes clearly increase with increasing H$_2$O:Si sol gel ratios. For example, it increases from 2 kg m^{-2} h^{-1} in H$_2$O–20 to 4 kg m^{-2} h^{-1} in H$_2$O–44 and 16 kg m^{-2} h^{-1} in H$_2$O–92 for pure water permeation at 25 ℃. These results also increase two-fold with increasing feed temperature to 60 ℃.

The superior performance produced by H_2O–92 membrane is attributed to the highest total pore volume, which has less transport resistance and, consequently higher fluxes. Likewise, in Chapter 5 the water flux in this chapter increased with increasing temperature, which is due to an increase in the driving force from a larger vapour pressure gradient. However, by increasing the salt concentration, the water flux of the H_2O–92 membrane for desalination of 3.5 wt% salt solution at 60 ℃ was not as outstanding as in other conditions, which is only 4.6 kg m^{-2} h^{-1}, similar as that of the H_2O–44 membrane.
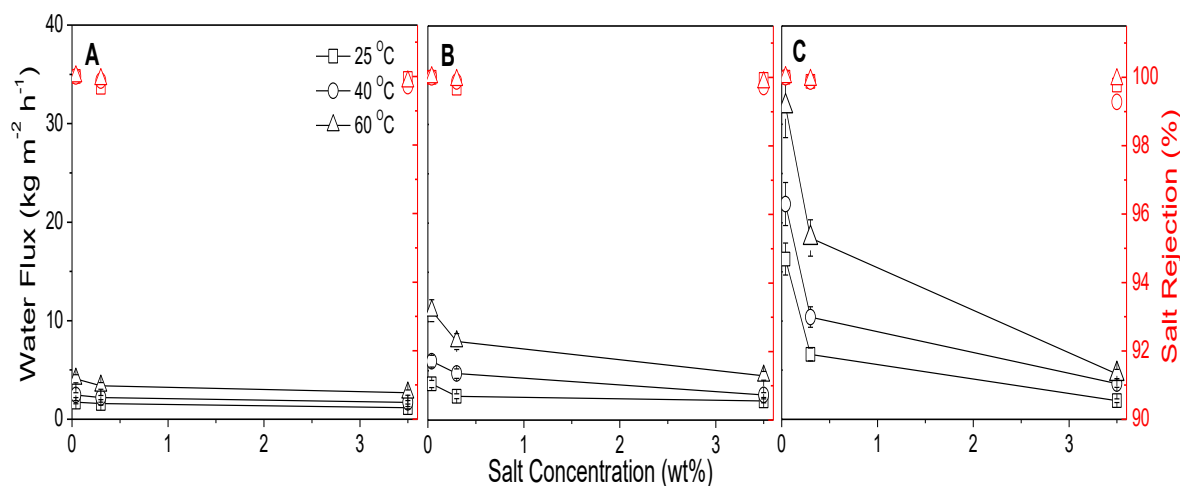
Figure 6.6 Water flux and salt rejection of H_2O–20 (A), H_2O–44 (B) and H_2O–92 (C) membranes as a function of salt concentration.

An important but often overlooked parameter of the membrane performance relates to its long term operation and hydrostability. Figure 6.7 shows the performance of the membranes tested up to 120 h as a function of temperature and feed salt concentration. Interestingly, it is observed that the membrane performance is stable within this testing timeframe with good stable flux and high salt rejections. However, on a closer inspection, the salt rejection of H_2O–20 membrane started to decline from >99% to 70% after 120 h at 60 ℃ in 3.5 wt% saline solution. Despite of this observation, the H_2O–44 and H_2O–92 membranes proved to deliver stable water fluxes and high salt rejections under all the testing conditions throughout this period. High temperature and high salt concentration affect the performance of inorganic membranes such as alumina-silicate zeolites [28], cobalt doped silica [13] and silica [2]. This problem is directly related to the ion exchange instability in zeolites, or hydro-instability of silica structures, coupled with silica sorption capacity towards salt ions [29].
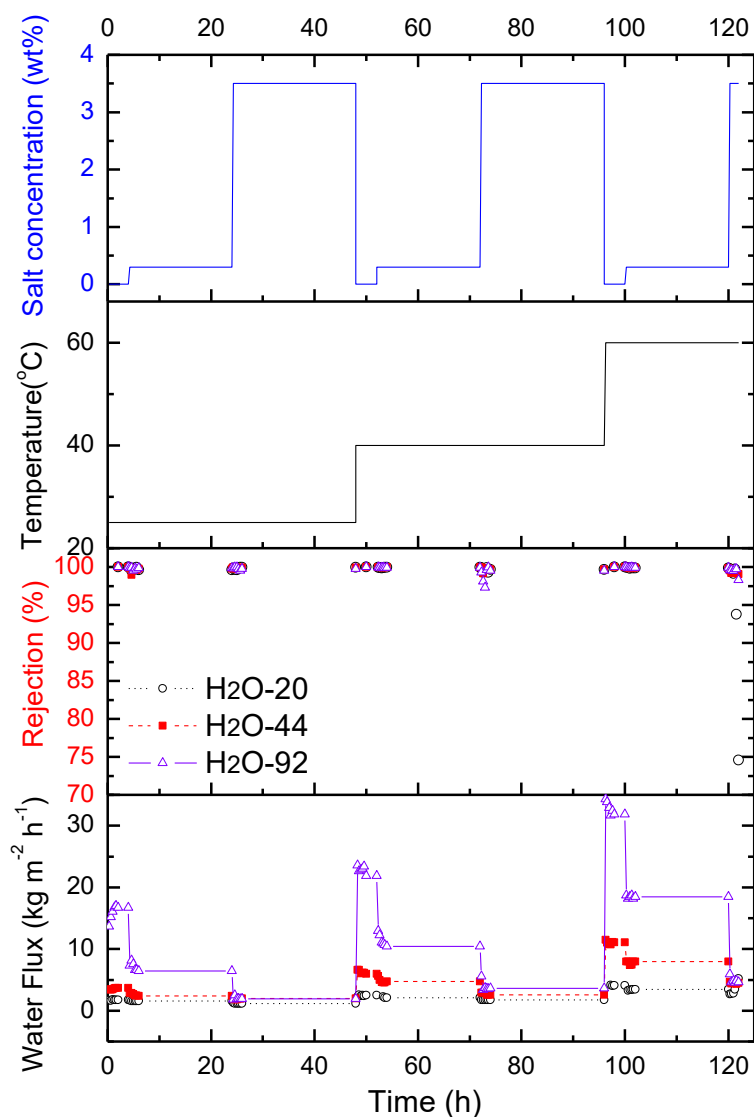
Figure 6.7 –120 h performance of pH 4 and pH 6 membranes for water flux (±10%) and salt rejection (±1%).

The more hydrostable H_2O–44 and H_2O–92 membranes underwent further stability testing at room temperature and 3.5wt% NaCl feed water concentration as displayed in Figure 6.8. The H_2O-44 membrane maintained the best stable performance for over 818 h. This membrane failed in the next measurement at ~860 h. This is evidenced by the small, marginal fluctuation of fluxes averaging at 2 kg m^{-2} h^{-1} and constant high salt rejections of greater than 99%. In comparison, the H_2O–92 membrane also produced constant performance of up to 300 h, after which the water fluxes increased by an average of 46%, from 2.8 to 4.1 kg m^{-2} h^{-1}. Although salt rejection was kept constant >99% all the way to 600 h for this membrane, the increase of water fluxes at 300 h suggests the onset process that the silica membrane layer underwent some degree of structural degradation. Furthermore, the water flux increased to 6.0 kg m^{-1} h^{-1} at 600 h, followed by pore wetting and membrane failure thereafter. These results suggest that the membrane layer was no

longer able to sustain the liquid-vapour interface as a result of structural failure, possibly caused by the creation of major defects or widening of the pore size.
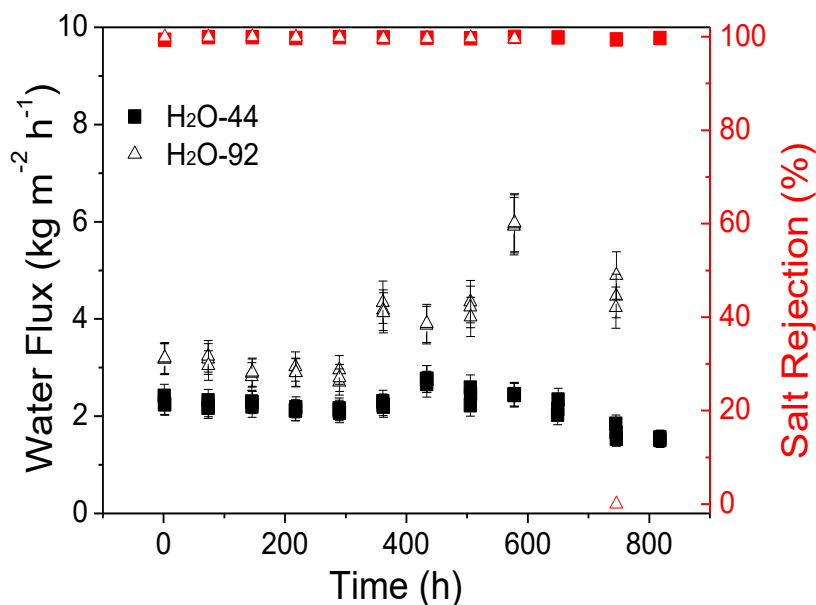

Figure 6.8 Water fluxes and salt rejections (± 1%) of the (A) H$_2$O–44, and (B) H$_2$O–92 membranes at NaCl 3.5 wt% at room temperature.

The hydrostability performance of the membranes is somewhat intriguing. For instance, there were no evident changes of the ratio of silanol to siloxane groups as measured by FTIR (Figure 6.3) and ^{29}Si NMR (Table 6.1). It is known that membranes with a higher amount of siloxane groups tend to be more stable contrary to those having a higher concentration of the hydrophilic silanol groups. The structural formation of the silica membranes is also very similar, showing tri-modal pore size distribution. The variations observed with the silica membranes as a function of the H$_2$O:Si ratio are related to surface area and pore volumes, though the nitrogen isotherms were characterised by microporous materials. In order to throw further light into the membrane performance, SEM analysis was carried out to provide the membrane morphology information.

Representative SEM images of the cross section of the H$_2$O–44 membrane are displayed in Figure 6.9. The α-Al$_2$O$_3$ porous substrate in Figure 6.9A shows the individual alumina particles ranging from 0.15 to 1.00 μm in size with various inter-particle voids. The RTP interlayer-free membrane in Figure 6.9B shows that a top-film layer was not formed as it conventionally occurs for silica membranes coated on interlayered supports. Indeed, the top surface aspect of the membrane shows a rough surface. However, the cross-section displays a deep impregnation of the sol-gel, which filled most of the inter-particle spaces, albeit there are a few areas which show medium (0.03 to

0.11 μm) and large (0.20 μm) size unfilled voids. The SEM results in this chapter is characteristics of the impregnation effect, which was discussed in Chapter 5, and it is caused by the initial high capillary forces upon contact of a liquid (sol) with and a dry porous surface (substrate). As salt rejections in each of the membrane were very high (> 99%), it is assumed that these voids are not deemed to be connected and the membrane structure was mainly controlled by small constrictions which hindered the passage of hydrated ions by pore size exclusion. It is interesting to observe how deep into the porous substrates was the penetration of the sol-gel, similar to Chapter 5.
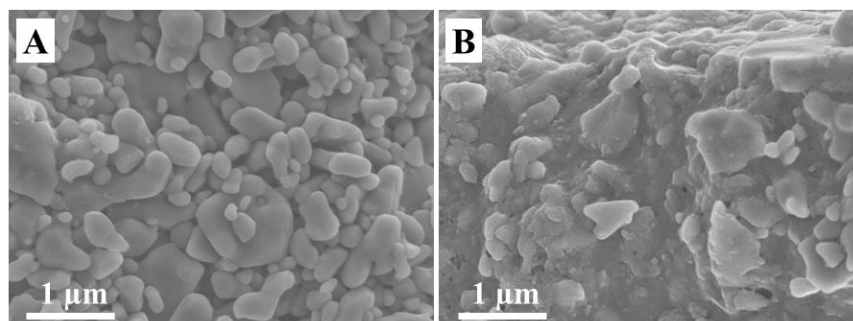
Figure 6.9 SEM images of (A) α-Al$_2$O$_3$ porous substrate, and (B) cross section of the RTP interlayer free silica H$_2$O–44 membranes.

Further investigation of the cross sections of all membranes post desalination testing was carried out by SEM analysis as shown in Figure 6.10. It reveals a broad impregnation depth with variations of 13.4-17.3 μm (H$_2$O–20 membrane, Figure 6.10A), 3.8-8.2 μm (H$_2$O–44 membrane, Figure 6.10B) and 5.4-16.2 μm (H$_2$O–92 membrane, Figure 6.10C). It is interesting to note that the H$_2$O–20 membrane with the highest silica thickness (13.4-17.3 μm), in addition to the lowest variation, was the membrane that failed first during long term hydrostability testing. Another interesting point to note is that the H$_2$O–44 membrane, with the lowest silica thickness, actually survived the hydrostability test of 818 h without failing.
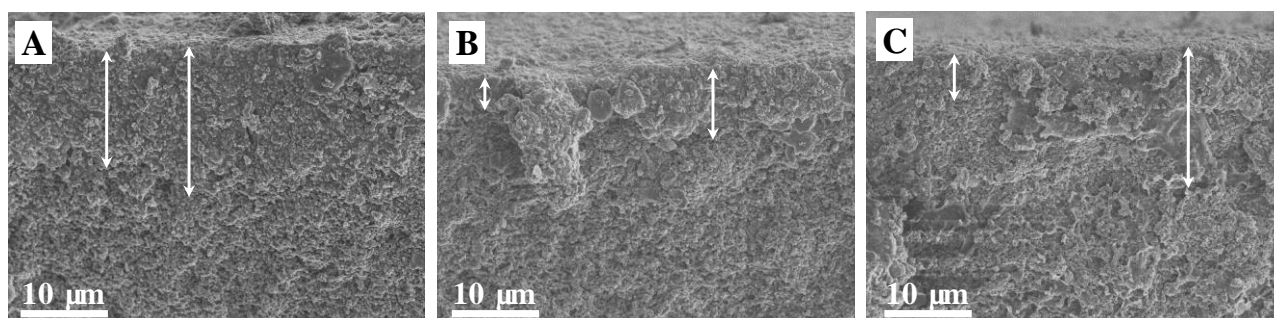
Figure 6.10 SEM images of (A) H$_2$O–20, (B) H$_2$O–44 and (C) H$_2$O–92 membranes post desalination long term testing.

This intriguing problem of membrane long term performance is therefore attributed to the substrate quality. In this thesis, cheap commercial substrates were purchased and used for the preparation of all membranes. Figure 6.9A clearly shows the substrates containing medium (0.03 to 0.11 μm) and large (0.20 μm) size pores, which are associated with small and large alumina particles. The variation of alumina particle sizes leads to the formation of a wide pore size distribution, and inhomogeneous porous substrates. In turn, this translates into different amounts of sol-gel penetrating the substrate at different depths during the sol-gel coating. On one hand, the novel method of interlayer free RTP silica membranes in this thesis is very robust, as it can also be used in the case of low quality substrates. On the other hand, improving the quality of the substrates, which can also increase costs quite considerably, will deliver the formation of impregnated homogeneous silica films.

Though affected by the low quality of the substrates, it is believed that compared to the sol-gel conditions, the thickness of silica layers is more likely to be the key factor in controlling the hydrostability of these membranes. This was observed in Chapter 5 for the pH 4 and pH 6 membranes where hydrostability was improved by using lower ethanol concentration to form thicker silica membranes. Moreover, the base-catalysed silica sols in Chapter 5 should be more hydrostable than the acid-catalysed silica sols as reported in Chapter 6 due to the further degree of condensation and crosslinking of the silica chains as discussed in Chapter 2. However, the resultant membranes gave the opposite desalination performance. Therefore, we conclude that the thickness of the silica layers is the key factor in controlling the hydrostability of the membrane. The thickness is determined by a combination of the sol-gel condition (including pH), the ethanol concentration (dilution) and the quality of the substrate, which have been systematically studied in this thesis.

6.3.3. Sol-gel effect in silica film formation

Upon the first RTP calcination, the integrity of the membrane to reject salt was not achieved, thus confirming an inhomogeneous pore size distribution containing several large pores leading to pore wetting. A superior pore size control to avoid pore wetting was achieved upon the deposition of a second layer and RTP calcination, confirmed by the high salt rejection in Figure 6.6. The structural evolutions of the membranes upon each RTP calcination cycle are schematically represented in Figure 6.11. In this approach, the pH 1 sols tend to coat the alumina particles of the substrate during the first coating step. The deep penetration of the sol is attributed to the initial high capillary forces related to the sol contacting a dry porous surface (substrate) as discussed in Chapter 5. Upon the second coating, the sol fills the remaining voids, thus forming microporous silica packed structure

between the alumina particles, as evidenced by the SEM images in Figures 6.9 and 6.10. After the two cycles of deposition and RTP calcination, a small number of micropores are expected to appear, and depicted in Figure 6.11 as red circles. This structural formation of the silica film for pH < 2 sols differs from that for pH > 2 sols as proposed in Chapter 5, as the latter had a large number of micropores and an observable division between the first macroporous layer and the top microporous silica layer (Figure 5.9 in Chapter 5). One possible reason that the membranes prepared in this Chapter are more hydrostable than those prepared in Chapter 5 may be directly related to the thickness of the impregnated silica films, which conferred a better structural integrity under desalination operation. In other words, thicker interlayer-free RTP silica membranes were prepared in this Chapter. This is also evidenced by the fact that water fluxes were generally lower is this Chapter (e.g. ~2.0 kg m^{-1} h^{-1} for 3.5 wt% seawater at 25 °C) than that of (~2.5 kg m^{-1} h^{-1}) in Chapter 5 because of the increased transport resistance from a thicker silica layer.
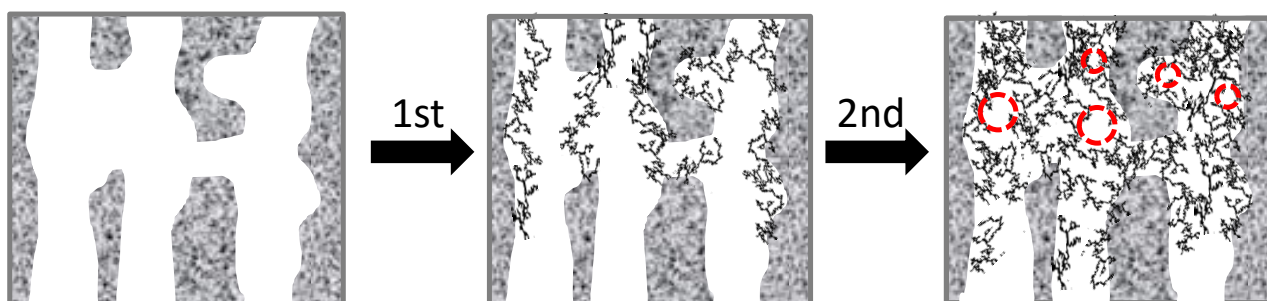
Figure 6.11 Conceptual schematic of the interlayer-free RTP membrane.

Another interesting point for discussion is that interlayer-free RTP silica membranes could be prepared using pH 1 sols as described in this chapter, but this was not achievable in Chapter 5. It is interesting that there are several similarities with the pH 1 sols from both chapters in terms of results and trends for nitrogen isotherms, pore size distribution and surface areas. The differences are the slightly higher concentration ratios of silanol to siloxane groups of 0.17-0.21 (this chapter) as compared to 0.15 (Chapter 5), and the EtOH:Si ratios of 150:4 (this chapter) and 255:4 (Chapter 5). Hence, an impinging question here is why it is possible to prepare interlayer-free RTP silica membrane with a high ethanol dilution ratio for pH > 2 membranes, but for pH < 2 membranes a much lower ethanol dilution ratio is required.

To rationalize these observations, we have to consider the fundamental of both the silica precursor characteristics and the sol-gel chemistry. As mentioned in Chapter 2 Literature Review, ES40 oligomers are pre-polymerized silica precursors that are prone to undergo cluster-cluster growth to confer a larger pore size and total pore volume in general [30, 31]. As ES40 precursor predominately contains Q^1 and Q^2 species [1], which are more acidic species in nature than the

unhydrolyzed Q^0 species, the final silica structures derived from ES40 are expected to be quite different. For instance, it is anticipated that condensation reaction occurs preferentially between the Q^1 species of the chain terminals and the more acidic Q^2 species of the chain pendants [1], such that resulted in an open fractal structure from a higher degree of condensation during the ES40 sol-gel process. This is also in good accord with these previous studies [30, 31].

However, the roles of pH and ethanol solvent concentration (dilution) in the sol-gel process must also be considered. The effect of pH is critical in controlling the pathway of sol-gel reactions. Generally, silica microstructure and textural properties are governed by the degree of hydrolysis and condensation reactions during the sol-gel process as discussed in Chapter 2. When pH of the sol is less than the iso-electric point of the silica species (IEP = 2) [1], the sol-gel reactions are governed by the acidic regime. Under this condition, acid catalysis favours hydrolysis reactions leading to the formation of long-chained weakly-branched silica oligomers [32]. As such, the proximity of these weakly-branched silica species is greatly increased in a diluted sol (concentration-limited), thereby reducing the degree of statistical crosslinking between the silica species (diffusion-limited). Therefore, interlayer-free silica membranes formed by pH < 2 sol will require a much lower ethanol ratio to overcome these limitations.

In contrast, increasing the sol pH above the silica IEP promotes condensation reactions during the early stage of hydrolysis. Under this condition, the ES40-derived silica species are characterized by highly-branched structure due to base catalysis sol-gel regime. As such, the highly-branched silica species will undergo a greater degree of random crosslinking between the comparatively larger molecules even under diluted conditions, hence a lower silanol to siloxane ratio is observed. This is the reason why it is possible to prepare interlayer-free RTP silica membranes with a higher ethanol dilution ratio (EtOH:Si = 255:4) for pH > 2 membranes, as evidenced by the pH 4 membranes discussed in Chapter 5. However, it should be heeded that excess ethanol can also retard the hydrolysis process by favoring the reverse reaction (alcoholysis) as ethanol is also a by-product of the sol-gel process. Furthermore, under the same given pH condition, increasing ethanol ratio can result in a diffusion-limited polymerization process with a longer gelation time, thereby leading to more microporous texture and a weaker microstructure [1, 33], especially under acidic regime.

The simplicity and robustness of the interlayer-free RTP preparation method paves the way to research opportunities to prepare interlayer-free silica membranes by the RTP method. This may include doping silica with other compounds to confer the silica films functionalities otherwise not available in pure silica films such as organic templates, hydrophobic molecules or metal oxides.

These functionalities may address improvements in hydrostability or adsorption, or using new organo-silica precursors to change the silica structure. In the case that organic materials are use, it may be necessary to keep or to carbonise the organic phase in the silica matrix. To this end, the RTP equipment will have to be designed using inert atmospheres, instead of the oxidising gas that was used in this thesis.

6.4. Conclusions

This chapter also shows that the ES40 sol-gel synthesis is flexible and can be tailored to prepare high quality interlayer-free RTP silica membranes for pH sols below the iso-electric point of silica (IEP = 2). This achievement was only possible by reducing the EtOH:Si ratio together with a refluxed sol-gel synthesis. Under the sol-gel acidic regime, the degree of statistical crosslinking between the silica species is diffusion-limited, coupled with the fact that weakly-branched silica species are hindered from proximity (concentration-limited). Therefore, interlayer-free RTP silica membranes require much lower ethanol dilution levels for pH < 2 sol to overcome these limitations as compared with ES40 sols at higher pH (> 2) values.

This chapter also proposes a different mechanistic model for the silica film formation. In the case of ES40 sols with pH < 2, the first layer tends to coat the substrate particles upon impregnation, whilst the second coat fills the remaining gaps between the coated particles. As a result, denser microporous silica films are formed, though a small number of macropores were also observed. This is contrary to the mechanism for ES40 sols with pH > 2 where macroporous were generally formed in the first coating whilst the second coating could not penetrate deeply into the substrate, thus forming a thinner microporous layer. These differences are associated with the acid and basic catalytic pathway of the sols below and above IEP = 2.

The prepared membranes performed well, delivering water fluxes up to 7 kg m^{-2} h^{-1} and excellent salt reject (>99%) for desalination of NaCl 3.5 wt% sea water. Increasing the feed solution temperature or reducing the salt concentration led to an increase in water fluxes for all membranes, an outcome related to increasing the driving force for water permeation. Long term testing showed that the best membrane (H$_2$O–44) was hydrostable for 818 h. This is a great improvement of over 518 h as compared to the membranes prepared with pH > 2 in Chapter 5. The other membranes failed at 600 h (H$_2$O–92) and 120 h (H$_2$O–20). However, the non-hydrostability of membranes was attributed to the non-homogeneous porosity of the substrates, which contain a large variation of particle sizes, and a large pore size distribution, rather than to the silica sol-gel properties.

Finally, the preparation method, coupled with the ES40 sol-gel synthesis and the long term hydrostability, suggests that the interlayer-free RTP method is robust and can be used even in the case of low quality non-homogeneous porous substrates. This demonstration opens a window of opportunities for further research to add functionalities otherwise not available in pure silica films such as organic templates, hydrophobic molecules or metal oxides.

Reference

[1] C.J. Brinker, G.W. Scherer, Sol-gel science: the physics and chemistry of sol-gel processing, Academic Press, Boston, 1990.

[2] M. Elma, C. Yacou, J. Diniz da Costa, D. Wang, Performance and Long Term Stability of Mesoporous Silica Membranes for Desalination, Membranes, 3 (2013) 136.

[3] A.M. Buckley, M. Greenblatt, A Comparison of the Microstructural Properties of Silica Aerogels and Xerogels, J Non-Cryst Solids, 143 (1992) 1-13.

[4] N.K. Raman, C.J. Brinker, Organic Template Approach to Molecular-Sieving Silica Membranes, J Membr Sci, 105 (1995) 273-279.

[5] R.M. de Vos, H. Verweij, Improved performance of silica membranes for gas separation, J Membr Sci, 143 (1998) 37-51.

[6] B.N. Nair, T. Yamaguchi, T. Okubo, H. Suematsu, K. Keizer, S.I. Nakao, Sol-gel synthesis of molecular sieving silica membranes, J Membr Sci, 135 (1997) 237-243.

[7] R.S.A. Delange, J.H.A. Hekkink, K. Keizer, A.J. Burggraaf, Formation and Characterization of Supported Microporous Ceramic Membranes Prepared by Sol-Gel Modification Techniques, J Membr Sci, 99 (1995) 57-75.

[8] J.C.D. da Costa, G.Q. Lu, V. Rudolph, Y.S. Lin, Novel molecular sieve silica (MSS) membranes: characterisation and permeation of single-step and two-step sol-gel membranes, J Membr Sci, 198 (2002) 9-21.

[9] M.C. Duke, J.C.D. da Costa, G.Q. Lu, M. Petch, P. Gray, Carbonised template molecular sieve silica membranes in fuel processing systems: permeation, hydrostability and regeneration J Membr Sci, 241 (2004) 325-333.

[10] M. Elma, D.K. Wang, C. Yacou, J.C.D. da Costa, Inter layer-free P123 carbonised template silica membranes for desalination with reduced salt concentration polarisation, J Membr Sci, 475 (2015) 376-383.

[11] M. Elma, D.K. Wang, C. Yacou, J. Motuzas, J.C.D. da Costa, High performance interlayer-free mesoporous cobalt oxide silica membranes for desalination applications, Desalination, 365 (2015) 308-315.

[12] X. Yang, T. Fraser, D. Myat, S. Smart, J. Zhang, J. Diniz da Costa, A. Liubinas, M. Duke, A Pervaporation Study of Ammonia Solutions Using Molecular Sieve Silica Membranes, Membranes, 4 (2014) 40.

[13] C.X.C. Lin, L.P. Ding, S. Smart, J.C. Diniz da Costa, Cobalt oxide silica membranes for desalination, J Colloid Interface Sci, 368 (2012) 70-76.

[14] B.P. Ladewig, Y.H. Tan, C.X.C. Lin, K. Ladewig, J.C.D. da Costa, S. Smart, Preparation, Characterization and Performance of Templated Silica Membranes in Non-Osmotic Desalination, Materials, 4 (2011) 845-856.

[15] S. Wijaya, M.C. Duke, J.C.D. da Costa, Carbonised template silica membranes for desalination, Desalination, 236 (2009) 291-298.

[16] A.G. Volkov, S. Paula, D.W. Deamer, Two mechanisms of permeation of small neutral molecules and hydrated ions across phospholipid bilayers, Bioelectroch Bioener, 42 (1997) 153-160.

[17] X.Y. Han, Y.F. Peng, Light-scattering characteristics of hydrated ions in dilute solutions of major sea salts, Optik, 127 (2016) 1455-1459.

[18] R.K. Iler, The chemistry of silica : solubility, polymerization, colloid and surface properties, and biochemistry Wiley, New York, 1979.

[19] G.R. Gallaher, P.K.T. Liu, Characterization of Ceramic Membranes .1. Thermal and Hydrothermal Stabilities of Commercial 40 Angstrom Membranes, J Membr Sci, 92 (1994) 29-44.

[20] G.R. Gavalas, C.E. Megiris, S.W. Nam, Deposition of H_2-permselective SiO2 films, Chem Engin Sci, 44 (1989) 1829-1835.

[21] D. Uhlmann, S. Smart, J.C.D. da Costa, High temperature steam investigation of cobalt oxide silica membranes for gas separation, Sep Purif Tech, 76 (2010) 171-178.

[22] D.K. Wang, J. Motuzas, J.C.D. da Costa, S. Smart, Rapid thermal processing of tubular cobalt oxide silica membranes, Int J Hydrogen Energ, 38 (2013) 7394-7399.

[23] S.N. Wang, D.K. Wang, S. Smart, J.C.D. da Costa, Ternary Phase-Separation Investigation of Sol-Gel Derived Silica from Ethyl Silicate 40, Sci Rep-Uk, 5 (2015).

[24] A. Bertoluzza, C. Fagnano, M.A. Morelli, V. Gottardi, M. Guglielmi, Raman and Infrared-Spectra on Silica-Gel Evolving toward Glass, J Non-Cryst Solids, 48 (1982) 117-128.

[25] A. Duran, C. Serna, V. Fornes, J.M.F. Navarro, Structural Considerations About Sio2 Glasses Prepared by Sol-Gel, J Non-Cryst Solids, 82 (1986) 69-77.

[26] M.I. Tejedor-Tejedor, L. Paredes, M.A. Anderson, Evaluation of ATR-FTIR spectroscopy as an "in situ" tool for following the hydrolysis and condensation of alkoxysilanes under rich H_2O conditions, Chem Mater, 10 (1998) 3410-3421.

[27] J.M. Kim, S.M. Chang, S.M. Kong, K.S. Kim, J. Kim, W.S. Kim, Control of hydroxyl group content in silica particle synthesized by the sol-precipitation process, Ceram Int, 35 (2009) 1015-1019.

[28] M. Drobek, C. Yacou, J. Motuzas, A. Julbe, L.P. Ding, J.C.D. da Costa, Long term pervaporation desalination of tubular MFI zeolite membranes, J Membr Sci, 415 (2012) 816-823.

[29] W.B.S. de Lint, T. Zivkovic, N.E. Benes, H.J.M. Bouwmeester, D.H.A. Blank, Electrolyte retention of supported bi-layered nanofiltration membranes, J Membr Sci, 277 (2006) 18-27.

[30] J. Mrowiec-Bialon, A.B. Jarzebski, L. Pajak, Z. Olejniczak, M. Gibas, Preparation and surface properties of low-density gels synthesized using prepolymerized silica precursors, Langmuir, 20 (2004) 10389-10393.

[31] D.K. Wang, J.C.D. da Costa, S. Smart, Development of rapid thermal processing of tubular cobalt oxide silica membranes for gas separations, J Membr Sci, 456 (2014) 192-201.

[32] C.J. Brinker, Hydrolysis and Condensation of Silicates - Effects on Structure, J Non-Cryst Solids, 100 (1988) 31-50.

[33] S.N. Wang, D.K. Wang, K.S. Jack, S. Smart, J.C.D. da Costa, Improved hydrothermal stability of silica materials prepared from ethyl silicate 40, Rsc Adv, 5 (2015) 6092-6099.

7 CONCLUSIONS AND RECOMMENDATIONS

7.1 Conclusions

This thesis focused on the investigation of the ES40 sol-gel method with the aim of preparing silica films directly on large pore substrates by the rapid thermal processing (RTP) method. In particular, this thesis endeavoured to understand how the ES40 sol-gel could be controlled and understood to deliver porous silica structures and how this, in turn, could be used to prepare high quality silica films to achieve high salt rejections in desalination application.

The first contribution of this thesis is the fundamental study of the ES40 sol-gel method, elucidating the miscible and non-miscible regions in a ternary phase diagram. A key finding of this work is related to the formation of dense and porous silica from miscible and non-miscible regions of ES40 sol-gel solution, respectively. This thesis initially focused on the homo/heterogeneous sol-gel system of ES40 in acidified water-ethanol solution. The ternary phase diagram of ES40–H_2O–EtOH showed that the ES40 sol-gel reactions can occur even in the phase-separated solutions. It was found that in phase-separated solutions, the sol-gel process commenced at the interface of the two phases, i.e. ES40 and the co-solvent. The silanol groups generated by hydrolysis at the interface could migrate to the co-solvent phase, contributing to condensation reactions, where silanol (Si–OH) and siloxane (Si–O–Si) groups were found to be affected by both the reaction temperature and the initial H_2O/Si ratios. Higher temperatures promoted sol-gel reactions due to an increase in the sol concentration as a result of faster solvent evaporation, thereby reducing the proximity of the reactive sites. Silica product with larger mesopores was obtained at 25 °C, compared to their micropores analogues produced at 40 and 60 °C, which was ascribed to the reduced drying stress. Consequently, the silica network compression was reduced by the slow solvent evaporation at low temperature, and the lower capillary forces, leading to the formation of larger pores derived from the silica cages of the ES40 oligomer precursor.

A second contribution is related to a systematic study of ES40 sol-gel ratios where the high water/Si and high acid/Si ratios and low ethanol/Si ratios delivered microporous features such as higher surface areas and pore volumes, and broader pore size distribution. A key finding is the formation of large silica particle clusters as revealed by small angle X-Ray scattering, structures of which were found to be more hydrostable when exposed to harsh conditions (550 °C and 75 mol% water vapour). Conversely, highly microporous silica matrices were favoured by using low water and low

acid catalyst ratios, and/or high ethanol ratio. The improved hydrostability of the silica xerogels was attributed to the formation of a more robust, open silica microstructure condensed by larger silica particles as revealed by SAXS data on one hand, and a lower proportion of silanol groups in the matrix as indicated by FTIR analyses on the other.

A third contribution is the first demonstration of the preparation of interlayer-free silica membranes by the RTP method. The membranes proved to have high salt rejection (up to 99%) in desalination application. A key finding is a significant reduction of the fabrication time, equivalent to 1% of that for a conventionally prepared silica membrane. Defect-free membranes with high salt rejection (> 99%) were obtained by adjusting the reactant ratios and reaction conditions during the ES40 sol-gel synthesis. Furthermore, it was found that the ES40 xerogels from RTP conferred a larger surface area and higher relative proportion of siloxane groups as compared to the CTP analogous. This was attributed to another key finding related to water being retained inside the xerogel pores at high temperatures (~200 °C) by the RTP method, promoting condensation reactions and the formation of siloxane bridges to further consolidate the membrane matrices.

The fourth contribution is associated with the systematic investigation of the effect of sol-gel conditions (i.e. pH, water/Si and ethanol/Si ratios) on the formation and performance of the resultant membranes. Interlayer-free membranes capable of achieving high salt rejection were successfully produced by changing the pH of the sol-gel reaction system to a pH 4 or 6. The best interlayer-free RTP silica membrane was prepared with a pH 4 sol, which reached high water fluxes of 17.8 kg m^{-2} h^{-1} at 60 °C and high salt reject (> 99%) for desalination of 3.5 wt% seawater. The dilution of the sol with ethanol also played an important role, as pH 4 membranes prepared with EtOH:Si ratio of 255:4 were stable for 120 h, whilst changing this ratio to 200:4 increased the effective desalination period to 300 h. This improvement is attributed to the thicker films derived from more viscous sols. The ES40 sol-gel also proved to be flexible, as further studies of low pH (~1) and changing water/Si ratio conferred high quality interlayer-free silica membranes by the RTP method. Of particular attention, the desalination experiment of pH 1 membranes prolonged a steady operation over 800 h without any hint of degradation, an improvement of by at least 500 h as compared to the best pH 4 membranes.

It was further found that pH played a fundamental role in the structural formation of the silica membranes. This is particularly evidenced by different structures formed below and above the silica iso-electric point (pH~2). At pH values above 2, the first layer impregnated on the substrate tended to form very porous silica structures. Subsequently, the second layer formed a dense microporous structure on top of the first layer. In the case of pH values below 1, the two layers were not

distinguished, as the films were generally dense and microporous, though a few macropores could be observed between the substrate particles. Therefore, the novel process to prepare interlayer-free silica membranes by the RTP method in this work produced more homogeneous silica films at pH values < 2, and heterogeneous silica structures at pH values > 2, which has a clear and definite association with the desalination performance of these membranes.

7.2   Recommendations

The work has demonstrated the potential of interlayer-free ES40 derived silica membranes fabricated by the RTP method for desalination applications. There are some interesting points based on major findings in this thesis which warrants for further investigation. Recommendations are given as follows:

1. The deep impregnation of the silica sol into the substrate requires further improvement. In this work, the sol infiltrated up to 10 μm, which is much thicker than conventional silica thin film membranes. Therefore, it is anticipated that by varying the sol-gel conditions and/or tuning the membrane dip coating and calcination process, the depth of impregnation could be significantly reduced, giving higher overall water fluxes whilst maintaining high salt rejections.

2. This thesis opens a window of research opportunities to prepare interlayer-free silica membranes by the RTP method. Of particular interest is doping silica with other compounds to confer the silica films functionalities otherwise not available in pure silica films. This may include doping the silica sol-gel with organic templates, hydrophobic molecules or metal oxides to improve hydrostability and adsorption, or possibly using new organo-silica precursors. These proposals will require further fundamental studies on the sol-gel method to coat the modified silica films directly on substrates with large pore sizes. In addition, designing new equipment is required for applying the RTP method under inert atmospheres to allow the retention of these organic groups, instead of the oxidising gas used in this thesis.

3. Investigation should also focus on the membrane performance using real seawater instead of the synthetic NaCl aqueous solutions employed in this thesis to further evaluate the practicality. This will provide further insights in terms of fouling, scaling, membrane degradation and cleaning processes in real-world environment.

4. There are a number of industrial applications which can be attractive for the deployment of cheap RTP silica membranes via pervaporation such as (i) ammonia recovery from waste water, (ii)

organic solvent and water separation and (iii) alcohols and water separation. For these applications, surface functionalisation as per recommendation 2 may be required. In addition, these recommendations would be warranted by demonstrating the scale up production of the RTP silica membranes for industrial applications.